



PROCESS EVALUATION OF UNDERGROUND COAL GASIFICATION: AN EXERGY ANALYSIS

MSc RESEARCH DISSERTATION SUBMISSION

Prepared by

Keeshan Moodley (348340)

*A dissertation submitted to the Faculty of Engineering and the Built Environment,
University of Witwatersrand, Johannesburg, in fulfilment of the requirements for the
degree of Master of Science in Engineering*

Supervisor: Dr. Shehzaad Kauchali

Johannesburg, 29 August 2016

Plagiarism Declaration

I, Keeshan Moodley, hereby declare that this work is my own effort under the supervision of my supervisor Dr. S. Kauchali, and where necessary, have given credit to the resources used.

This research is in submission is for the Degree of Masters of Science in Chemical Engineering to the University of Witwatersrand and has not been submitted before for any Degree or examination to this or any other university

Keeshan Moodley

Date

Abstract

This study discusses underground coal gasification (UCG) and the analysis thereof. Two main methods were used. The first is the Bond Equivalent Diagram, which gives an ideal of where operations should take place in relation to their coal and product gas compositions. This method was used to analyze several real life sites for their idealized and actual operations. The second consisted of a comparative exergy simulation study. This was done for an air-blown UCG plant with a downstream Fischer-Tropsch reactor and an oxygen-blown UCG plant with upstream air separation. The plants were analyzed by their overall exergy efficiency as well as their exergy outputs with respect to coal inputs (fuel). It was discovered that the air-blown simulation with downstream Fischer-Tropsch was the better choice from an exergy point of view due to it having higher efficiencies (1.5 for overall, 1.38 for fuel) as opposed to the oxygen-blown simulation (0.77 overall, 0.8 for fuel). This coupled with other design and safety factors led to the conclusion that the air-blown simulation was better.

Dedication

I would like to dedicate this work to my grandfather, Ganesan Naidoo, in memory of his wish that his grandchildren could reach the academic heights that were not afforded to his children.

Acknowledgements

I would firstly like to thank my HR manager, Diamantina Messaris, for making this opportunity possible and allowing me to fully develop and further my academic endeavours.

I would also like to thank my family for supporting me through this – without you, I would have never come this far.

A big vote of thanks goes out to my supervisor, Dr Shehzaad Kauchali for acting as my mentor through this. Your dedication with me has really inspired me since my undergraduate days and words cannot express how big a role you have had in shaping this.

There were many a time where I wondered why I was doing this, but the clarity and encouragement of my friends have always been there. A special thank you goes out to Kenishia Naidoo and Werner Coetzee for being my guides throughout this journey.

Table of Contents

Abstract.....	ii
List of Figures.....	vii
List of Tables	viii
Nomenclature.....	x
List of Abbreviations	xi
1 Introduction.....	1
1.1 Overview.....	1
1.2 Problem Statement & Research Motivation	3
1.3 Dissertation Structure	3
2 Literature Review	5
2.1 Underground Coal Gasification	5
2.1.1 Introduction.....	5
Site Selection	5
Drilling Procedure.....	8
Oxidant Selection.....	10
2.1.2 Reaction Description.....	14
2.1.3 Environmental Impact.....	17
2.2 Fischer-Tropsch Synthesis	19
2.2.1 Introduction.....	19
2.2.2 Reaction & Product Description	20
2.2.3 Catalyst Selection	22
2.3 Air Separation	29
2.3.1 Process Description.....	29
2.3.2 Environmental Impact.....	30
2.4 Exergy.....	33
2.4.1 Introduction.....	33
2.4.2 Analysis	35

2.4.3	UCG Exergy Analysis.....	38
2.4.4	FTS Exergy Analysis	38
2.4.5	Air Separation Exergy Analysis.....	43
3	Theory.....	46
3.1	Bond Equivalent Diagram.....	46
3.2	Bond Equivalent Analysis of UCG.....	51
3.3	Exergy Analysis.....	53
3.3.1	General Assumptions	54
4	Results & Discussion	56
4.1	Bond Equivalent Diagram Analysis.....	56
4.1.1	Hoe Creek	56
4.1.2	Chinchilla.....	61
4.1.3	Rocky Mountain	65
4.1.4	Laboratory Gasification Study	69
4.1.5	Comparative BED Discussion	72
4.2	Exergy Analysis.....	76
4.2.1	Air-Blown UCG & FTS.....	76
4.2.2	Oxygen (ASU) UCG.....	82
4.2.3	Comparative Simulation Discussion.....	87
4.2.4	Hoe Creek Simulation.....	89
4.2.5	Improvements	92
5	Conclusion	96
6	References.....	98
	Appendix A: Bond Equivalent Diagram.....	A
	Appendix B: Exergy Analysis	K

List of Figures

Figure 1: UCG geological interaction (Kumar, 2014)	6
Figure 2: Illustration of UCG (Self <i>et al</i> , 2010).....	14
Figure 3: UCG molecular view (Bell <i>et al</i> , 2011)	16
Figure 4: ASF product distribution independent of carbon number(van de Loosdrecht et al, 2013)	21
Figure 5: Arrangement of typical Co catalyst (van de Loosdrecht <i>et al</i> , 2013).....	26
Figure 6: Process Flow for a typical air separation (Smith & Klosek, 1998)	29
Figure 7: Grassman diagram of reference case exergy flow (Iandoli & Kjelstrup, 2007 - streams below 15MW are not shown).....	41
Figure 8: Exergy Losses for different variability cases (Iandoli & Kjelstrup, 2007)	42
Figure 9: ASU Model (Cornelissen & Hirs, 1998)	44
Figure 10: Pure O ₂ process flow diagram	47
Figure 11: Air & FT conversion UCG process flow diagram	48
Figure 12: Bond equivalent diagram - basic CHO system (Pillay, 2013).....	49
Figure 13: BED of Hoe Creek coal and syngas (adapted from Thorsness <i>et al</i> , 1979 - dry basis)	59
Figure 14: Closeup of Hoe Creek thermally balanced region.....	60
Figure 15: BED of Chinchilla coal and syngas.....	63
Figure 16: Chinchilla thermally balanced region close-up	64
Figure 17: BED for Rocky Mountain coal and syngas	67
Figure 18: Rocky Mountain thermally balanced region close-up.....	68
Figure 19: BED for lab study coal and syngas.....	71
Figure 20: Laboratory study thermally balanced region close-up	72
Figure 21: Air UCG-FTS simulation diagram	76
Figure 22: Exergy flow diagram of air-blown UCG with downstream FTS	80
Figure 23: ASU-UCG simulation diagram	82
Figure 24: Exergy flow Oxygen-blown (ASU) UCG	85
Figure 25: Hoe Creek simulation diagram	89
Figure 26: Process flow diagram of air separation via adsorption (Smith & Klosek, 2001).....	94

List of Tables

Table 1: UCG water tests (adapted from Kapusta <i>et al</i> , 2013).....	7
Table 2: Classification criteria for UCG (Bialecka, 2009)	8
Table 3: Analysis of UCG trial projects (adapted of Kačur <i>et al</i> , 2014)	11
Table 4: Ideal FTS iron catalyst categorization (adapted from van de Loosdrecht <i>et al</i> , 2013).....	23
Table 5: EIGA environmental concerns (EIGA, IGC 94/11/E, 2011).....	31
Table 6: Difference between energy and exergy (Romero and Linares, 2014)	35
Table 7: Biomass FTS exergy analysis results (adapted from Soheli & Jack, 2011)	39
Table 8: Rational exergy efficiency of ASU integrated with biomass gasifier (adapted from Sapali & Raibhole, 2013).....	43
Table 9: Exergy efficiency quantification of an ASU (adapted from Cornelissen and Hirs, 1998)	44
Table 10: Enthalpy of reactions at 650K	52
Table 11: Thermally balanced reactions	53
Table 12: Ultimate analysis of Hoe Creek coal as recieved (adapted from Thorsness <i>et al</i> , 1977).....	56
Table 13: Hoe Creek gas composition (mol%, adapted from Thorsness <i>et al</i> , 1977)	57
Table 14: Table of balanced reaction scheme for Hoe Creek coal	57
Table 15: Thermally balanced reactions for Hoe Creek coal	58
Table 16: Ultimate analysis of Chinchilla coal, dry and ash free (adapted from Queensland Department of Mines and Energy, 1999).....	61
Table 17: Molar composition of syngas from Chinchilla (adapted from Kacur <i>et al</i> 2014).....	61
Table 18: Balanced reaction scheme for Chinchilla coal.....	62
Table 19: Thermally balanced reactions for Chinchilla coal	62
Table 20: Ultimate analysis of Rocky Mountain coal, dry (adapted from National Energy Technology Laboratory, 2012).....	65

Table 21: Rocky Mountain syngas molar composition (adapted from Dennis, 2006).....	65
Table 22: Balanced reactions for Rocky Mountain coal.....	66
Table 23: Thermally balanced reactions for Rocky Mountain coal.....	66
Table 24: Ultimate analysis of laboratory in coal (adapted from Prabu & Jayanti, 2012).....	69
Table 25: Molar syngas composition of UCG experiment (Prabu & Jayanti, 2012).....	69
Table 26: Balanced reaction scheme for lab coal	70
Table 27: Thermally balanced reactions	70
Table 28: Comparison of Hoe Creek & Chinchilla syngas composition (dry and without nitrogen)	73
Table 29: Oxygen-blown UCG operations comparison.....	74
Table 30: Main UCG & FTS simulation results	78
Table 31: Total exergy results of Air UCG & FTS.....	79
Table 32: Equipment exergy analysis	79
Table 33: Distillation unit summary	83
Table 34: Main UCG composition results	83
Table 35: Total exergy analysis of oxygen (ASU) UCG simulation	84
Table 36: Equipment exergy analysis	84
Table 37: Comparison of UCG product stream exergies.....	87
Table 38: Hoe Creek simulation exergy results	90
Table 39: Hoe Creek simulation exergy efficiency	91
Table 41: ASPEN Simulation results for air-FTS simulation.....	L
Table 42: ASPEN Simulation results for ASU UCG.....	M
Table 43: ASPEN Simulation results for Hoe Creek.....	N

Nomenclature

atm	Atmosphere
C	Carbon (chemical element)
CARBO-01	Carbon (ASPEN component)
CARBO-02	Carbon Monoxide (ASPEN component)
CARBO-03	Carbon Dioxide (ASPEN component)
CH ₄	Methane (chemical compound)
C ₈ H ₁₈	Octane (chemical compound)
CO	Carbon Monoxide (chemical compound)
CO ₂	Carbon Dioxide (chemical compound)
GW	Gigawatt
HYDRO-01	Hydrogen (ASPEN component)
H ₂	Hydrogen (chemical element)
H ₂ O	Water (chemical compound)
J	Joule
K	Kelvin
kW	Kilowatt
METHA-01	Methane (ASPEN component)

MW	Megawatt
mol	Moles
N ₂	Nitrogen (chemical element)
N-OCT-01	Octane (ASPEN component)
NITRO-01	Nitrogen (ASPEN component)
O ₂	Oxygen (chemical component)
OXY-01	Oxygen (ASPEN component)
Pa	Pascal
r# or R#	Reaction Number
R	Universal Gas Constant

List of Abbreviations

ASU	Air Separation Unit
BED	Bond Equivalent Diagram
CRIP	Controlled Retractable Injection Point
FTS	Fischer Tropsch Synthesis
KES	Kölbel-Engelhardt Synthesis
UCG	Underground Coal Gasification
WGS	Water Gas Shift

1 Introduction

1.1 Overview

Coal has been an integral part of mankind's technological development, playing an important role within the fuel industry and making a significant economic contribution to countries that possess feasible deposits. Its calorific value makes it an ideal source of power via its combustion, though its status as a fossil fuel presents an urgent issue that forces the reconsideration of its consumption. Though cheaper than most renewable sources of energy, coal cannot generate itself quickly enough to meet the growing energy demand across the globe. Though the resource heavily invests itself in carbon dioxide emissions, it continues to be an influential driving force in the energy market and thus requires an innovative solution in order to slow down its depletion and help to prevent rising energy costs (Self, Reddy & Rose; 2012).

One way to counter the above problem would be to access coal deposits that would have normally been ignored under conventional mining protocols. Self *et al* argues that current coal consumption averages at about 15 to 20% of the total global reserve by mining standards, with the balance being deemed unrecoverable for economic or safety reasons. Given that mining not only brings about its own concerns with regards to ecological contamination and hazardous working conditions, it becomes obvious that one must regard other methods of harnessing coal. One such method is underground coal gasification (UCG).

UCG follows the same process as surface coal gasification, whereby coal is converted to synthetic gas (syngas) via an oxidizing agent, with one main difference: the reactions take place within the coal seam itself rather than in an external reactor. Injection and production wells are drilled into the coal bed for oxidant insertion and syngas extraction respectively. The end product can be used for various purposes depending on its composition, calorific value and how much cleaning it requires. Usually, syngas can be used as a means of combustion to

generate power or as a chemical feedstock for other processes. Not only does UCG offer a lower capital investment by absence of a reactor set-up and coal mine operations, but potential UCG sites offer themselves to be integrated with carbon capture and sequestration (CCS), thus lowering carbon dioxide emissions (Brown, 2012).

As stated earlier, an oxidant is needed for the reaction pathways to occur, the details of which will be described later on. According to Bialecka (2009), the best choice of oxidant would be pure oxygen as it causes the syngas to have a higher calorific value than compared to air or steam. However, the financial implications of using pure oxygen are great – since UCG is a continuous process, an air separation unit/unit (ASU) would require a tremendous capital investment and operating cost, which may outweigh the UCG profit margins. To consider an alternative, the syngas produced from air-blown gasification may be converted to liquid hydrocarbon fuels using Fischer-Tropsch synthesis (FTS). Mirzaei *et al* (2013) defines FTS as a catalytic set of simultaneous reactions which convert syngas into linear and branched hydrocarbons. This process has experienced a new surge of interest due to its low sulphur-, nitrogen- and aromatic-based emissions as well as fluctuating crude oil prices affecting the hydrocarbon fuel market (Choudhury & Moholkar, 2013)¹.

In terms of analyzing efficiency, the traditional energy balance follows the fundamental ‘First Law’ of thermodynamics, which is based upon the principle that energy is conserved in different forms and is unable to ascertain the quality of energy available in a stream. This can be solved by considering an exergy analysis instead, which is defined as calculating the maximum potential work of a stream if brought to equilibrium with its surroundings. By performing this analysis, one is able to ascertain exactly how much work potential the final product streams contain and exactly which process units cause the most amount of exergy loss.

1.2 Problem Statement & Research Motivation

With coal resources under strain and renewable energy resources proving costly, new methods are needed to effectively use coal deposits and access seams that are deemed unfeasible by mining methods.

The purpose of this research is thus to:

- Analyze UCG site operations in terms of the Bond Equivalent Diagram (BED)
- Simulate the following processes for exergy evaluation:
 - Oxygen-blown UCG to produce syngas for downstream combustion
 - Air-blown UCG with FT conversion of syngas to liquids for downstream combustion
 - The Hoe Creek UCG operation

1.3 Dissertation Structure

This dissertation is divided into 8 different sections, including appendices and the introduction (section 1).

Section 2 covers the literature review of the four main topics mentioned in this thesis. The UCG process is described in detail in terms of its chemistry and physical conditions. The processes of Fischer-Tropsch Synthesis (FTS) and cryogenic air separation are also described and expanded upon. The last idea covered in this section is defining exergy and how it is applied to each of the aforementioned systems.

Section 3 covers the practical theory of the study. In 3.1, the Bond Equivalent Diagram (BED) is introduced to give a clearer understanding to UCG and how its mass and energy balances operates. 3.2 covers the exergy analysis applied to the study and gives a list of assumptions made in the simulations.

Section 4 details the analysis and discussion of the study. 4.1 deals with the BED analysis of the syngas production operations at the Hoe Creek, Chinchilla and Rocky Mountain UCG seams; as well as considering a laboratory-scale gasification study done by Prabu & Jayanti (2012). The heat of reactions that come from the reaction scheme help determine the Thermally Balanced Line (TBL), a method used to show whether a site operates endothermically, exothermically or is thermally balanced in principle. 4.2 covers the exergy analysis of an air-blown UCG site coupled with downstream FTS in comparison to an air separation unit plant (ASU) producing pure oxygen for a downstream UCG reactor. The exergy represents the workable energy a stream possesses, and efficiencies are defined with respect to the system feeds to determine how much work is conserved across the process. Improvements for further study are also made.

Section 5 is the conclusion of the report and summarizes the work done.

Appendix A and B deals with the ancillary calculations used in the BED and exergy calculations respectively

2 Literature Review

2.1 Underground Coal Gasification

2.1.1 Introduction

Bhutto, Bazmi & Zahedi (2013) characterizes UCG as a combination of mining activities and gasification that removes the need for much of the labour, and thus offers a production method that is safe to both human control operations and the environment. The reaction mechanism is similar to that of *ex-situ* gasification (Self *et al*; Bialecka; Brown) and offers a product that may be utilized for energy generation or as a feed stock into another process.

The following sections will cover the progression of UCG:

- Site selection
- Drilling Procedure
- Oxidant Selection
- Reaction Mechanism
- Environmental Impact

Site Selection

Figure 1 below offers an insight into the geological interactions that the UCG process has at different levels. When considering a potential site, it is important to take the overburden material (the rock and soil above the coal seam) and any aquifers that are around the area. Both Bialecka and Brown propose that a potential UCG site should ideally be free of any surrounding water bodies as any unwanted water influx would lead to compromised gasification efficiency. Bhutto expands on this concept, stating that the groundwater regime must be properly defined both within and around the selected operations site. Groundwater influx can impact on the oxidant injection pressure and the UCG chemistry.

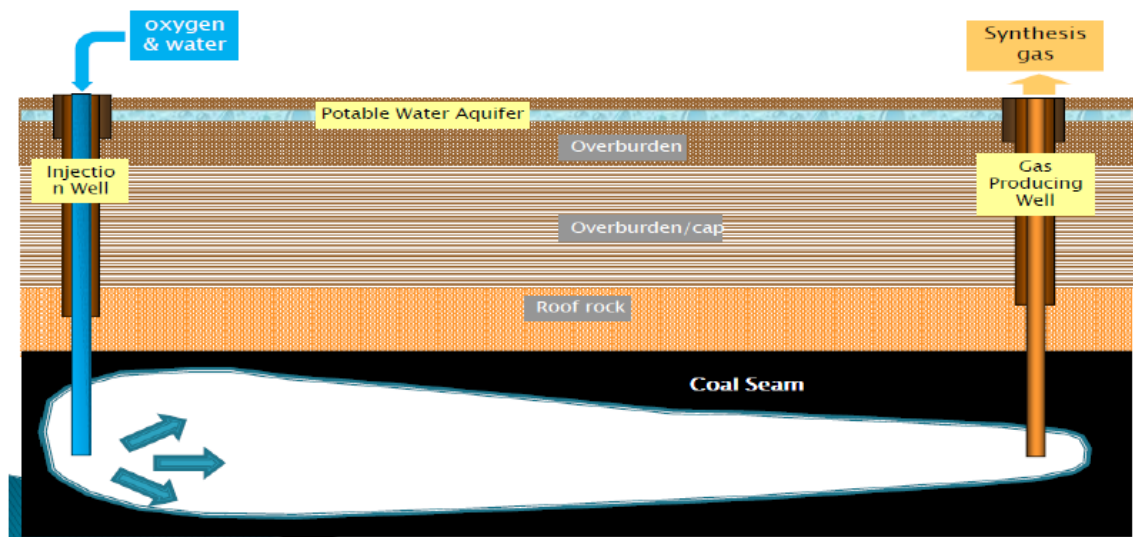


Figure 1: UCG geological interaction (Kumar, 2014)

Groundwater contamination is cited by Kapusta, Stańczyk, Wiatowski and Chećko (2013) as one of the major environmental challenges that oppose UCG operation. During any phase of the UCG process, surrounding water bodies may become polluted by the products of the chemical reactions occurring within the coal seam, many of which are considered to be environmentally hazardous, with typical contaminants being characterized as phenolic compounds, benzene derivatives, polycyclic aromatic compounds and N-heterocyclic compounds for organic groups and ammonia, chlorides and sulphates for inorganic groups. Kapusta *et al* conducted a study on the experimental mine site known as ‘Barbara’ in Poland and measured levels of the previously mentioned chemicals as well as heavy metals and cyanides in five different sampling points in and around the coal seam’s post processing waters, which are summarized in table 1 below:

Table 1: UCG water tests (adapted from Kapusta *et al*, 2013)

<u>Contaminant</u>	<u>Unit of measurement</u>	<u>Production phase value</u>	<u>Cooling phase value</u>
Conductivity	μS/cm	14 425	11 805
pH	-	6.29	5.95
Total nitrogen	mg/L N	2003	1425
Total chlorides	mg/L	1660	643
Total cyanides	mg/L	1.26	1.03
Total sulphates	mg/L	3220	6305
Mercury (Hg)	mg/L	<0.005	<0.005
Nickel (Ni)	mg/L	0.243	0.140
Iron (Fe)	mg/L	650	1110
Lead (Pb)	mg/L	0.044	<0.05
Total organic carbon	mg/L	616	1490
Phenolics	mg/L	484	610
Total BTEX (benzene, toluene, ethylbenzene & xylene)	μg/L	55.8	15.3
Total PAH's (polycyclic aromatic hydrocarbons)	μg/L	1912	378
Total N-heterocycles	μg/L	6.47	11.69

It was noted that the production levels of these contaminants decreased rapidly after UCG operations were terminated in the coal seam, and was concluded that the pollutant levels decrease with increasing time after operation termination and distance from the operation site. Kapusta and Brown agree that groundwater contamination can be avoided by operating the reactor space at a pressure lower than the hydrostatic pressure in the area to prevent the influx and settling of any water into the surrounding reactor area.

Brown cites Hoe Creek in Wyoming to suffer from “poor site characterization and operation”, which eventually caused the cavity roof in the coal seam to collapse and the process gas to escape into the local groundwater system.

Table 2 subsequently summarizes the ideal criterion for a potential UCG site:

Table 2: Classification criteria for UCG (Bialecka, 2009)

Criterion	Characteristics/Remarks
Coal type	Any
Coal physiochemical properties	High volatile matter content, low agglomerating capacity, ash content less than 50% by weight
Seam depth	Profitability criterion
Bed thickness	More than 1m
Angle of inclination	Any
Type & tightness of surrounding rock mass	Should be tight & firm with slightly permeable layers in the overburden area (clays, silts, shale clays)
Hydrological conditions	No surrounding water bodies
Coal quantity	Profitability criterion
Methane presence	None
Deposit tectonics	No fissures or faults
Infrastructure conditions	Lack of urbanized development is preferred

Drilling Procedure

Self *et al* identifies two standard methods which have been used successfully with regards to UCG drilling – shaft and shaftless.

Shaft methods make use of coal mine galleries and shafts to transport oxidants and the UCG product streams into and out of the reaction space. These sometimes require the creation of shafts and drilling of openings through underground labour. These methods are only employed in closed coal mines for economic and safety reasons. Some of the more commonly used methods in this category are:

- Chamber/warehouse method: this is best utilized for highly permeable coal types. Brick walls are used to separate coal panels, whilst oxidants are supplied to a side of the panel that has already been ignited and the

product is withdrawn from the other side. Self *et al* notes that this method produces low syngas flow rates.

- Borehole producer method: the coal seam is separated into parallel horizontal galleries all connected by a series of boreholes. Remote electric ignition is used in each borehole to begin the UCG process. This method is best used for extremely flat coal seams.
- Stream method: best utilized for coal seams orientated in a sharp inclination, parallel galleries are created which follow the contour of the seam, all of which are connected at the bottom via a horizontal gallery known as a fire-drift. Fire is introduced at the bottom gallery and the hot coal face moves up the seam's natural slope as oxidants are fed through one gallery and syngas is withdrawn from the other. The residual ash drops down on the void space and does not interfere with the coal.
- LLT gasification method: here, long and large tunnel (LLT) systems are drilled - a main gasification channel, two auxiliary holes (between the injection and production wells for air and water vapour injection or as gas discharge systems) and two auxiliary tunnels. The tunnels are sealed to contain combustible gases. A third tunnel may exist which is constructed of bricks and prevents blockage in the main gasification channel.

More recently, shaftless methods have been developed which make use of directional drilling, whereby wells are made in an angular fashion. These do not require the use of an underground labour workforce, thus making it much safer for operational personnel. There are two main methods here:

- Linked vertical well (LVW) method: the most basic of UCG technologies, this involves production and injection wells into the seam and using the natural pathways of the coal to direct the oxidant flow. Ideally, this method should involve a series of injection wells, as the coal face migrates further away from the injection well as the gasification continues; decreasing both syngas quality and system control. This method is best

when used for low rank coals such as lignites due to their natural permeability. High rank coals such as anthracites do not fare as well.

- Controlled retractable injection point (CRIP) method: a combination of conventional and directional drilling, the CRIP method is used to access the coal and form a link between the injection and production wells. A vertical section of predetermined depth is drilled, after which directional drilling is used to expand the hole and drill underneath the coal seam, creating an almost horizontal injection well. A burner attached to retractable coiled tubing is used to start ignition. The ignition point can be moved to anywhere along the injection well should a previous part of the seam be consumed and abandoned. This offers far more accurate control than any of the previously mentioned methods, though it is still fairly new and not commonly used.

Oxidant Selection

One of the key success criteria listed by Kačur, Durdán, Liaciak & Flegner (2014) of the UCG process is the calorific value of the generated syngas. This is generally of a low to medium BTU calorific nature. Table 3 subsequently categorizes some of the UCG trial projects taken around the world since the early 1900's and analyzes them in terms of oxidant used and gas calorific value. As can be seen, processes that use a combination of oxygen and air as opposed to the latter only produce a gas that has a higher calorific value.

Table 3: Analysis of UCG trial projects (adapted of Kačur *et al*, 2014)

<u>Country</u>	<u>Site</u>	<u>Year</u>	<u>Chosen oxidant</u>	<u>Coal type</u>	<u>Syngas calorific value (MJ/m³)</u>
Former Soviet Union (USSR)	Lisichansk	1935	Air	Bituminous	3.8
	Podmoskovna	1947	Air	Lignite	3.4
	Angreskajna	1961	Air	Bituminous	4.1
	Yuzno-Abinskaja	1955	Air	Lignite	3.4
USA	Hanna I	1973	Air	High volatile bituminous	4.2
	Hanna II	1975	Air	High volatile bituminous	5.3
	Hanna III	1977	Air	High volatile bituminous	4.1
	Hoe Creek I	1976	Air	High volatile bituminous	3.6
	Hoe Creek IIA	1977	Air	High volatile bituminous	3.4
	Hoe Creek IIB	1977	O ₂ /H ₂ O	High volatile bituminous	9.0
	Hoe Creek IIIA	1979	Air	High volatile	3.9

				bituminous	
	Hoe Creek IIB	1979	O ₂ /H ₂ O	High volatile bituminous	6.9
	Pricetown I	1979	Air	Bituminous	6.1
	Rawlins IA	1979	Air	Sub-bituminous	5.6
	Rawlins IB	1979	O ₂ /H ₂ O	Sub-bituminous	8.1
	Centralia A	1984	O ₂ /H ₂ O	Sub-bituminous C	9.7
	Centralia B	1984	O ₂ /H ₂ O	Sub-bituminous C	8.4
	Rocky Mountain IA	1987	O ₂ /H ₂ O	Sub-bituminous	9.5
	Rocky Mountain IB	1987	O ₂ /H ₂ O	Sub-bituminous	8.8
UK	Newman – Spiney P5	1949	Air	Sub-bituminous	1.4
Belgium	Thulin	1986	Air	Anthracite	7.0
Spain	El Tremedal	1997	O ₂ /H ₂ O	Sub-bituminous	10.9
Australia	Chinchilla	2000	Air	Sub-bituminous	6.6

The experiment in Kačur *et al* further goes on to simulate a UCG reactor system using two gasifiers set in parallel. The use of air only as an oxidant was the first variable analyzed, with the results showing that the syngas produced from the

reactor reached a maximum value of 4.43 MJ/m^3 at an air flow of $19.28 \text{ m}^3/\text{hr}$. The second experiment ran a mixture of air and oxygen as an oxidant with varying ratios of the latter. A maximum calorific value occurred at 8.21 MJ/m^3 at an air flow of $3.93 \text{ m}^3/\text{hr}$ and oxygen flow of $1.84 \text{ m}^3/\text{hr}$. A third experiment also ran a mixture of oxygen and air, this time in larger quantities. A maximum calorific value 13.79 MJ/m^3 was achieved at an air flow of $12.06 \text{ m}^3/\text{hr}$ and oxygen flow of $9.01 \text{ m}^3/\text{hr}$. Although it is concluded that increasing the oxygen ratio in the air does help gasification performance, an optimal ratio must be found: low contents can hinder temperature profile growths and reaction rates and excess contents can result in unwanted oxygen in the syngas.

2.1.2 Reaction Description

Self *et al* states that UCG is similar to surface (ex situ) gasification, and that syngas production is governed by the same set of chemical reactions. This definition is confirmed by both Brown (2012) and Bialecka (2009). The UCG progression is illustrated by figure 2 below:

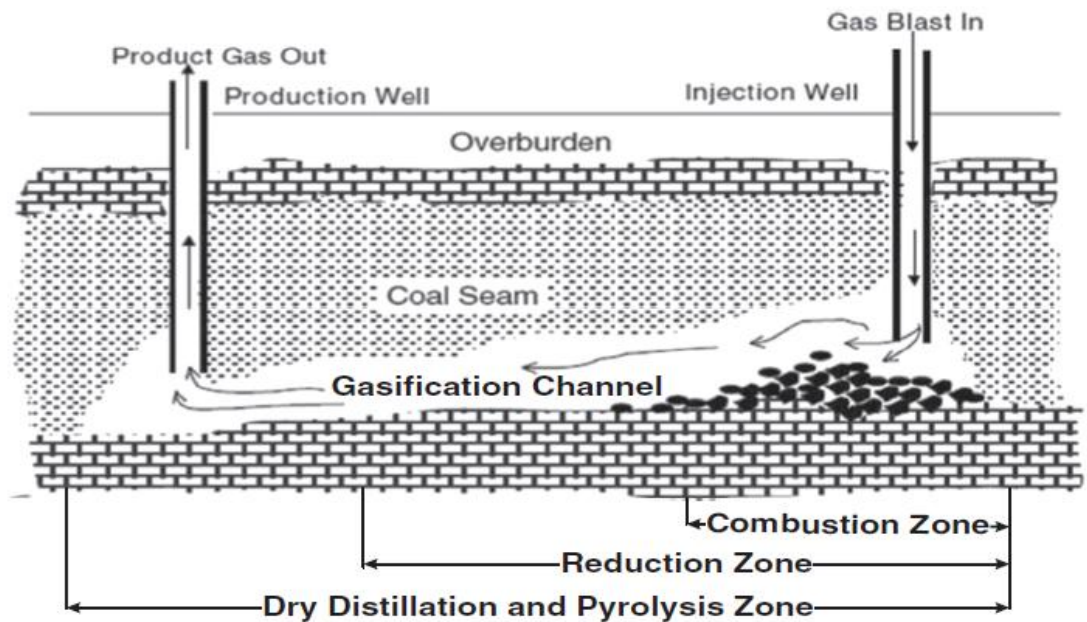


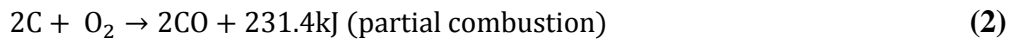
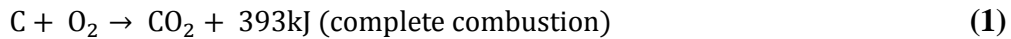
Figure 2: Illustration of UCG (Self *et al*, 2010)

Injection and production wells are drilled into the coal seam. The former acts a channel which allows a continuous flow of compressed oxidants to enter the coal body and form part of the set of reactions which produce raw syngas together with other contaminants depending on the coal composition. Ignition can be either through the use of an electric coil or gas firing at the face of the seam. Bialecka (2009) states that the conditions of these reactions are difficult due to the reaction mechanism occurring on a compact surface with only the topmost layer exposed to the oxidant flow; however goes further on to state that this would depend on the depth of coal – most UCG operations occur within the gas permeable region of brown coal beds and young hard coal formations at a depth of approximately 300 meters. Strongly swelling and coking coals are noted by Bialecka to block gas

flow across the entire coal bed and thus hinder the reaction by restricting the mass transfer of the oxidant into the carbon network.

The UCG reactions scheme can be divided into three main zones, discussed both in Self *et al* and Kumar, Udayakumar, Stojcevski & Oo (2014), and shown in figure 2, and will now be considered in detail. These zones follow the oxidant flow direction and exist simultaneously, a key feature in differentiating between UCG and surface (*ex situ*) gasification.

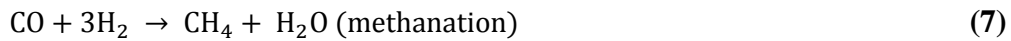
The first zone is known as the combustion or oxidation zone, where oxygen contained within the oxidant stream reacts with the carbon in the coal, and is represented by equations 1 to 3 (Self *et al*; Kumar *et al*). Due to the high release of energy, the highest temperatures within the UCG process occur within this zone, sometimes exceeding 1500K.



The second zone is known as the reduction zone, whereby water vapour (from the oxidant stream or released from the coal body) and carbon dioxide are reduced to form carbon monoxide and hydrogen, represented by equations 4 and 5. Since these reactions are endothermic, they make use of the heat released in the combustion zone.



Kumar *et al* notes that the water vapour present in this phase also promote the water gas shift (WGS) reaction, which influences the H₂/CO ratio. Both Kumar *et al* and Self *et al* state that a methanation reaction can occur at this point, which consumes hydrogen and carbon monoxide.



The final zone is called the dry distillation or pyrolysis zone, whereby the coal seam decomposes into multiple volatiles including light hydrocarbons, tars and volatile gases. At this point, the syngas can be extracted from the production well, containing mostly CO, H₂ and CH₄; though it can contain other contaminants such as heavy metals, ash and sulphur products depending on the coal composition.

Bell, Towler & Fan (2011) quantifies The UCG process on a molecular scale, as seen by Figure 3 below:

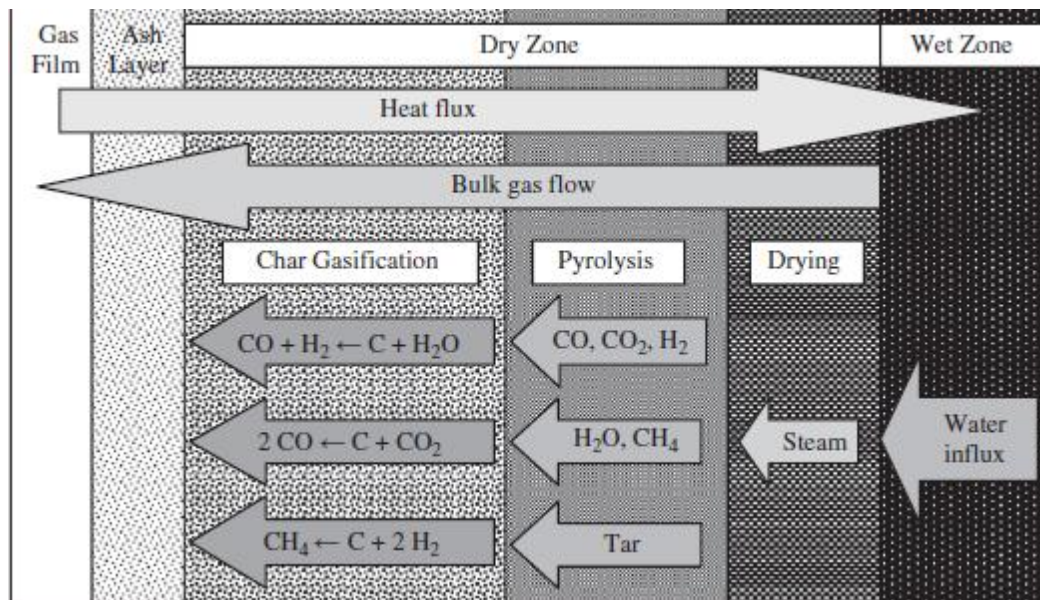


Figure 3: UCG molecular view (Bell *et al*, 2011)

Heat from the bulk gas zone is transferred to the coal seam across the gas film and ash layers. The water contained in the micropores of the dry zone is evaporated and the temperature drops as it approaches the wet zone, where bulk water is evaporated into steam (known as the drying zone). In the pyrolysis zone, the char network is thermally decomposed. Finally, in the char gasification zone, the network is converted to gas by a combination of steam & carbon dioxide

gasification as well as hydrogenation. Bell *et al* states that the overall gasification rate is highly influenced by this last step.

2.1.3 Environmental Impact

UCG offers benefits mainly associated with its lack of economic constraints, though it does also offer significant environmental advantages as well. Imran *et al* (2014) states that large areas of land are not removed from use as most of the activity occurs well underground. With this comes the added gain of underground ash disposal and minimal surface waste extraction and reduced occupational health hazards for operational personnel as no manpower would be required underground. Minimal atmospheric pollution is generated and the process consumes less water than *ex-situ* gasification, which needs a high steam-to-air ratio to prevent slagging. The properties of the overburden material act as a natural insulating material and thus create a higher thermal efficiency for UCG as opposed to its *ex-situ* counterpart.

Compared with conventional coal mining techniques, UCG tends to be preferable due to its independence from activities such as mining, cleaning, transport and storage. Each of these steps require capital and operating costs and put forward the problem of dealing with solid, liquid and gaseous residues that must be treated prior to disposal of their respective waste streams. UCG combines this into a single operation that is not only environmentally friendly, but has a lower cost (Imran *et al*). Compared to other power-generating processes, UCG offers an electricity cost of €66 per MWh when combined with CCS and CCGT (combined cycle gas turbine) as opposed to other 'clean' energies such as nuclear (€67 per MWh), clean coal (€115 per MWh), CCG combined with CCS (€105 per MWh) and generic renewable energy sources (€172 per MWh). Kumar *et al* agrees with this, stating that the only close competitor of UCG is nuclear energy.

Imran *et al* (2014) also delves into the environmental concerns of UCG. Carbon dioxide emissions are still a major concern since the process still utilizes a fossil

fuel as a feedstock, though Brown (2012) proposes that this can be countered with CCS as there is a high degree of coincidence between UCG and CCS sites. Additionally, many types of coal plasticize and swell in the presence of CO₂, thus sealing any fractures within the exposed surface of the coal bed.

Ground subsidence is also a major concern. As the void within the reactor space grows, surface material moves downward as they are not supported by the coal bed. Though the magnitude of subsidence depends on the type of rocks, depth of the bed and geometry of void; it should be noted that this is not a unique problem to UCG or conventional mining in general. Brown mentions that monitoring equipment can be installed to measure the rate and extent of subsidence and that it can be managed by conventional mining methods.

Bhutto *et al* (2013) states that contamination of surrounding groundwater through outward gas flow from the reactor seam can be managed by operating the pressures below hydrostatic pressure. This also helps by using the groundwater as an additional oxidant. Bhutto *et al* further goes on to say that main contaminants from UCG sites post operation include polyaromatic hydrocarbons, phenols and ash leachate (inorganic matter). Ideally, UCG sites should be as far away from groundwater sources as possible, though if this is not achievable, regular water testing and treatment should form part of operations.

2.2 Fischer-Tropsch Synthesis

2.2.1 Introduction

The FTS process is a set of catalytic reactions which are used to convert syngas or raw natural gas into predominantly straight-chain hydrocarbons. This technology has been reviewed with great interest since the 1920's under the context of converting remote natural gas into liquid fuels (Arabpour, Rahimpour, Iranshahi & Raeissi, 2012; van de Loosdrecht *et al*, 2013). Gas-to-liquid conversion allows for an increase fuel supply to meet the growing demand, particularly within the Pacific and Asian sectors.

FTS has the main advantages of producing a wide hydrocarbon spectrum with very little sulphur- and nitrogen-based compounds (Lillebø *et al*, 2013) as well as low aromatic compound content (Mirzaei *et al*, 2013). By using a natural gas feedstock or syngas, it is possible to produce liquid hydrocarbons in bulk that can further be refined and separated into fuels such as petroleum and diesel.

Van de Loosdrecht *et al* gives a detailed history of FTS, starting in 1920's when Franz Fischer and Hans Tropsch patented the method of converting syngas to hydrocarbons via iron- and cobalt-based catalysts. The first commercial plant was piloted in 1936, with several others coming online at a later stage to provide Germany and Japan with synthetic fuel during the Second World War, with China piloting plants from the 1940's through to the 1960's.

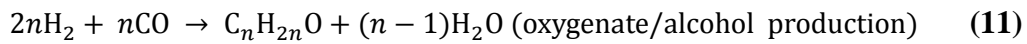
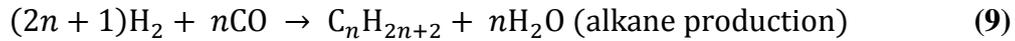
After the war, the Allied Forces came into contact with FTS technology through the interrogations of scientists and engineers who were involved in running the synthetic fuels industry. Based on this, the US Bureau of Mines developed a two-stage high temperature FTS, whilst Sasol piloted both a high- and low-temperature process for the production of petrol and waxes respectively. The former was expanded on in the 1970's due to the increasing oil prices.

2.2.2 Reaction & Product Description

van de Loosdrecht *et al* describes the reaction mechanism as a polymerization mechanism in essence, in keeping with the product spectrum previously mentioned. This is demonstrated in the equation below:



Both Choudhary & Moholkar (2013) and Hu, Yu & Lu (2012) expand on equation 8, by dividing the product spectrum into several simultaneous reactions that group each set of hydrocarbons according to their chemical classification:



van de Loosdrecht *et al* states that the entire process can essentially be summarized as a carbon monoxide hydrogenation reaction, with the carbon-to-carbon bonds that make up the chain growth governed by the Anderson-Schulz-Flory (ASF distribution). This is a statistical model that is based on the probability of hydrocarbon chain growth (α). For a particular class of product containing n carbon atoms:

$$C_n = n(1 - \alpha)\alpha^{n-1} \quad (13)$$

Should α be independent of the carbon number, the product distribution will align itself accordingly as in Figure 4 below:

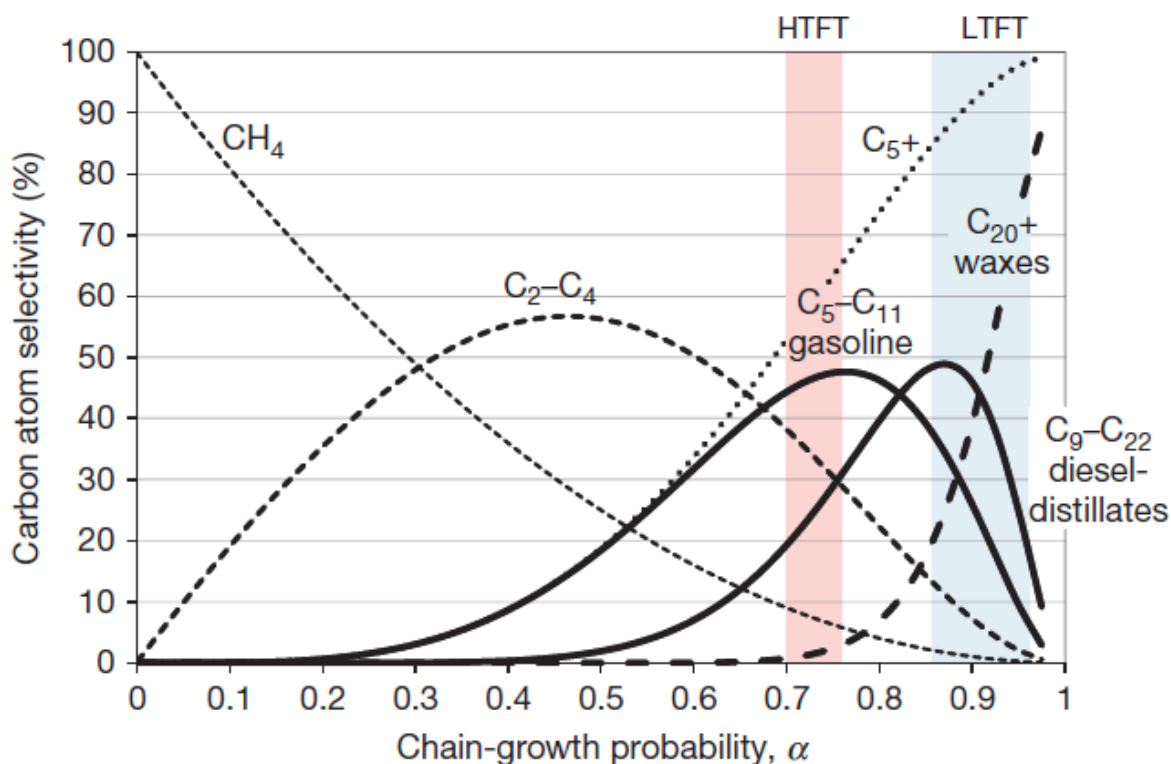


Figure 4: ASF product distribution independent of carbon number(van de Loosdrecht et al, 2013)

According to Hu *et al* and van de Loosdrecht *et al*, FTS can be categorized into a high or low temperature operating range, depending on the products desired and the type of catalyst used:

High temperature FTS (HTFTS) occurs at temperatures ranging between 320°C to 350°C. At these operating conditions, all products are in the gas phase, thus making the system a gas-solid system. Fixed fluidized bed reactors are recommended for this type of process. Cobalt catalysts produce methane within this operation, whilst the commercially-used iron catalysts with alkali promoters mainly produce gasoline (petroleum) spectrum hydrocarbons with light olefins and oxygenates as byproducts.

Low temperature FTS (LTFTS) occurs at temperatures ranging between 200°C to 250°C. Commercially, both cobalt and iron catalysts can be used, with the former being used at the lower end of the temperature range. LTFTS tends to be more difficult to operate than HTFTS – the products are mainly heavier hydrocarbons

(waxes) and thus create a three-phase reaction system. Catalyst particles have to be bigger than they would in the higher temperature operation in order to limit the pressure drop if a fixed bed reactor is used. This tends to cause problems in differences between hydrogen and carbon monoxide diffusion rates and reduces the catalyst utilization.

The subsequent section will delve further into catalyst selection.

2.2.3 Catalyst Selection

Although metals such as nickel and ruthenium can be used as catalysts, commercially only iron and cobalt based catalysts are used in the FT reactor system. Iron generally produces more oxygenates and olefins than cobalt and is thus considered to have a lower hydrogenation count than the latter.

Looking at iron, it is a cheap raw material when compared to cobalt and produces a lighter hydrocarbon spectrum that is suitable for the fuel and chemical industry. Ideal temperatures occur between 320° to 350°C, where the α parameter sits at an average value of 0.7, thus making it appropriate for HTFTS and helping to yield most of the products at gasoline chain length. It is also more tolerant of catalyst poisons such as sulphur and is more responsive to the addition of promoters and changes in process parameters (namely temperature, pressure and feed composition) to enhance selectivity. However, iron catalysts tend to deactivate quickly and must be regenerated or replaced more often than their cobalt-based counterparts.

Iron catalysts that are used for commercial purposes are mainly iron oxides, hydroxides or oxy-hydroxides that require a treatment step such as reduction or syngas pre-treatment. Below, are ideal catalysts for different conditions:

Table 4: Ideal FTS iron catalyst categorization (adapted from van de Loosdrecht *et al*, 2013)

<u>FTS Process</u>	<u>Reactor</u>	<u>Catalyst Properties</u>	<u>Raw Material</u>	<u>Synthesis Method</u>
HTFT - 320°C to 350°C	Circulating or fixed fluidized bed reactors	<ul style="list-style-type: none"> • Low surface area (less than 10g/m²) • High density • High strength 	Mill scale	Fusion method followed by crushing and milling
LTFT - 220°C to 250°C	Tubular fixed bed reactor	<ul style="list-style-type: none"> • High surface area • High strength 	Fe(NO ₃) ₃ and silica	Precipitation followed by extrusion and shaping
	Slurry bed reactors	<ul style="list-style-type: none"> • High surface area • Small particle size 	Fe(NO ₃) ₃ and silica	Precipitation followed by spray drying and calcination

Iron catalyst preparations include:

- Fusion is a method that produces iron catalyst particles of low surface area and high particle density. This ensures that the particles are of high strength and are suitable for reactors such as circulating fluidized bed reactors whereby flow movements would destroy more fragile catalysts. Iron oxides are used as a feed and melted in arc furnaces along with

promoters. The molten mix is then set in ingots and then milled to the required size. A disadvantage of this process are the impurities set in these ingots – during cooling, the alkali promoters bind themselves to inorganic additions such as silica and aluminium oxides and negate their promotion effect.

- Precipitation of iron catalysts is one of the earliest forms of iron catalyst preparation. In the 1930's, this method was adapted on a large commercial scale, coinciding with the FTS boom in that era. Iron (III) nitrate solution is reacted with a base to precipitate out iron (III) oxide-(oxy)hydroxide. By controlling process conditions such as temperature, pH and precipitation rate; catalyst properties such as surface area and crystallite size can be controlled to the desired condition. The slurry stream is then filtered and washed to remove soluble salts such as ammonium nitrate and impregnated with structural promoters such as silicon and aluminium to increase catalyst strength as well as chemical promoters. The particles are finally spray-dried and calcinated to get rid of volatiles. When compared with fusion, precipitation offers increased catalyst strength, better catalyst shape and increased promoter distribution without negation.

As previously mentioned, iron catalysts can be more easily manipulated than cobalt ones in terms of selectivity adjustment. van de Loosdrecht *et al* states that iron catalyst composition produces higher responsiveness to FTS selectivity than process conditions. Addition of alkali promoters tend to allow yields which deviate from the ASF model and require two α parameters instead of one.

Deactivation of iron catalysts used in the FTS process can be attributed to:

- Free carbon formation
- Phase transformation actions, such as oxidation
- Mechanical break-up due to flow
- Deposition of catalyst poisons from the syngas feed
- Sintering

Free carbon formation is the most prevalent cause of catalyst deactivation in HTFTS where dissociated carbon atoms from the CO molecule in the syngas feed react with each other to produce carbon deposition. This can be suppressed by the types of chemical promoters added to the catalyst. In LTFTS, sintering and oxidation are the key deactivation factors, whereby the interconversion of the different iron carbides from the catalyst mechanism can lead to a stoichiometric excess of carbon and thus weakening of catalyst particles.

Cobalt catalysts are mentioned in the original FTS patent made by Fischer and Tropsch in 1925. Germany and Japan adapted large scale FTS processes using only cobalt catalysts from 1938 to 1945, after which focus shifted to iron catalysts.

Generally, cobalt is up to 250 times more expensive than iron and thus needs to be used effectively, so a high density of cobalt metal sites is available.

Cobalt catalysts are used exclusively for LTFTS. They are currently used by Sasol and QP in the Oryx GTL plant in Qatar and by Shell in the SMDS plant in Bintulu, Malaysia (Saiba, Moodley, Cibîca *et al*, 2010).

Many modern cobalt catalysts are similar to the ones first described by Fischer and Tropsch, with cobalt on a metal oxide support. Cobalt is the active metal, with a weight composition of anywhere from 10 to 30%. A noble metal is used as a reduction promoter, with a weight composition of 0.05 to 1%, and a structural oxidic promoter making up anywhere from 1 to 10%. The balance is a modified refractory oxidic support. They are usually arranged as per the figure below:

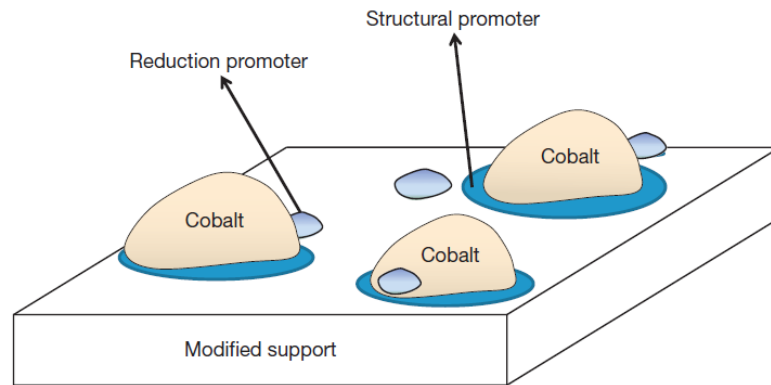


Figure 5: Arrangement of typical Co catalyst (van de Loosdrecht *et al*, 2013)

Methods of cobalt catalyst preparation include:

- Coprecipitation of catalysts can be done as a batch or continuous process at constant pH. The cobalt precipitates as α -Co(OH)₂ or β -Co(OH)₂. As with iron catalyst precipitation, crystallite size can be controlled by temperature, precursor salt, precipitation agents and reaction atmosphere. The precipitate is then filtered and washed. The particles are impregnated with a structural support promoter, then spray-dried to obtain the correct size distribution for bubble bed reactors or pelletized for fixed bed reactors.
- Impregnation of cobalt (in the form of oxides or metal) onto pre-shaped supports.

Van de Loosdrecht *et al* states that when judging cobalt catalyst performance, they are more active in slurry bed reactors, which normally operate at an average temperature of 230°C, which is suited for LTFTS. Here, products are heavier hydrocarbons: although this would induce a higher calorific value product (Domalski, 1972) and the operation control becomes more difficult due to the reactor acting as a multi-phase system.

Saiba *et al* (2010) states that cobalt catalyst deactivation methods can be attributed to the following:

- Oxidation – this was originally thought to have been due to product water molecules from the multiple reactions, though recent studies have proven that this is a function of crystallite size and dependant on operating conditions. Above sizes of 2nm will not undergo oxidation
- Mixed-metal support interaction – this is a rare occurrence. Although the reactions are thermodynamically feasible, they need a CoO intermediate which will not form under normal FTS conditions.
- Carbon deposition and carburization – this will result in pore blockages and limit mass transfer into and out of the catalyst. This can be decreased to some effect by ruthenium and boron.
- Sintering – a thermodynamically driven process whereby smaller unstable particles join together to form larger stable ones which are lower in surface energy. This is affected by reaction temperature and water partial pressure. This can be controlled by choosing the right structural support such as alumina or silica.
- Poisoning – this is especially significant in coal-to-liquid systems. Sulphur-based poisoning can be prevented by the addition of zinc- or lead-oxide guard beds whilst nitrogen-based poisoning can be undone with mild hydrogen treatment.
- Surface reconstruction – thermodynamically driven process whereby surface energy is lowered. Unfortunately further study is needed in this area.

As can be expected, much study has gone into the study of catalysts and their overall effects on the FTS system. Yao *et al* (2014) did a comparative study on cobalt catalysts by analyzing the effects of cobalt catalysts, one supported by SiO₂ and one by ZSM-5. Using the polyethylene glycol-additive method (a subtype of the co-precipitation method), both catalysts were developed, with the SiO₂ supported catalyst using ruthenium as a promoter. The ZSM-5 supported catalyst was discovered to have a better CO conversion but a lower turnover frequency. The strong interactions between the hydrogen species and the catalyst was unfavourable to hydrogenation of carbon intermediates and is thus considered to be the rate determining step. In contrast, the Ru-promoted catalyst improved

cobalt oxide reducibility and an improved turnover frequency. In this case, the hydrogen interactions with the catalyst were significantly weaker than in the former case and produced liquid hydrocarbons in the gasoline range. It was concluded that the ZSM-5 catalyst could have a higher activity if further research went into weakening hydrogen interactions with the catalyst.

Schulz (2013) studied the constraints based on iron and cobalt catalysts. Using co-precipitated iron and cobalt catalysts, the study makes use of both fixed bed reactors for studying the initial changes of catalyst selectivity and CSTR slurry reactors for control of full control of the process parameters. The product streams were analyzed using gas chromatography. The study revealed the following points:

- The product distribution was proven to be independent of carbon number
- Although hydrocarbon chain growth is typically a function of the carbon number, it was discovered that the CSTR (continuous stirred tank reactors) experiment displayed increasing probability of chain growth with time whilst desorption of chains was increasingly suppressed on cobalt catalysts. On iron catalysts, the chain growth probability only changed during the initial stage of the experiment, with the rest of the experiment remaining static. It was noted that cobalt catalysts are far more sensitive to changes in feed concentration.
- Schulz explicitly states that methanation is undesirable due to methane not forming a part of FTS and is considered a ‘waste’ in a sense. Nickel, cobalt and ruthenium catalysts tend to enhance this formation, with the feed composition and temperature acting as supporting factors. In cobalt, methane is assumed to form on inactive surface areas. Iron catalysts depend on CO partial pressures for formation.

2.3 Air Separation

2.3.1 Process Description

Air separation is a general term given to the production of pure, or at least concentrated, streams of oxygen, nitrogen and argon. Though many processes exist in this regard, both cryogenic and non-cryogenic, both Smith & Klosek (2001) and Cornelissen & Hirs (1998) state that cryogenic distillation is the only method that can be used for high purities and production rate, thus it is the only method that will be considered as part of UCG.

Air separation units make use of cryogenic distillation with the use of the double-column distillation process developed by Carl von Linde in the early 1900's. Though many plants may differ from one another with regards to the actual process layout in order to meet their specific energy or product requirements, the basic principles on which they are based remain the same. The process described below is based on Smith & Klosek, Wilson, Woodward & Erickson (1988) as well as Cornilissen & Hirs.

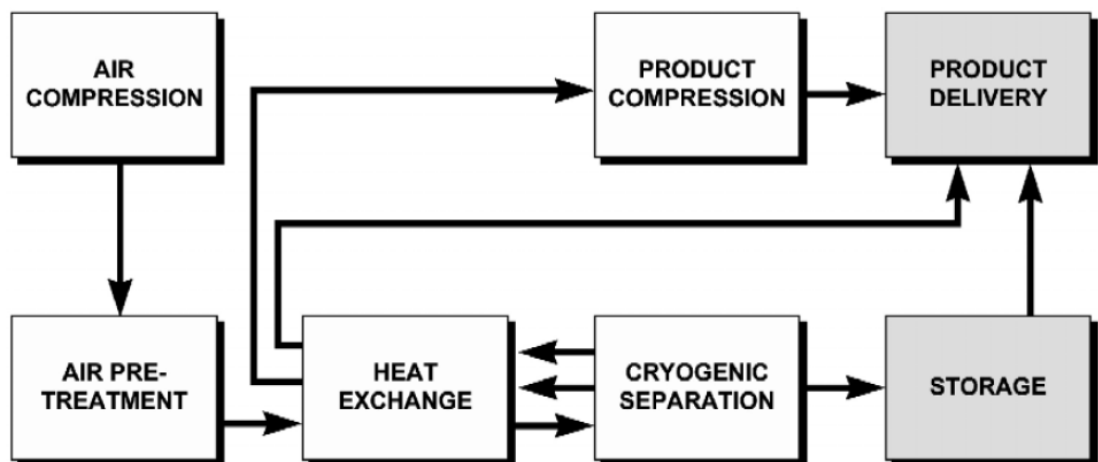


Figure 6: Process Flow for a typical air separation (Smith & Klosek, 1998)

Air is compressed to approximately 6bar via a compressor and inter-stage coolers, and then filtered to get rid of dust particles that contaminate the ambient air. The

stream is fed through an after-cooler or spray tower which lowers the temperature after the final compression stage. The air is then fed through the front end purification or pre-treatment, known as molecular sieves contains activated packing material to absorb water and carbon dioxide that would otherwise freeze under the subzero temperatures in the following process stages and block pipes. There are usually two molecular sieves located in parallel. Whilst one is active, the other will regenerate its packing to release the absorbed water and carbon dioxide by a heated waste nitrogen stream. Once this is done, the flow will be diverted to the newly regenerated molecular sieve and the other will undergo regeneration.

The air stream is then cooled to -172°C in the main heat exchanger, flowing in a counter-current manner to the liquid products of nitrogen, oxygen and argon. Depending on the design, a fraction of the air feed at this point may be diverted to a turbine to recover energy associated with refrigeration and another fraction may be condensed and fed to the distillation column (Wilson *et al*). The air after the heat exchanger is fed to the bottom of the high pressure (HP) column. Two pure nitrogen refluxes are produced – one for the itself and one for the low pressure (LP) column, whilst the overhead condenser of the HP column provides the reboil duty for the LP column.

The bottom liquid of the HP column is vaporized to provide the overhead condenser duty for the argon column. The upper part of the LP column is where pure nitrogen can be withdrawn, whilst the bottom liquid is fed to the argon column to provide pure oxygen and crude argon. An additional column is required to separate pure argon from oxygen.

2.3.2 Environmental Impact

The European Industrial Gases Association (EIGA) has compiled a list of environmental concerns in their Environmental Impacts of Air Separation Units (IGC Doc 94/11/E, 2011) that is summarized in the table below. EIGA maintains a philosophy of minimizing waste and pollution of any kind and disposing of

these in a safe and environmentally conscious way. These are the main concerns affecting ASU operations and production and are by no means an exhaustive list.

Table 5: EIGA environmental concerns (EIGA, IGC 94/11/E, 2011)

<u>Concern</u>	<u>Risk</u>	<u>Mitigation Measure</u>
Compression energy	Indirect impact on production and supply from power plants and the local municipality electricity system	Continuous improvement in energy efficiency of ASU's by operating procedures, equipment design and maintenance
Oil	Oil discharge to the environment from compressors, hydraulic systems and/or transformers	<ul style="list-style-type: none"> • Installation of a bund or pit at each compressor and transformer to collect oil • Installation of cyclonic or electrostatic oil demisters • Preventative maintenance to ensure that leaks (if any) are caught before it becomes a hazard
Volatile organic compounds (VOC's)	Irritation of human eyes, nose and throat, massive global warming risk depending on which gas is released	<ul style="list-style-type: none"> • Use refrigerants with no ozone depleting potential and lower global warming potential

		<ul style="list-style-type: none"> • Identify all points where leaks could possibly occur and ensure that they are hermetically sealed • Design of process so that the refrigerant and the solvent can be used reused instead of adding fresh feed • Avoid excess use of refrigerant and solvent and review safe working practices near refrigeration area
<p>Contaminated water discharge</p>	<p>Contaminated water may pollute surrounding water bodies or areas with heavy metals that deplete organic matter necessary for ecological balance as well as introducing improper temperature gradients to the surrounding areas</p>	<ul style="list-style-type: none"> • Minimize leaks through preventative maintenance of cooling towers and heat exchangers • Reduce controlled losses in cooling towers by looking at bleed losses and concentration cycles

		<ul style="list-style-type: none"> • Use corrosion inhibitors to extend equipment life • Operate cooling towers to optimum concentration cycles to minimize chemical loss, wastewater discharges and makeup water consumption • Use the minimum quantity of treatment chemicals • Use local legal requirements for water discharge in terms of concentration and temperature
--	--	--

2.4 Exergy

2.4.1 Introduction

Since coal is a non-renewable resource, it is imperative that the most be made of its thermodynamic capabilities. Although there is a shift to renewable sources of energy, there is also a powerful drive to make coal-related processes more

efficient and more productive per unit mass of coal consumed. The First Law of Thermodynamics deals with the conservation of energy throughout its different forms. Though this is useful, it does not give detailed insight into the quality of energy studied within the system. It is more productive to employ the Second Law of Thermodynamics with this regard, whereby the exergy or the potential work of a system can be determined (Srivastava, 1988; Ghamarian & Cambel, 1982).

Exergy is defined as the potential of a resource to do work based on the difference between its physical parameters and the dead state considered (Boroumandjazi, Rismanchi, & Saidur, 2013; Eftekhari, van der Kooi & Bruining, 2012). This can be with regards to a combination of temperature, pressure or composition. It is a useful analytical and optimization tool as it is possible to derive the maximum performance of a considered system under a certain set of conditions as well pinpoint possible sources of irreversibility that negate the potential within a process. If this idea is expanded to a chemical process such as UCG, it becomes possible to identify which process units ‘consume’ the most exergy and where improvements can be made. Srivastava states that this provision allows for the proper design of equipment, which in turn reduces operating and maintenance costs.

In the past, exergy analysis was limited to Eastern Europe, where Srivastava states that extensive research on this topic was conducted within the Soviet Union. Lior, Sarmiento-Darkin & Al-Shaqawi (2006) states that the analysis also offers the calculation of thermodynamic optima where compromises between the desire to accelerate reaction rates and undesirable entropy generation.

Romero & Linares (2014) take a more global approach to exergy, citing it as an important indicator for energy sustainability. Energy on its own does not offer a proper study into the relationship between a thermodynamic system under study and its environment due to the irreversibility (entropy) generation that will degrade energy. They define exergy as the difference between energy and these irreversibilities, thus making it the energy available for work, though it is not a property of the material(s) under consideration – it is the thermodynamic link

between the system and its environment. If this connection is broken, the available energy is considered to be chemical potential energy. The table below offers further insight into differentiating between exergy and energy:

Table 6: Difference between energy and exergy (Romero and Linares, 2014)

<u>Energy</u>	<u>Exergy</u>
Dependant on characteristics of flow and independent of environment	Dependant on characteristics of flow and environment
Refers to motion or ability to induce motion	Work or ability to induce work
Always conserved in a process due to transfer in different forms	Conserved in a reversible process only
Value is different from 0 when in equilibrium with reference environment	Value is 0 when in equilibrium with reference environment

2.4.2 Analysis

Sapali and Raibhole (2013, in their exergy study to be mentioned later on) quantify exergy as:

$$\dot{E} = \dot{E}_k + \dot{E}_p + \dot{E}_{phys} + \dot{E}_{chem} \quad (14)$$

Where:

- \dot{E} is the total rate of exergy in a stream in J/s
- \dot{E}_k is the kinetic exergy (associated with speed) of a stream in J/s
- \dot{E}_p is the potential exergy (associated with altitude) of a stream in J/s
- \dot{E}_{phys} is the physical exergy (work obtainable from a substance through a reversible process) of a stream in J/s

- E_{chem} is the chemical exergy (work obtainable from a substance through heat transfer and matter exchanges with the environment) of a stream in J/s

It is important to note that exergy does not ‘balance’ in the same way that energy does. Since exergy can be lost due to entropy production, equation 14 cannot be used for balances over mass or energy boundaries and does not condone a simple IN equals OUT case.

Physical exergy, also known as thermo-mechanical exergy, can be defined as:

$$E_{\text{phys}} = \dot{m}[(h - h_0) - T_0(S - S_0)] \quad (15)$$

Where:

- \dot{m} is the stream flow rate in kg/s
- $h - h_0$ refers to the enthalpy difference of the stream at its current state (T, P) and the ‘dead’ or reference state in J/kg (T₀, P₀) respectively (Note – environmental considerations are in K and Pa for temperature and pressure respectively)
- $S - S_0$ refers to the entropy difference of the stream at its current state and the dead state in J/kg.K

For solids and liquids, the physical exergy can be defined as:

$$E_{\text{phys}} = \dot{m} \left[C \left((T - T_0) - T_0 \ln \frac{T}{T_0} \right) - v_m (P - P_0) \right] \quad (16)$$

Where:

- C is the heat capacity of the solid or liquid in J/kg.K
- v_m is the specific volume of the solid or liquid at temperature T₀ in m³/kg

Chemical exergy can be defined as:

$$E_{chem} = \dot{m} \sum_i x_i (e_{0,i} + RT_0 \ln x_i) \quad (17)$$

Where:

- x_i is the molar fraction of the component i in the stream
- $e_{0,i}$ is the standard chemical exergy of the stream in J/kg
- R is the universal gas constant – 8.314J/K.mol

The simple, or overall, exergy efficiency of the process is defined as:

$$\eta = \frac{E_{out}}{E_{in}} \quad (18)$$

Where:

- E_{in} and E_{out} are the exergies of the streams flowing into and out of a particular system boundary in J/s

The overall exergy represents the amount of workable energy that is conserved from all the inputs within the system in relation to that of the outputs. This ratio considers the universal inputs and outputs, regardless of the stream's intended purpose. A high value for this does not necessarily mean that the system is efficient as waste streams could still contain significant work that could be utilized elsewhere in the process instead of simply dissipating.

The fuel exergy efficiency takes individual components or desired components and compares them to the exergy of the coal feed:

$$\Psi = \frac{E_{desired\ component(s)}}{E_{coal\ feed}} \quad (19)$$

The fuel efficiency, while similar to the overall efficiency, relates the exergy conserved from the coal feed to the final desired product. This ratio is a judge of how much of the coal's initial exergy into the system is conserved in the various forms of work taking place, which result in the desired product. A high value for

this means that the coal's workable energy is mostly conserved throughout the process and ends up within the desired product stream.

2.4.3 UCG Exergy Analysis

Eftekhari *et al* performed an exergy analysis on a UCG plant with simultaneous CCS storage. Using a chemical equilibrium model to analyze the effect of process parameters on product composition, three different scenarios were analyzed: ideal operations, practical operations (defined from state-of-the-art technologies) and zero CO₂ emissions, all with the aim of maximizing hydrogen content and minimizing carbon dioxide emissions. The results showed that whilst the UCG can recover 52 to 68% of the coal's chemical exergy in the first two cases, though the zero emissions scenario shows a negative recovery, indicating that current CCS technology cannot be productively utilized. Further study is needed once new developments occur.

2.4.4 FTS Exergy Analysis

Sohel & Jack (2011) compared a biomass gasification process coupled with FTS with a biochemical process that converted a biomass feed to ethanol. The biomass feed selected was sawdust, dried via excess heat from the FTS reaction heat and then gasified with air. The resultant gas was then cooled and then cleaned of ash and salts before being compressed, shifted using the WGS reaction and fed to a FT reactor. No mention is made of what kind of catalyst is made use of, though the feed composition is given (by weight) as 26% H₂, 12% CO, 17% CO₂, 44% N₂ and small amounts of methane. Approximately 10.19kg/s of biomass is converted to 1.54kg/s of diesel fuel and a net electricity production of 4MW, with the exergy losses being quantified in the table below:

Table 7: Biomass FTS exergy analysis results (adapted from Sohel & Jack, 2011)

<u>Process unit</u>	<u>Exergy loss (%)</u>
Biomass drying	4.3
Biomass gasification	34.2
Syngas cleaning	0.6
Syngas compression	4.8
WGS reactor	0.8
FTS reactor	2.9
Biofuel separation	2.0
Heat recovery	14.2
Power generation	36.2

The overall exergy efficiency was calculated to be 36.4% as opposed to 34.7% of the biochemical process. Both processes experienced heavy losses in the heat recovery and power generation sections, and were concluded to be similar in their exergetic natures though the FTS process had a high conversion efficiency and somewhat minimized the entropy generation, thus accounting for the slightly higher efficiency in exergy.

Iandoli & Kjelstrup (2007) simulated a GTL process that combined syngas production, FTS and a product upgrading unit using Pro/II (Aspen/SimSci) simulation software, though the latter was not considered as part of the exergy analysis. Natural gas feed is preheated and mixed with steam and oxygen from an ASU (also not considered by the study). The three components were reacted in an autothermal reformer at 1300K and is converted to syngas. The syngas is then cooled to separate and condense out water whilst the excess heat is recovered in a waste heat reboiler that produces both high pressure (110bar) and low pressure (5bar) steam. The syngas is then fed to a slurry-phase FT reactor that uses cobalt-based catalyst due to its high selectivity. The maximum conversion per pass was assumed to be 60% and the tailgas is recycled back into the process. To focus on the FT unit of the process, three cases were developed where certain variables

were changed to test exergetic efficiency: a reference case based on LTFTS, increasing catalyst selectivity by 5% against the reference case and increasing the hydrogen conversion to 90% per pass.

Figure 7 shows the exergy flow of the reference case. As can be seen, the FT recycle stream contains a significant amount of work that would have been wasted if it had been vented or discarded. The FT unit in the reference case shows a exergy efficiency of 93% owing to the fact that it is not considered to be adiabatic in its modelling and heat produced from the FT reactions must be directly recovered to keep the operating temperature constant. Overall, the losses amounted to 20% within the FT unit and the entire GTL process (excluding product upgrading and the ASU) was 62%.

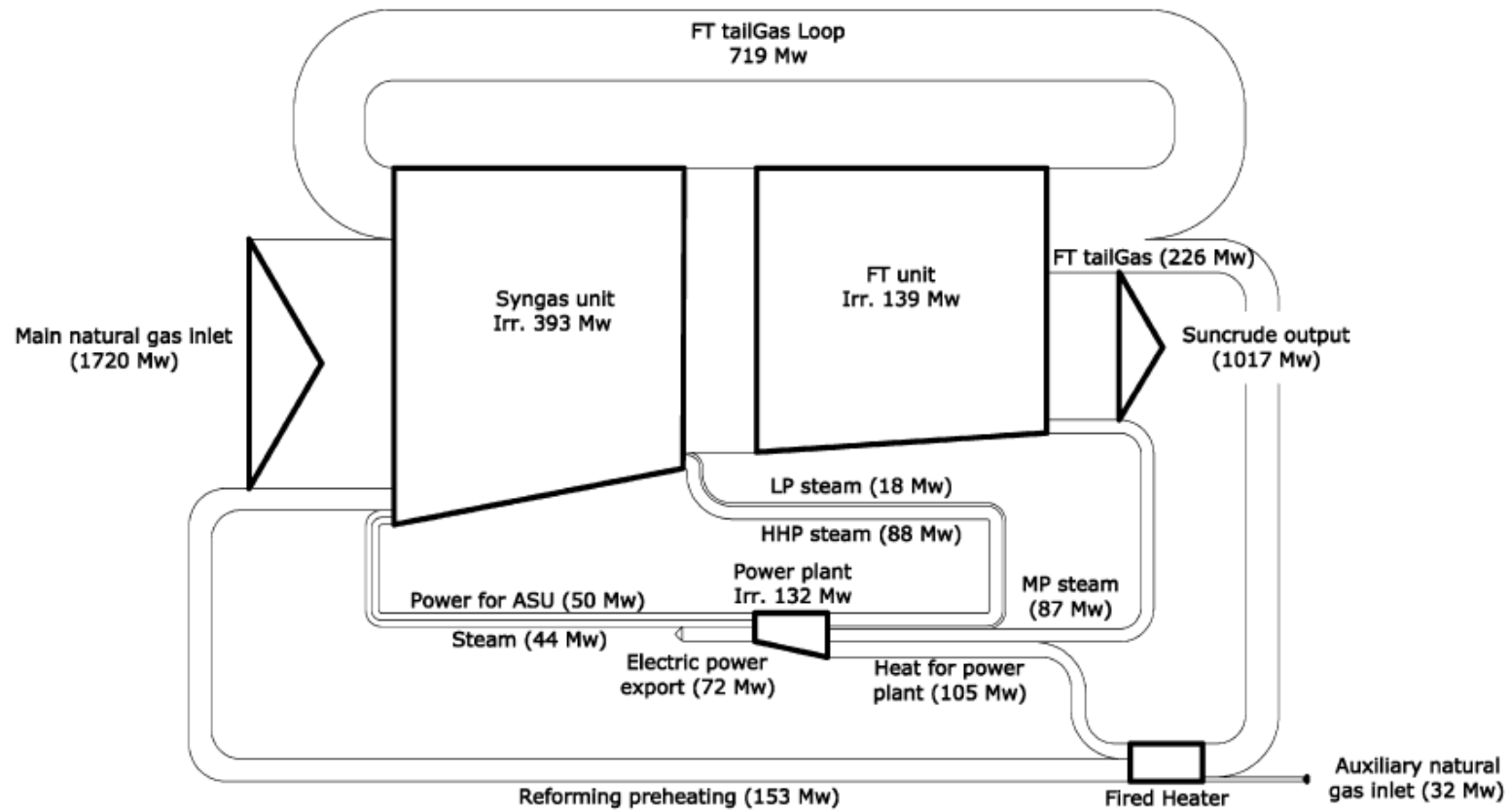


Figure 7: Grassman diagram of reference case exergy flow (Iandoli & Kjelstrup, 2007 - streams below 15MW are not shown)

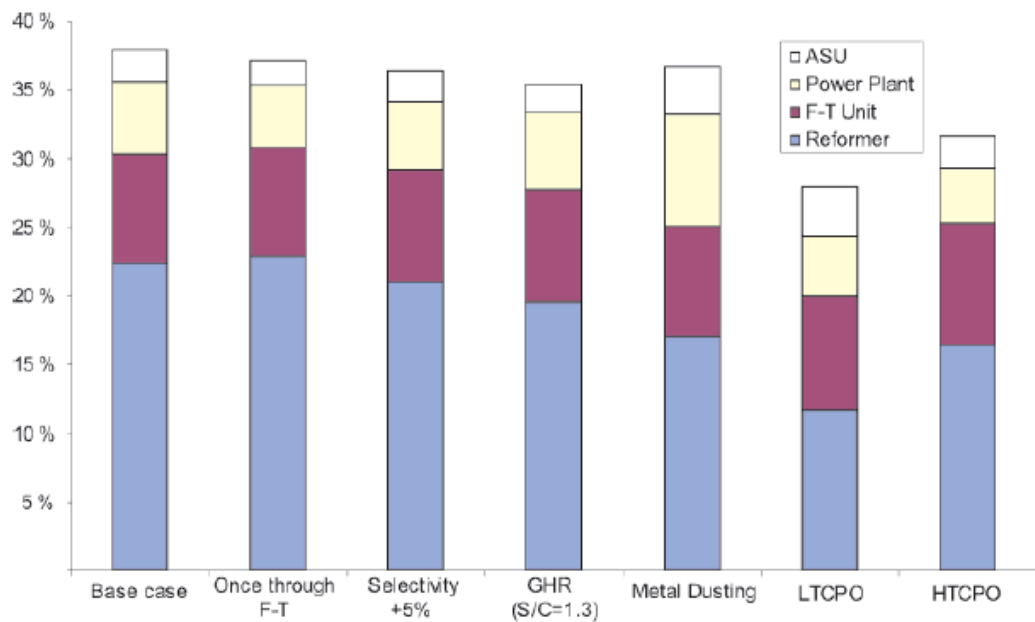


Figure 8: Exergy Losses for different variability cases (Iandoli & Kjelstrup, 2007)

Figure 8 shows the exergy losses from the study according each of the variables changed within the reference case, though only the first three are of interest in this context as these apply directly to the FT unit. Iandoli & Kjelstrup concluded that increasing the single pass conversion of hydrogen did not make any difference to the exergy of the FT unit whilst increasing catalyst selectivity 5% upward of the base case only improved the FT unit by 2 to 3%.

Prins, Ptasinaki & Janssen (2004) performed an exergy analysis study on the exergetic optimization of a biomass gasification process integrated with a Fischer-Tropsch reaction system. Sawdust is dried to 10% moisture by weight by using the residual heat from the FT reactor. The sawdust is autothermally gasified by air at 900°C at atmospheric pressure. The resulting gas is cooled to 90°C and generates steam of 50barg and 20barg to be used in steam cycles for electricity production. The syngas is cleaned by filtration and washed with water before being compressed to 25bar and catalytically shifted using a WGS reactor, having a composition and 26% hydrogen, 12% carbon monoxide, 17% carbon monoxide, 44% nitrogen and small amounts of methane. The FT reactor then converts this to liquid hydrocarbons in the ranges of naphtha (C5 to C8), diesel (C9 to C12) and

wax (C23+). The tail gas from this process is used to generate electricity by being incinerated in a steam turbine.

It was discovered that the largest exergy losses occur in the biomass gasification due to the gasification process decreasing the heating value in the conversion from biomass to syngas. This is unavoidable, though it can be mitigated by optimizing the gasification temperature. Significant exergy losses can occur in the power generation section of the process, which can be reduced by improving liquid hydrocarbon recovery and using more efficient electrical energy generation technology. Overall, the process had a 36.4% rational exergetic efficiency which is increased to 46.2% if recommendations are taken into account.

2.4.5 Air Separation Exergy Analysis

Sapali & Raibhole (2013) simulated a medium oxygen purity ASU in an attempt to integrate it with a biomass gasifier that uses a steam and oxygen mixture as the gasifying agent. Using the ASPEN process simulation software, oxygen was obtained at a purity of 96.2% from a feed of 850scmh (standard cubic meters per hour). The table below summarizes the rational efficiencies of the ASU components:

Table 8: Rational exergy efficiency of ASU integrated with biomass gasifier (adapted from Sapali & Raibhole, 2013)

Process Unit	Rational Efficiency (%)
Multi-Stage Compressor	64.43
Booster	63.05
Sub-cooler	88.19
Main heat exchanger	56.41
Expander	50.22
HP column	50.24
LP column	54.01
Biomass gasifier	72

It can be seen that the distillation columns, which are essentially the driving force behind the ASU operation, ‘destroy’ the most exergy.

Cornelissen & Hirs (1998) did an exergy analysis on a cryogenic air separation unit in order to study the possibilities of fuel saving. Expanding on equation 20, the study defined the exergy used as the sum of the desired component and the exergy loss within the system considered. By simulating the ASU with the ASPEN software (see figure below), the plant was divided into five different areas and analyzed for the rational efficiency as can be seen from table 9:

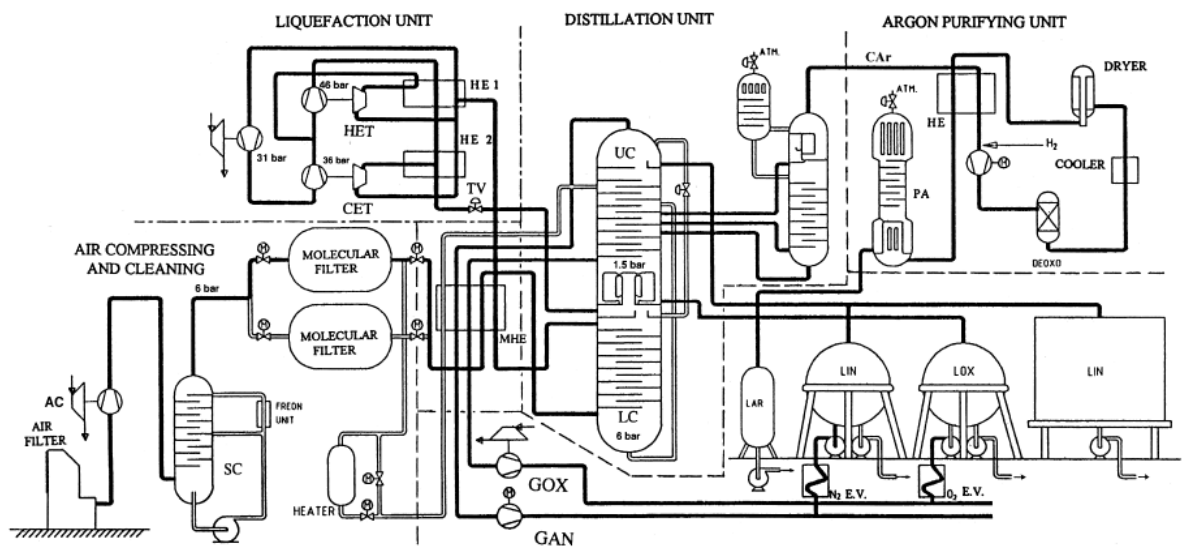


Figure 9: ASU Model (Cornelissen & Hirs, 1998)

Table 9: Exergy efficiency quantification of an ASU (adapted from Cornelissen and Hirs, 1998)

Unit	Exergy Loss (kW)	Rational Efficiency (%)
Air compressor and front-end purification	2751	48
Main heat exchanger	333	86
Distillation unit	788	46
Liquefaction unit	4853	25
Argon purifying unit	85	2
Total	8810	28

- The main air compressor lost about 1708kW, which is caused by the compression of 6.2bar. This ASU uses steam to regenerate the molecular sieves by heating purge gas from downstream to 170°C. The steam turbines have a rational efficiency of 0.86, though the exergy is lost as the purge gas is vented to the atmosphere after regenerating the molecular sieves (225kW from steam at 11bar and 210°C).
- The main heat exchanger loses exergy based on differences between the hot and cold streams and the pressure drops associated with these. The mean temperature difference was calculated to be 4.2K.
- The distillation column unit loses 62kW in the lower column, 487kW in the upper and argon purification columns and 125kW in the throttling between the two columns. Overall, the unit has an exergetic efficiency of 46%, though Cornelissen and Hirs suggest that this doesn't give an overall view as the energy transformation from mechanical to thermal is not taken into account.
- In total, the overall rational exergy efficiency was calculated to be 0.28. The main component of this comes from the physical exergy of the desired components. If the focus is shifted to the chemical exergy, the efficiency drops to 0.071.

Improvements that were recommended in the study were:

- Increasing the polytropic efficiency of the main air compressor from 0.7 to 0.85 which will reduce power consumption by 880kW. This saves the steam turbine 139kW. If the nitrogen compressor in the liquefaction unit has its polytropic efficiency increased from 0.75 to 0.85, the steam turbine saves a further 108kW. The rational exergy efficiencies of both compressors go up to 0.77.
- Further savings could be made by changing the operating pressures in the distillation columns. If the lower column operates at slightly below atmospheric pressure and the upper column at atmospheric pressure, exergy loss is reduced. If the products could be compressed to

environmental pressure, 400kW of exergy could be saved, though this causes a 15K temperature difference in the columns which offsets the saving and purity of products may be compromised.

3 Theory

3.1 Bond Equivalent Diagram

In order to analyze the full effects of the processes to be considered, it is necessary to develop the comparative processes that will eventually be considered in the exergy analysis. This will eventually help with the process simulation and develop the mass and energy balance and lead to the exergy analysis.

What follows is a brief description of each of the UCG-related systems that will be used. It is important to note that these are simple process flow diagrams in order to get a generic idea of what will be entailed in the simulation. The process complexities will be noted and developed later on.

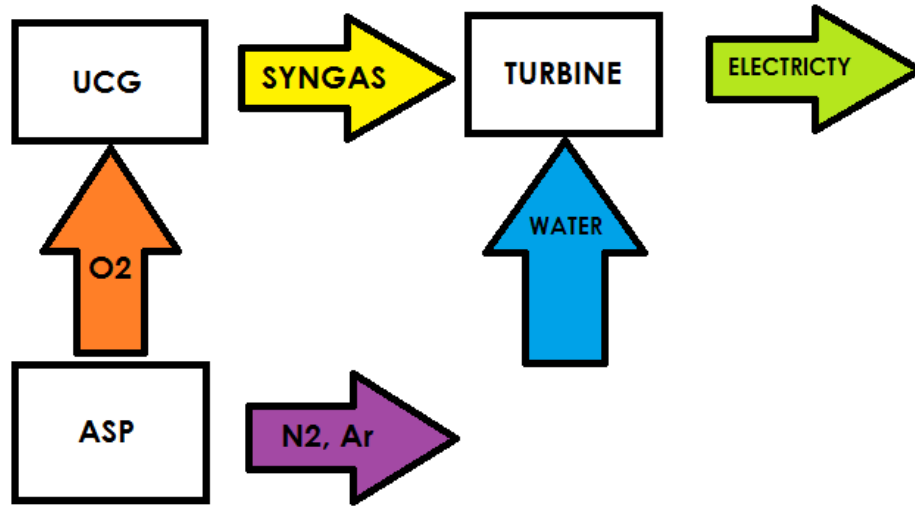


Figure 10: Pure O₂ process flow diagram

Figure 10 above represents the process flow diagram that incorporates oxygen from an air separation unit into the UCG process. Gaseous oxygen is sent from the ASU to the main UCG process as an oxidant whilst nitrogen and argon are produced as by-products that can be kept for storage and sold separately for further commercial gain.

The oxygen is then reacted with the coal bed as part of the gasification process to produce syngas with a composition determined from the reactions listed in equations 1 to 7. Once cleaned of impurities, it is combusted to produce steam which will drive a turbine to produce electricity. Though the exergy study will assess the effectiveness of the process up until the turbine stage, electricity production mainly depends on the calorific value of the syngas and is not the main part of this research.

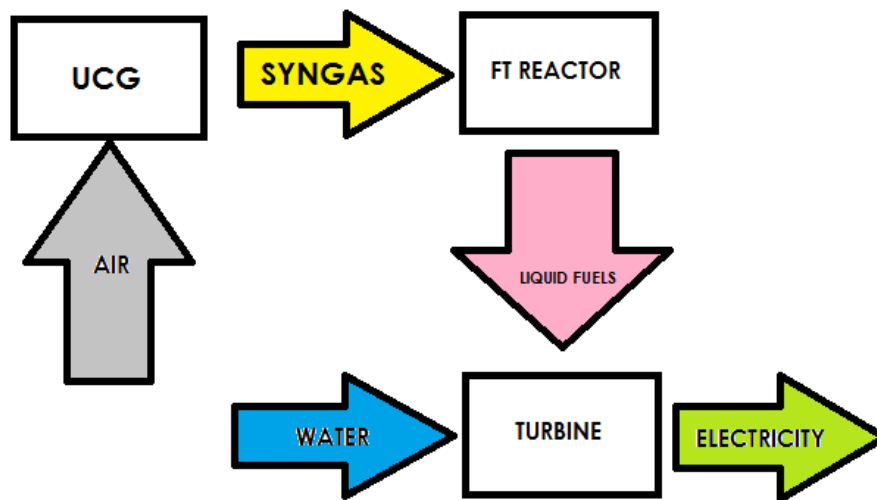


Figure 11: Air & FT conversion UCG process flow diagram

Figure 1 above represents the process flow diagram that incorporates air into the UCG process with downstream FTS conversion. Air is compressed and used as an oxidant in the gasification process that will produce syngas. Once cleaned, the syngas enters a catalytic FT reactor that converts to liquid hydrocarbons via the reactions expressed in equations 8 to 12. The liquid fuels are then combusted to produce steam which will drive a turbine to generate electricity. As with the pure oxygen process, this last step is not the main concern of this research as it is a function of calorific value rather than electricity.

In order to consider how the various systems interact with each other, it is useful to consider them on a bond equivalent diagram. This type of diagram shows the bonding capability of each element considered in the system (Pillay, 2013), in this case carbon, hydrogen and oxygen as these are the main elements in the UCG process. This process is useful as it not only shows how various systems interact with each other, but gives a theoretical insight into complex reaction schemes before design and operations can be taken into account

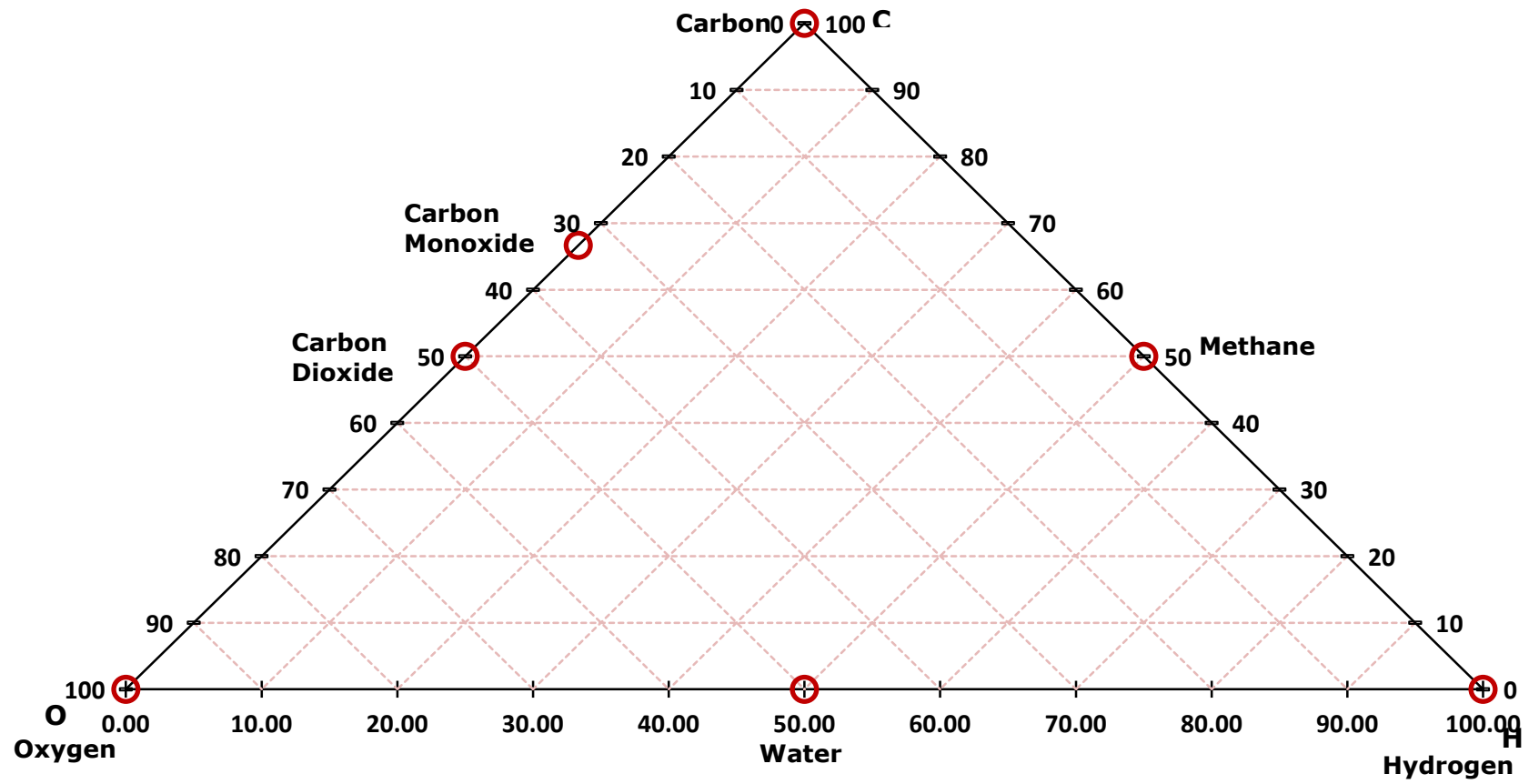


Figure 12: Bond equivalent diagram - basic CHO system (Pillay, 2013)

Figure 12 represents a basic CHO ternary system with the most basic compounds shown. Each apex of the triangle represents pure carbon, oxygen and hydrogen, whilst the gridlines represent the reactions that occur between the elements at a particular composition.

To plot a particular point on the diagram, the molar composition of a compound or mixture must be known in terms of the elements considered. Pillay (2013) states that the co-ordinates can be obtained by multiplying the molar fractions by the number of valence electrons of each element and dividing it by the overall total. These are represented by the next three equations:

$$C = \frac{4x_C}{4x_C + x_H + 2x_O} \quad (20)$$

$$H = \frac{x_H}{4x_C + x_H + 2x_O} \quad (21)$$

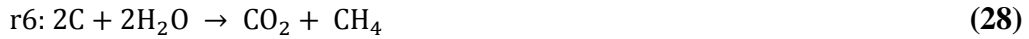
$$O = \frac{2x_O}{4x_C + x_H + 2x_O} \quad (22)$$

Whilst bond equivalent diagrams can quantify the aims and what reaction drivers of various CHO processes should be, it does not show how to reach the desired end goal. External factors such as production costs, process efficiencies and associated expenses & investments must be considered as decision tools.

3.2 Bond Equivalent Analysis of UCG

In order to fully consider UCG operations, one must first consider what reactions occur within the UCG system, a set of reactions must be defined. The following reactions form the basis for the considered reaction scheme as they do not produce feed material or consume products:





Each reaction is classified as either endothermic or exothermic based on the whether the heat of the reaction is positive or negative. Heat of reactions are influenced by the temperature and pressure of the system. In this case, ideal gas behaviour is assumed and the influence of system pressure is ignored. The heat of reaction is given by:

$$\Delta H_{rxn} = \sum n\Delta H_{products} - \sum m\Delta H_{reactants} \quad (29)$$

Where:

- ΔH_{rxn} is the heat of reaction in kJ
- $\sum n\Delta H_{products}$ is the sum of the product between the stoichiometric coefficients of the products and their respective heat of formations in kJ
- $\sum m\Delta H_{reactants}$ is the sum of the product between the stoichiometric coefficients of the reactants and their respective heat of formations in kJ

Table 10 below summarizes the heat of reactions at 1200K:

Table 10: Enthalpy of reactions at 1200K

Reaction	Enthalpy (kJ/mol)
r1	-110.4
r2	-394.1
r3	135
r4	96.6
r5	185.6
r6	12.2

As can be seen, only reaction r1 and r2 is classified as exothermic, whilst the rest are endothermic. When plotted, the reactions produce a polygon referred to as the stoichiometric region, in which operations are considered to operate as per the reaction scheme in relation to the coal feed and oxidant, without excess of either. The above information will help in determining the thermally balanced region, an

area on the BED (bond equivalent diagram) whereby no excess energy is added or lost by the system and is considered to be adiabatic. In this scenario, the exothermic reactions are balanced by the endothermic reactions. On the BED, this region is classified as a quadrant on the BED. In order to plot this area, ratios of the exothermic reactions must be added to reaction x so that the overall heat of reaction is zero. This yields the thermally balanced line without methanation and a thermally balanced region or polygon with methanation, upon which no energy is added or lost to a system and is classified as adiabatic, and ideally, most operations should occur here for the practicality of not having to add or take out energy out of the system.

Table 11 below represents the thermally balanced reactions and the linear combinations of the previously mentioned reactions:

Table 11: Thermally balanced reactions

	Reaction	Linear combination
A	$C + 0.275O_2 + 0.45H_2O \rightarrow CO + 0.45H_2$	$r1 + 0.818r3$
B	$C + 0.197O_2 + 1.606H_2O \rightarrow CO_2 + 1.606H_2$	$r2 + 0.64r4$
C	$C + 0.18O_2 + 0.427H_2O \rightarrow 0.786CO + 0.214CH_4$	$r1 + 0.595r5$
D	$C + 0.015O_2 + 0.985H_2O \rightarrow 0.508CO_2 + 0.492CH_4$	$r2 + 0.031r6$

If a system operates above the line or region, it is considered to be endothermic and needs external energy. The reverse is true if the system is found below the line or region.

Section 4.1 will better represent the UCG operations (coal and syngas) at the Chinchilla, Rocky Mountain and Hoe Creek sites as well as a laboratory gasification study.

3.3 Exergy Analysis

In order to fully compare and determine an optimal UCG process in terms of work efficiency, two processes will be simulated in order to compare oxidant choice.

The first process will be air-blown UCG coupled with downstream traditional Fischer-Tropsch synthesis to produce petrol. The second process will couple an

air separation unit to produce oxygen for downstream UCG. Each of the processes was modelled using the ASPEN simulation software, with the exergy calculated as per section 2.4.2.

3.3.1 General Assumptions

- The exergy quantification in equation 14, similar to the traditional energy balance, is simplified in the calculations to include only the chemical and physical exergy terms:

$$\dot{E} = E_{phys} + E_{chem} \quad (30)$$

- For ease of calculations, the following assumptions were made:
 - Instead of coal, carbon (in graphite form was used) to make the UCG reaction scheme easier
 - Air has been simulated to contain 79% nitrogen and 21% oxygen only
 - It is assumed that all carbon entering the reactor is used in the UCG reaction scheme defined in equations
 - The UCG reaction scheme has been defined as per equations 35 to 40 with the following conversions assumed and an empirical coal formula replacing the pure carbon and balancing out the rest of the equation:
 - R1: 0.412
 - R2: 0.111
 - R3: 0.331
 - R4: 0.095
 - R5: 0.051
 - R6: 0
 - Water vapour is combined with the carbon to simulate a coal stream. The water vapour amount is stoichiometric, based on the

reactions set above, so the ratios of carbon to water in both simulations are the same.

- It is assumed that no pressure drops occur across the system unless specified by a particular piece of equipment.

4 Results & Discussion

4.1 Bond Equivalent Diagram Analysis

The following subsections represent the analysis of historical UCG operations in terms of the BED. As stated previously, the diagram offers insight into complex reaction schemes in carbon-hydrogen-oxygen processes and helps determine whether an operation is endothermic or exothermic. Processes can thus be optimized by maintaining parameters such that the system neither requires nor produces excess energy.

4.1.1 Hoe Creek

Hoe Creek, Wyoming is the first operation that will be analyzed and interpreted using the BED. Relevant data for calculations involve the coal and product gas compositions and a set reaction scheme.

The following data represents the Hoe Creek system obtained from experiments performed and monitored by Thorsness, Hill & Stephens (1977). The purpose of this experiment was to create a commercially viable UCG process by using explosives to fracture the coal and increase gas permeability throughout the seam.

Table 12 below represents the Hoe Creek coal composition:

Table 12: Ultimate analysis of Hoe Creek coal as received (adapted from Thorsness *et al*, 1977)

Hoe Creek coal	
Carbon	66.96
Hydrogen	4.99
Nitrogen	1.28
Chlorine	0.08
Sulphur	0.88
Ash	9.00
Oxygen	16.87

By converting the ultimate analysis to mol %, the empirical coal chemical formula was found – $\text{CH}_{0.45}\text{O}_{0.033}$. By using the calorific value specified in Thorsness *et*

al, the heat of formation of the coal was found (-94.552kJ/mol). This will be needed later to calculate the heats of reactions.

The following table represents the UCG product gas from the Hoe Creek operations:

Table 13: Hoe Creek gas composition (mol%, adapted from Thorsness *et al*, 1977)

Hoe Creek gas	
Water	30.4
Nitrogen	38.1
Hydrogen	11.9
Carbon monoxide	6.1
Carbon dioxide	11
Methane	1.1
Tar	1.4

The next step of plotting the operations on the BED is to define the reaction scheme. The set of reactions not only show how the different pathways interact with each other, but also helps determine whether the system is exothermic or endothermic. The following reaction scheme (which will be used in the subsequent analyses of all other operations) is adapted from reactions 23 to 28, with the coal empirical formula inserted in place for pure carbon.

Table 14: Table of balanced reaction scheme for Hoe Creek coal

No.	Reaction	Heat of reaction (kJ/mol)
r1	$\text{CH}_{0.45}\text{O}_{0.033} + 0.4835\text{O}_2 \rightarrow \text{CO} + 0.225\text{H}_2$	-15.85
r2	$\text{CH}_{0.45}\text{O}_{0.033} + 0.9835\text{O}_2 \rightarrow \text{CO}_2 + 0.225\text{H}_2$	-299.55
r3	$\text{CH}_{0.45}\text{O}_{0.033} + 0.967\text{H}_2\text{O} \rightarrow \text{CO} + 1.192\text{H}_2$	260.52
r4	$\text{CH}_{0.45}\text{O}_{0.033} + 1.967\text{H}_2\text{O} \rightarrow \text{CO}_2 + 2.192\text{H}_2$	262.62
r5	$\text{CH}_{0.45}\text{O}_{0.033} + 0.57\text{H}_2\text{O} \rightarrow 0.397\text{CH}_4 + 0.603\text{CO}$	357.24
r6	$\text{CH}_{0.45}\text{O}_{0.033} + 0.871\text{H}_2\text{O} \rightarrow 0.548\text{CH}_4 + 0.452\text{CO}_2$	153.69

As can be seen, R1 and R2 are exothermic, whilst all other reactions are endothermic. In order to find the TBL (thermally balanced line), these reactions must be paired and balanced. R1 & R3 and R2 & R4 are paired up as they produce the same products. For the methanation reactions to be considered, R1 is

paired with R5 and R2 with R6. The balanced reactions and the resulting BED can be seen below:

Table 15: Thermally balanced reactions for Hoe Creek coal

No.	Reaction	Combination
A	$17.4\text{CH}_{0.45}\text{O}_{0.033} + 7.9294\text{O}_2 + 0.967\text{H}_2\text{O} \rightarrow 17.4\text{CO} + 4.882\text{H}_2$	16.4r1 + r3
B	$2.1\text{CH}_{0.45}\text{O}_{0.033} + 0.9835\text{O}_2 + 2.1637\text{H}_2\text{O} \rightarrow 2.1\text{CO}_2 + 2.6362\text{H}_2$	r2 + 1.1r4
C	$10.9\text{CH}_{0.45}\text{O}_{0.033} + 4.78665\text{O}_2 + 0.57\text{H}_2\text{O} \rightarrow 10.503\text{CO} + 2.2275\text{H}_2 + 0.397\text{CH}_4$	9.9r1 + r5
D	$3.5\text{CH}_{0.45}\text{O}_{0.033} + 0.9835\text{O}_2 + 2.1775\text{H}_2\text{O} \rightarrow 2.13\text{CO}_2 + 0.225\text{H}_2 + 1.37\text{CH}_4$	r2 + 2.5r6

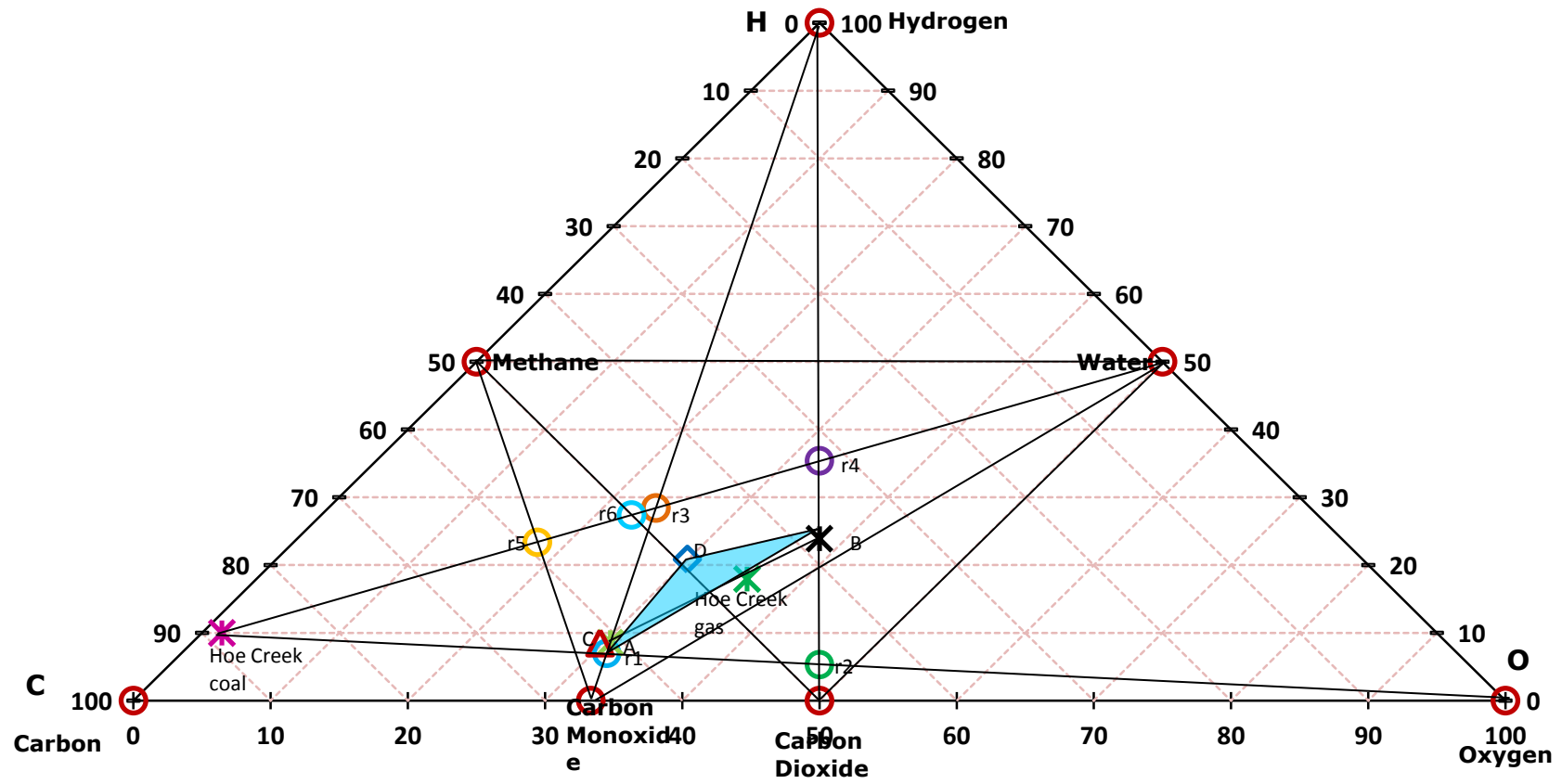


Figure 13: BED of Hoe Creek coal and syngas (adapted from Thorsness *et al*, 1979 - dry basis)

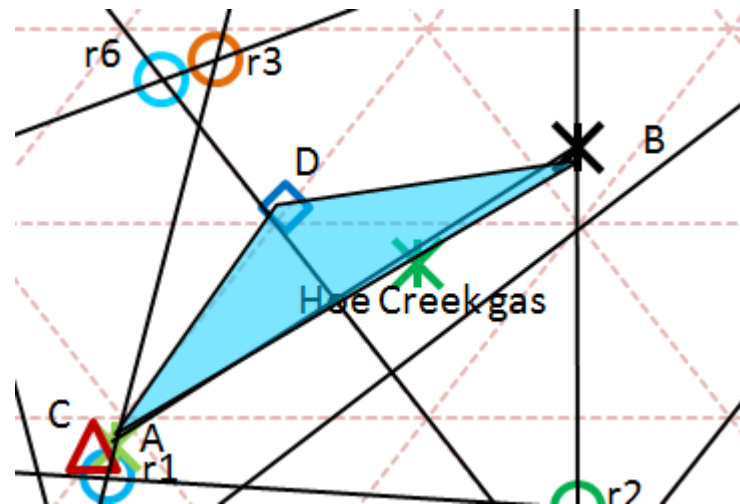


Figure 14: Closeup of Hoe Creek thermally balanced region

The gas was plotted without water and nitrogen so as to compare it to the Chinchilla and Rocky Mountain operations, both of which were given without moisture content.

Balanced reaction A lies extremely close to r3, which represents the hydrogen-carbon monoxide reaction. This is due to the ratio of C:H:O in the balanced reaction, which is similar to that of r3. The relatively small magnitude of r1's heat of reaction compared to that of r3 is also a contributing factor and is this responsible for the high ratio that is needed to add up to A.

The syngas composition was plotted without moisture. The point lies under the thermally balanced region (which is generated by balancing the methanation reactions with the exothermic ones to give a region instead of a line), indicating that the process is exothermic overall and thus produces heat. Since this operation used air as oxidant, there is a significant amount of inert nitrogen contained within the operation. Air operations are difficult to operate in the sense that if the air flow rate is not properly controlled, the inert nitrogen may cause the coal ignition in the seam to slow down and eventually stop. Of interest, Thorsness *et al* notes that doubling the air flow rate or the noted water influx into the gasification seam does not cause a significant change in the product gas composition. Surprisingly, there is a considerable amount of hydrogen contained in the syngas for an air operation, which may be attributed to the initial moisture content of the coal (29.2% by weight).

4.1.2 Chinchilla

Chinchilla coal data was obtained from the Queensland Department of Mines and Energy publication of the use of Walloon coals (subbituminous) for power generation. Though analysis for coal was recorded for both as received and dry and ash free scenarios, the product gas was only reported in Kačur *et al* (2014) as moisture free. For this reason, the Chinchilla points are plotted as dry only, as seen by the tables below.

Table 16: Ultimate analysis of Chinchilla coal, dry and ash free (adapted from Queensland Department of Mines and Energy, 1999)

Chinchilla coal	
Carbon	80.2
Hydrogen	6
Nitrogen	1.5
Sulphur	0.7
Oxygen	11.6

Table 17: Molar composition of syngas from Chinchilla (adapted from Kacur et al 2014)

Components	Chinchilla value (%)
Nitrogen	43
Hydrogen	22
Carbon monoxide	7
Carbon dioxide	19
Methane	8

Using the same method as Hoe Creek, the chemical formula for Chinchilla's coal is $\text{CH}_{0.45}\text{O}_{0.054}$, with the heat of formation being -151.93kJ/mol .

The following tables represent the reaction set used to define the Chinchilla operation and the balanced reactions from the ratio of endothermic to exothermic heats of reactions:

Table 18: Balanced reaction scheme for Chinchilla coal

No.	Reaction	Heat of reaction (kJ/mol)
r1	$\text{CH}_{0.45}\text{O}_{0.054} + 0.473\text{O}_2 \rightarrow \text{CO} + 0.225\text{H}_2$	41.53
r2	$\text{CH}_{0.45}\text{O}_{0.054} + 0.973\text{O}_2 \rightarrow \text{CO}_2 + 0.225\text{H}_2$	-242.17
r3	$\text{CH}_{0.45}\text{O}_{0.054} + 0.946\text{H}_2\text{O} \rightarrow \text{CO} + 1.171\text{H}_2$	311.90
r4	$\text{CH}_{0.45}\text{O}_{0.054} + 1.946\text{H}_2\text{O} \rightarrow \text{CO}_2 + 2.171\text{H}_2$	314.00
r5	$\text{CH}_{0.45}\text{O}_{0.054} + 0.556\text{H}_2\text{O} \rightarrow 0.39\text{CH}_4 + 0.61\text{CO}$	210.61
r6	$\text{CH}_{0.45}\text{O}_{0.054} + 0.8605\text{H}_2\text{O} \rightarrow 0.54275\text{CH}_4 + 0.45725\text{CO}_2$	268.45

Table 19: Thermally balanced reactions for Chinchilla coal

No.	Reaction	Combination
A	$1.2\text{CH}_{0.45}\text{O}_{0.054} + 0.6676\text{O}_2 \rightarrow \text{CO} + 0.2\text{CO}_2 + 0.27\text{H}_2$	r1 + 0.25r2
B	$2.3\text{CH}_{0.45}\text{O}_{0.054} + 1.2649\text{O}_2 + 0.946\text{H}_2\text{O} \rightarrow 1.3\text{CO}_2 + \text{CO} + 1.4635\text{H}_2$	r3 + 1.3r2
C	$2.3\text{CH}_{0.45}\text{O}_{0.054} + 1.946\text{H}_2\text{O} + 1.2649\text{O}_2 \rightarrow 2.3\text{CO}_2 + 2.4635\text{H}_2$	r4 + 1.3r2
D	$1.87\text{CH}_{0.45}\text{O}_{0.054} + 0.556\text{H}_2\text{O} + 0.84651\text{O}_2 \rightarrow 0.39\text{CH}_4 + 0.9\text{CO}_2 + 0.61\text{CO} + 0.19575\text{H}_2$	r5 + 0.9r2
E	$1.9\text{CH}_{0.45}\text{O}_{0.054} + 0.8757\text{O}_2 + 0.8605\text{H}_2\text{O} \rightarrow 1.35725\text{CO}_2 + 0.54725\text{CH}_4 + 0.2025\text{H}_2$	r6 + 0.9r2

Compared to Hoe Creek, Chinchilla's only exothermic reaction is r2. This is due it being the main carbon dioxide production reaction, which is normally an extremely exothermic reaction. When coupled with the rest of the reactions, r2 produces the reactions seen in table 19. The following diagram represents the BED for the Chinchilla:

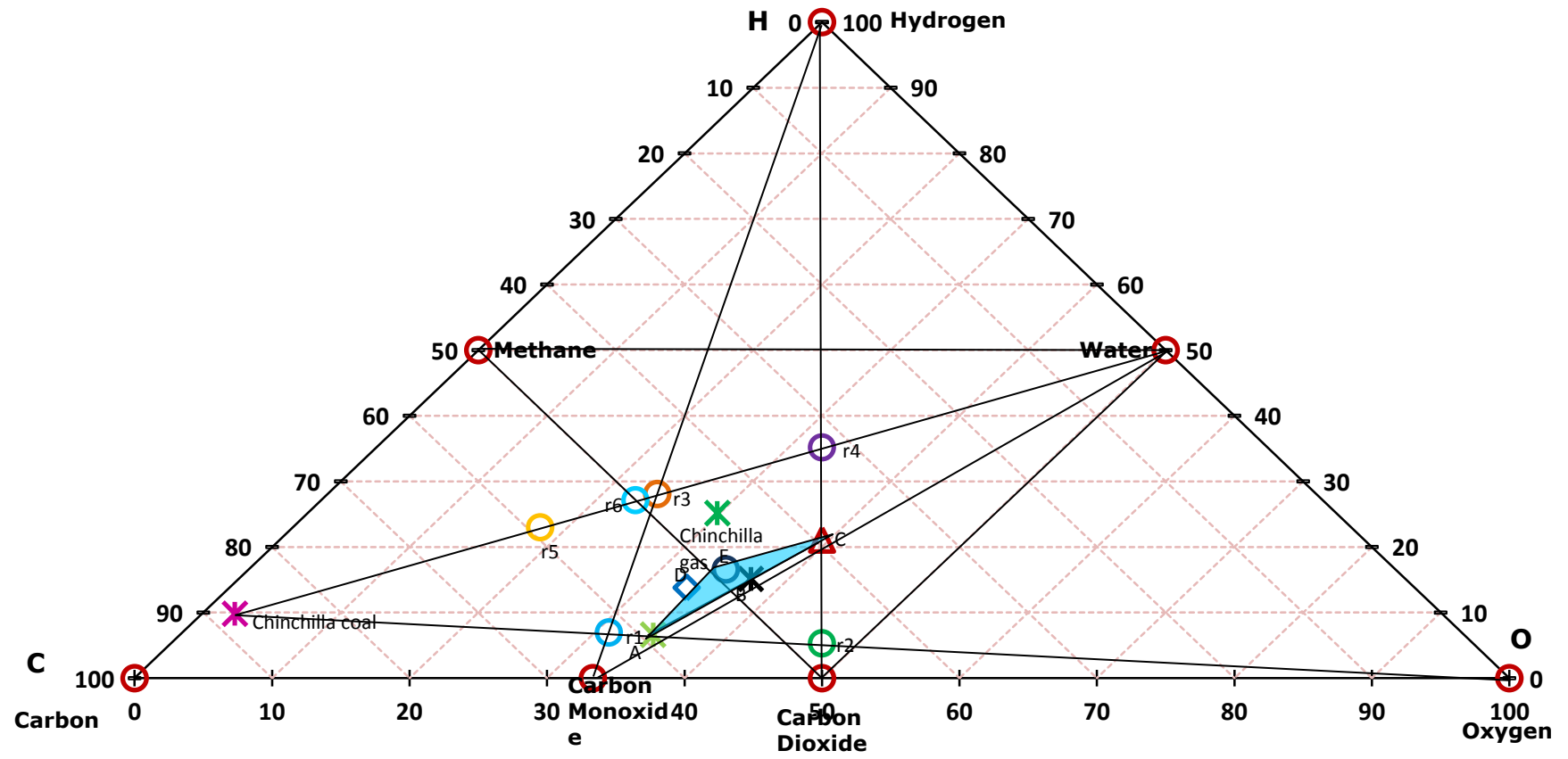


Figure 15: BED of Chinchilla coal and syngas

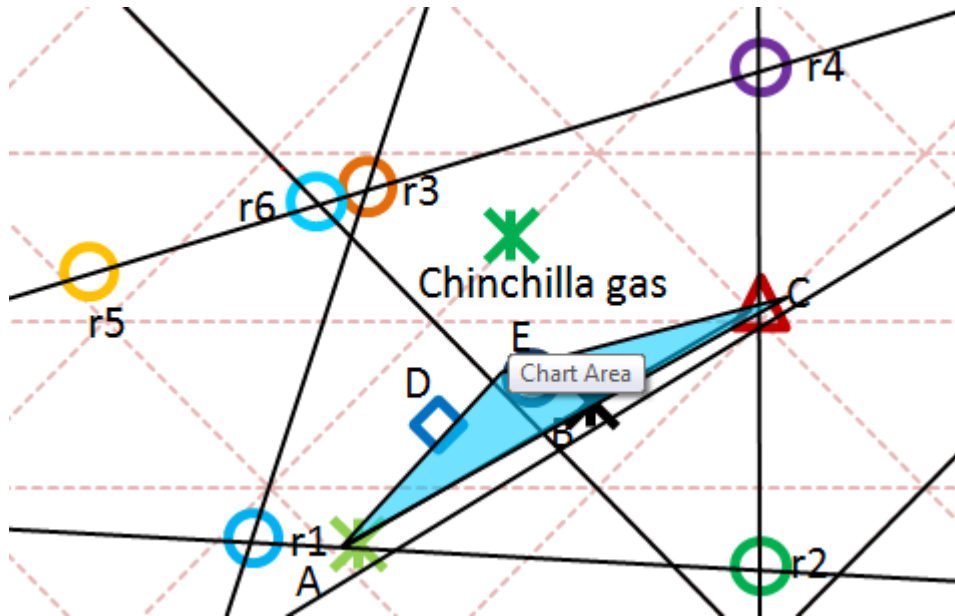


Figure 16: Chinchilla thermally balanced region close-up

Chinchilla offers an interesting perspective by producing a thermally balanced region (in a triangular form) instead of a line, running through reactions A, B and C with the methanation reactions D and E lying close to the line. Unlike Hoe Creek, the Chinchilla syngas comes out above the thermally balanced region, indicating the operations are endothermic overall. This indicates that work must be added to the system, most likely in the form of heating the air stream before sending it underground through the coal seam. Practically, this would require additional energy expenses contained within the operating costs.

As with Hoe Creek, Chinchilla's syngas contains a significant amount of nitrogen, which could lower the seam temperature and stop the ignition if not carefully controlled. As with Chinchilla, there is a significant amount of hydrogen produced, roughly equal to the amount of carbon dioxide. Both air blown operations contain an ideal ratio of hydrogen to carbon monoxide for FTS to produce liquid hydrocarbons from the product gas. Chinchilla contains approximately eight times more methane than Hoe Creek, thus making it the likely factor as to why the syngas lies above the TBL. If the thermally balanced region is expanded to include the methanation reactions, Chinchilla still lies far above it, thus confirming its endothermic status.

4.1.3 Rocky Mountain

The Rocky Mountain, like Chinchilla, site uses subbituminous coal for UCG, which can easily be seen by the similar composition both on the BED and the table below. The chemical formula for this coal is $\text{CH}_{0.41}\text{O}_{0.08}$ and its heat of formation is -165.2kJ/mol . Tables 20 and 21 below detail the coal's ultimate analysis and syngas composition respectively.

Table 20: Ultimate analysis of Rocky Mountain coal, dry (adapted from National Energy Technology Laboratory, 2012)

Rocky Mountain coal	
Carbon	67.45
Hydrogen	4.56
Nitrogen	0.96
Sulphur	0.98
Chlorine	0.01
Ash	11.03
Oxygen	15.01

Table 21: Rocky Mountain syngas molar composition (adapted from Dennis, 2006)

Rocky Mountain Gas		
Component	ELW	CRIP
Hydrogen	32.7	39.6
Methane	10.1	10.3
Carbon monoxide	8.2	11.9
Carbon dioxide	45.7	35.3
Hydrogen sulphide	0.8	0.6
Nitrogen	0.5	0.5
Argon	0.2	0.1
Higher hydrocarbons	1.8	1.7

The final technical report on the site (Dennis, 2006) tested two technologies, both using a combination of steam and oxygen as oxidants. The report details the dry gas composition for extended well linking (ELW) and controlled retracting injection point (CRIP) operations. The ELW site had a steam to oxygen ratio of approximately 1.88 (83716:44461 MSCF) and the CRIP site a ratio of approximately 2.04 (176904:86650 MSCF).

Table 22 and 23 represent the reaction scheme adapted for the Rocky Mountain coal and the balanced reactions respectively.

Table 22: Balanced reactions for Rocky Mountain coal

No.	Reaction	Heat of reaction (kJ/mol)
r1	$\text{CH}_{0.41}\text{O}_{0.08} + 0.46\text{O}_2 \rightarrow \text{CO} + 0.205\text{H}_2$	54.80
r2	$\text{CH}_{0.41}\text{O}_{0.08} + 0.96\text{O}_2 \rightarrow \text{CO}_2 + 0.205\text{H}_2$	-228.90
r3	$\text{CH}_{0.41}\text{O}_{0.08} + 0.92\text{H}_2\text{O} \rightarrow \text{CO} + 1.125\text{H}_2$	277.27
r4	$\text{CH}_{0.41}\text{O}_{0.08} + 1.92\text{H}_2\text{O} \rightarrow \text{CO}_2 + 2.125\text{H}_2$	235.29
r5	$\text{CH}_{0.41}\text{O}_{0.08} + 0.545\text{H}_2\text{O} \rightarrow 0.375\text{CH}_4 + 0.625\text{CO}$	199.92
r6	$\text{CH}_{0.41}\text{O}_{0.08} + 0.8575\text{H}_2\text{O} \rightarrow 0.53125\text{CH}_4 + 0.46875\text{CO}_2$	148.05

Table 23: Thermally balanced reactions for Rocky Mountain coal

No.	Reaction	Combination
A	$\text{CH}_{0.41}\text{O}_{0.08} + 0.55658\text{O}_2 \rightarrow 0.806838\text{CO} + 0.19316\text{CO}_2 + 0.806838\text{H}_2$	r1 + 0.2r2
B	$\text{CH}_{0.41}\text{O}_{0.08} + 0.416\text{H}_2\text{O} + 0.52588\text{O}_2 \rightarrow 0.4522\text{CO} + 0.5478\text{CO}_2 + 0.621\text{H}_2$	r3 + 1.2r2
C	$\text{CH}_{0.41}\text{O}_{0.08} + 0.94656\text{H}_2\text{O} + 0.4867\text{O}_2 \rightarrow \text{CO}_2 + 1.15157\text{H}_2$	r4 + 1.02r2
D	$\text{CH}_{0.41}\text{O}_{0.08} + 0.4476\text{O}_2 + 0.2909\text{H}_2\text{O} \rightarrow 0.2\text{CH}_4 + 0.466\text{CO}_2 + 0.334\text{CO} + 0.09557\text{H}_2$	r5 + 0.87r2
E	$\text{CH}_{0.41}\text{O}_{0.08} + 0.5207\text{H}_2\text{O} + 0.377\text{O}_2 \rightarrow 0.677\text{CO}_2 + 0.0805\text{H}_2 + 0.3225\text{CH}_4$	r6 + 0.65r2

As with Chinchilla, the only exothermic reaction in the system is R2 at 650K. This was balanced with the rest of the reactions to find the TBL for this mine.

Figure 17 represents the BED for Rocky Mountain:

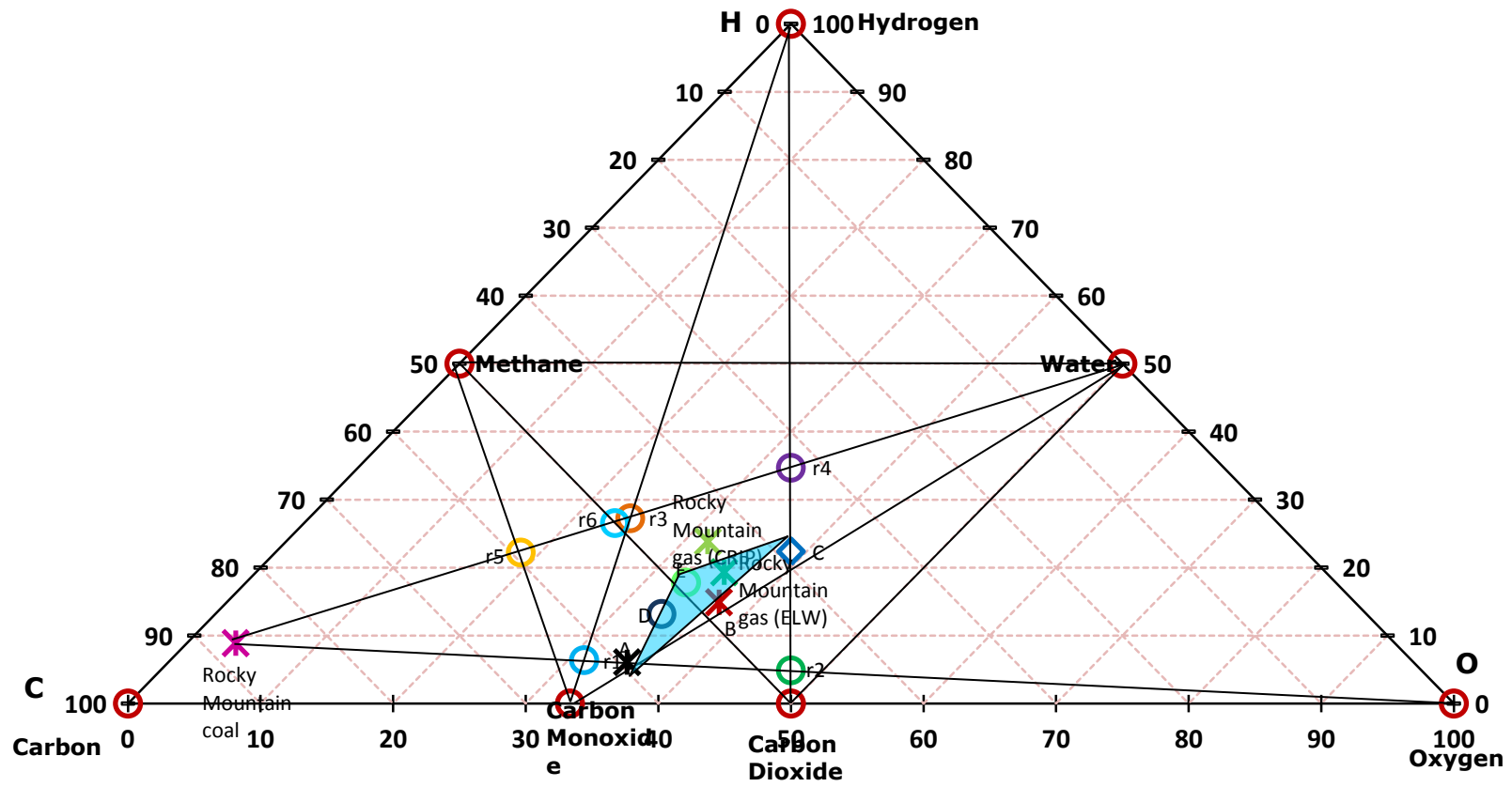


Figure 17: BED for Rocky Mountain coal and syngas

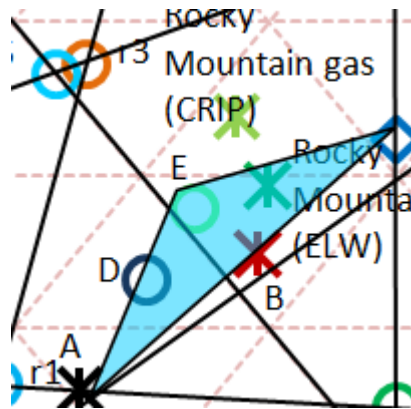


Figure 18: Rocky Mountain thermally balanced region close-up

Like Chinchilla, Rocky Mountain produces a thermally balanced region in the shape of a triangle. The two distinct syngas production methods present an appealing scenario.

The CRIP method lies above the region, similar to Chinchilla, meaning that this particular process is overall endothermic and requires energy input. The ELW method lies within the thermally balanced region, meaning that the process neither requires or produces excess energy. All gaseous products are at the same temperature as the reactants, meaning that no unnecessary energy costs will occur. If one looks at the composition of the two gas processes, the CRIP method contains a higher hydrogen content (in both the elemental gas and methane), thus pushing it above TBL boundary. It can be concluded that a higher energy (heat) input is required for more hydrogen to occur in the final gas. This is an indication that there is a cycle performed to increase the seam's temperature by first using an oxygen-rich oxidant followed by gasification.

When compared to the air blown processes, Rocky Mountain contains the most methane and hydrogen in its syngas. This is expected as UCG operations that use oxygen, as a gasifying agent, produce a syngas that has a higher calorific value than those that use air. The significant hydrogen and methane in both Rocky Mountain technologies contribute to this. There is also a higher carbon dioxide content in both gases, particularly in ELW. Oxygen-blown sites produce a higher temperature in the coal seam, thus allowing for complete combustion of the

carbon content to produce CO₂ rather than the partial combustion mechanism to produce CO.

4.1.4 Laboratory Gasification Study

A series of laboratory scale experiments performed by Prabu & Jayanti (2012) in a study to simulate UCG on high-ash content coals for carbon-neutral power generation. Using coal from a thermal power station in Chennai, India and acacia wood as a comparison, several sets of experiments were done in air and oxygen environments to ascertain product composition. The ultimate analysis of the coal and the product gas were reported without moisture.

Table 24: Ultimate analysis of laboratory in coal (adapted from Prabu & Jayanti, 2012)

Component	C	H	O	N	S
Coal 2	77.41	6.96	14.99	0.142	0.5

Table 25: Molar syngas composition of UCG experiment (Prabu & Jayanti, 2012)

Component	Coal 2 (air)	Coal 2 (oxygen)
Hydrogen	4.8	9.66
Carbon monoxide	2.92	29.47
Oxygen	13.96	15.54
Methane	4.19	6.84
Carbon dioxide	14.5	38.48
Nitrogen	59.63	-

Coal 2 was used in both air and oxygen runs. The air run was interrupted every two hours to record the coal sample's cavity shape. The air flow rate used was 3.5L/min, which accounts for the excess nitrogen and oxygen in the product gas, though there is a relatively low amount of carbon dioxide in the feed. The low amount of carbon suggests that not all the carbon was reacted due to the interruptive nature of the experiment.

Tables 26 and 27 below represent the reaction scheme for the laboratory coal ($\text{CH}_{0.54}\text{O}_{0.07}$, -180.85kJ/mol) as well as the balanced reactions for the TBL:

Table 26: Balanced reaction scheme for lab coal

No.	Reaction	Heat of reaction (kJ/mol)
r1	$\text{CH}_{0.54}\text{O}_{0.07} + 0.465\text{O}_2 \rightarrow \text{CO} + 0.27\text{H}_2$	70.45
r2	$\text{CH}_{0.54}\text{O}_{0.07} + 0.965\text{O}_2 \rightarrow \text{CO}_2 + 0.27\text{H}_2$	-213.25
r3	$\text{CH}_{0.54}\text{O}_{0.07} + 0.93\text{H}_2\text{O} \rightarrow \text{CO} + 1.2\text{H}_2$	336.24
r4	$\text{CH}_{0.54}\text{O}_{0.07} + 1.93\text{H}_2\text{O} \rightarrow \text{CO}_2 + 2.2\text{H}_2$	338.34
r5	$\text{CH}_{0.54}\text{O}_{0.07} + 0.53\text{H}_2\text{O} \rightarrow 0.6\text{CO} + 0.4\text{CH}_4$	232.36
r6	$\text{CH}_{0.54}\text{O}_{0.07} + 0.83\text{H}_2\text{O} \rightarrow 0.45\text{CO}_2 + 0.55\text{CH}_4$	202.21

Table 27: Thermally balanced reactions

No.	Reaction	Combination
A	$1.3\text{CH}_{0.54}\text{O}_{0.07} + 0.7545\text{O}_2 \rightarrow \text{CO} + 0.3\text{CO}_2 + 0.351\text{H}_2$	r1 + 0.3r2
B	$2.6\text{CH}_{0.54}\text{O}_{0.07} + 0.93\text{H}_2\text{O} + 1.544\text{O}_2 \rightarrow \text{CO} + 1.6\text{CO}_2 + 1.632\text{H}_2$	r3 + 1.6r2
C	$2.6\text{CH}_{0.54}\text{O}_{0.07} + 1.93\text{H}_2\text{O} + 1.544\text{O}_2 \rightarrow 2.6\text{CO}_2 + 2.632\text{H}_2$	r4 + 1.6r2
D	$2.1\text{CH}_{0.54}\text{O}_{0.07} + 0.53\text{H}_2\text{O} + 1.0615\text{O}_2 \rightarrow 0.6\text{CO} + 1.1\text{CO}_2 + 0.4\text{CH}_4 + 0.297\text{H}_2$	r5 + 1.1r2
E	$1.9\text{CH}_{0.54}\text{O}_{0.07} + 0.8575\text{H}_2\text{O} + 0.8685\text{O}_2 \rightarrow 1.36875\text{CO}_2 + 0.53125\text{CH}_4 + 0.243\text{H}_2$	r6 + 0.9r2

Figure 19 represents the BED for the laboratory study:

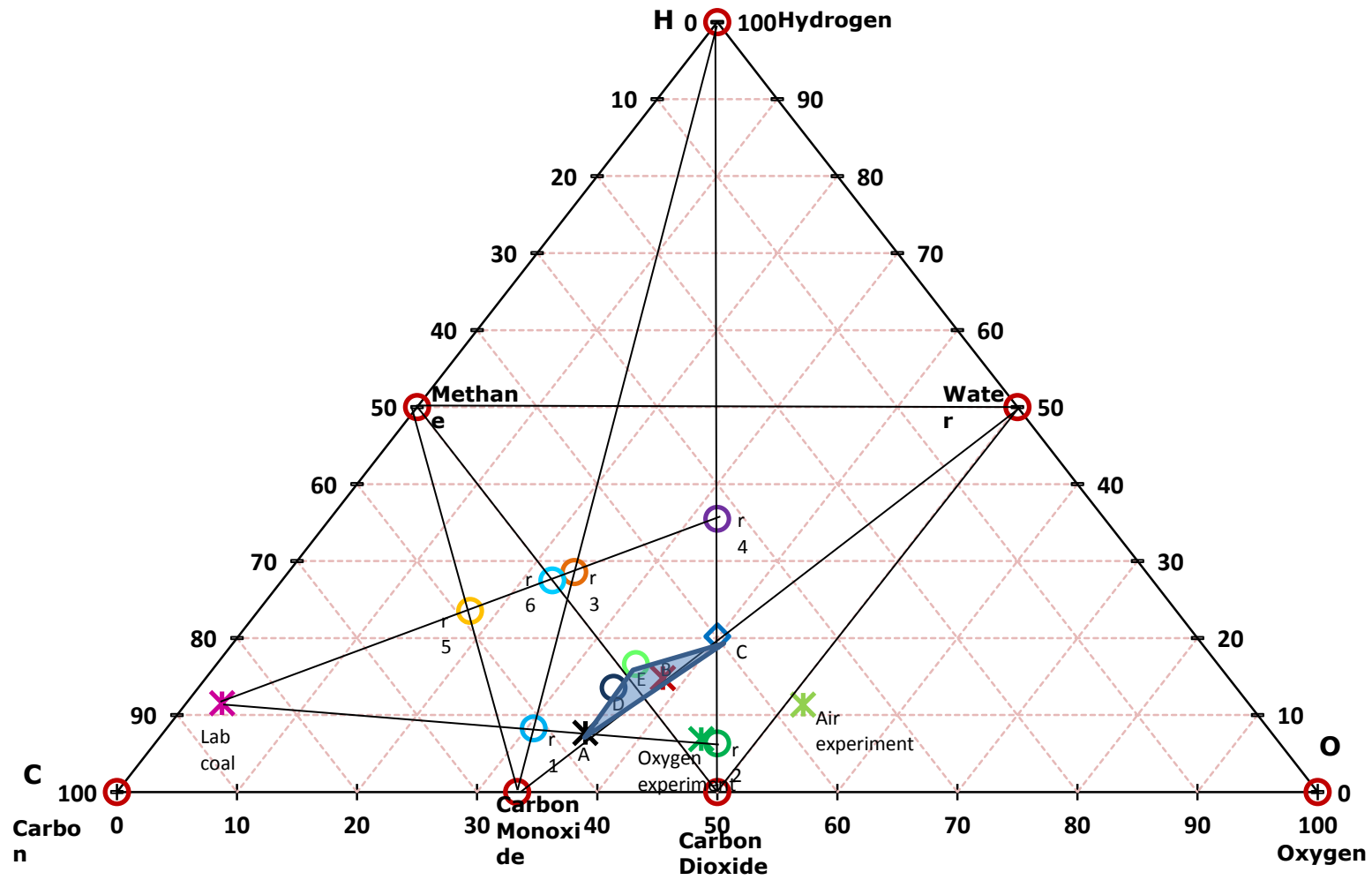


Figure 19: BED for lab study coal and syngas

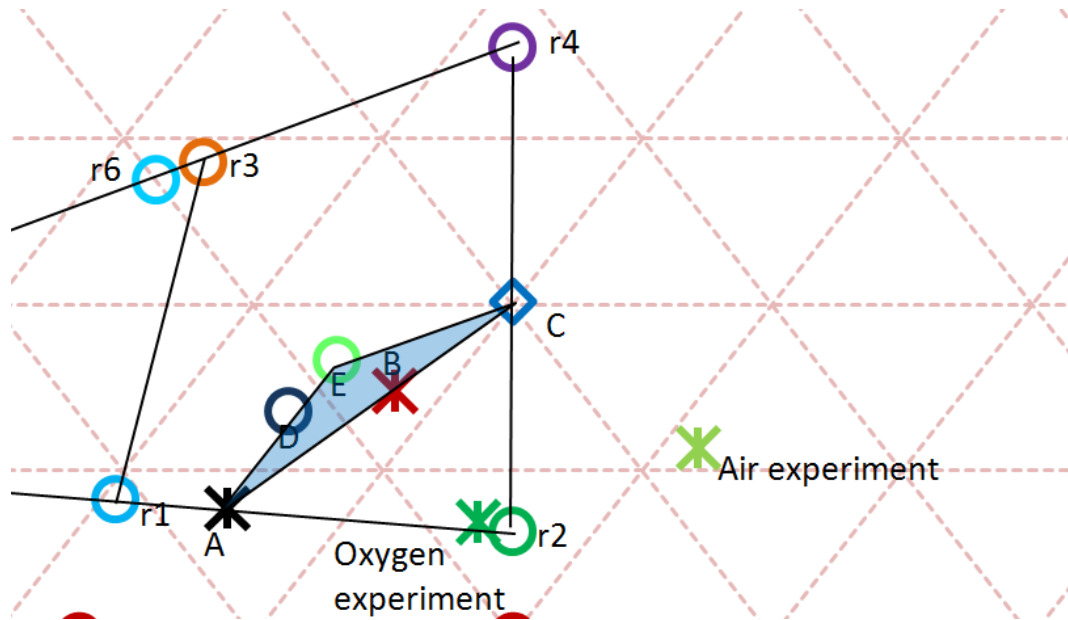


Figure 20: Laboratory study thermally balanced region close-up

As can be noted, the air experiment lies beyond the water-carbon dioxide line due to the significant presence of oxygen in the syngas. This can be attributed to the interrupted nature of the experiment and not allowing the entire coal sample to be gasified. As expected, the oxygen experiment lies underneath the thermally balanced region/triangle within the stoichiometric region, thus indicating that this process is an exothermic one.

4.1.5 Comparative BED Discussion

When comparing the air blown operations, it can be noted that each of the diagrams produce different scenarios:

- Hoe Creek production lies below its TBL, indicating exothermic operations
- Chinchilla lies above the thermally balanced region, indicating endothermic operation
- The laboratory air study produces gas that does not lie within the stoichiometric quadrant

Due to the interrupted nature of the laboratory study it can be considered to be an outlier compared to Hoe Creek and Chinchilla. Both contain a significant amount

of nitrogen from using air as an oxidant, which as stated previously, can cause the ignition within the coal seam to die off if not controlled carefully. The following tables analyze the CHO component analysis (dry) and the dry gas composition for the two seams without nitrogen:

Table 28: Comparison of Hoe Creek & Chinchilla syngas composition (dry and without nitrogen)

Components	Chinchilla	Hoe Creek
Hydrogen	39.29	39.53
Carbon monoxide	12.5	20.27
Carbon dioxide	33.93	36.54
Methane	14.29	3.65

As can be seen, the hydrogen and carbon dioxide values are quite similar to each other. What differs is the carbon monoxide and methane content – Hoe Creek contains 7.8% more carbon monoxide, whilst Chinchilla contains 10.6% more methane. Though the inclusion of methane formation within the reaction scheme allows the TBL to become a region (i.e. it allows for flexible operations as the operating range for thermally balanced seams becomes bigger) , the formation of excess methane can thus be seen as a hindrance to the optimal thermal operations of the UCG seam as it absorbs energy that could be used for balancing endothermic reactions.

The following scenarios are present for the oxygen-blown scenarios:

- Rocky Mountain CRIP lies above the thermally balanced region, which indicates endothermic operations
- Rocky Mountain ELW lies within the thermally balanced region, indicating optimal thermal operations
- The laboratory study oxygen simulation lies under the thermally balanced region, indicating exothermic operations

The following table compares the above three situation in terms of their dry syngas composition:

Table 29: Oxygen-blown UCG operations comparison

Component	ELW	CRIP	Laboratory Study
Hydrogen	33.82	40.57	9.66
Methane	10.44	10.64	6.84
Carbon monoxide	8.48	12.3	29.47
Carbon dioxide	47.26	36.48	38.48
Oxygen	0	0	15.54

One of the noticeable comparisons that can be made is the carbon dioxide composition in each of the simulations. Whilst CRIP and the laboratory study contain similar values, the ELW contains approximately 9% more carbon dioxide. This is offset by the low carbon monoxide content when compared to the other two simulations.

Rocky Mountain makes use of steam and oxygen as oxidants. The ELW has a steam to oxygen ratio of 1.88, whilst the CRIP has a ratio of 2.04. One can conclude that the higher steam ratio is conducive to producing a higher hydrogen and carbon monoxide content while lowering the carbon dioxide amount. This is due to the higher steam content lowering the temperature of the seam, thus creating favourable conditions to produce hydrogen and carbon monoxide.

A significant variation also occurs within the hydrogen content, with the CRIP method containing the highest amount. The laboratory study has the lowest amount of hydrogen across the three, though it contains the highest amount of carbon monoxide. The laboratory study is the only study out of the three to contain excess oxygen, thus indicating that the syngas production was not stoichiometric. This would explain why position of the oxygen-blown syngas point on the laboratory BED is almost out of the stoichiometric region.

The oxygen-blown studies, on average when compared to their air-blown counterparts, contain more carbon dioxide and less carbon monoxide. Similar to Rocky Mountain's CRIP run, oxygen-blown UCG runs produce far higher temperatures than air-blown simulations, which are conducive to carbon dioxide formation due to the higher oxidant content.

It can thus be concluded that excessive methane formation within the syngas production can prove to push UCG operations out of the thermally balanced region and into the endothermic section of the stoichiometric quadrant, hence causing a deficiency of energy within the process. Excessive oxidant usage within a coal seam can push operations out of the stoichiometric region completely and is considered a waste for operations. Optimal UCG seams lies either on a thermally balanced line or within a thermally balanced region, though oxidant selection and composition of the product gas depends on the desired downstream processing.

4.2 Exergy Analysis

The previous section covered real-life UCG operations based on their reported coal and syngas compositions. By using the BED method, it is possible to obtain a conclusive view of how a particular operation is carried out and where the production operates from an energy perspective. From section 4.1, it is concluded that UCG is best carried out under balanced conditions from its reaction scheme to avoid an excess of energy or a lack thereof.

This section covers the exergy analysis. Exergy represents the ability of the system to do work based on its various properties. If a system or process has the ability to retain most of the exergy within its feed, it means that work losses are minimized and operations are carried out efficiently. By using the exergy analysis, it is possible to identify key losses across equipment and learn to minimize these through changing operating conditions, reaction schemes or considering alternative methods of performing the same action.

There are two options that can be considered for UCG operations:

- Using cryogenic air separation (distillation) to produce pure oxygen for syngas with a high calorific value that can be used for combustion
- Use air-blown UCG to produce syngas that is then reacted in FTS to produce syncrude with a high calorific value that can be used for combustion

This section aims to understand which option is better.

4.2.1 Air-Blown UCG & FTS

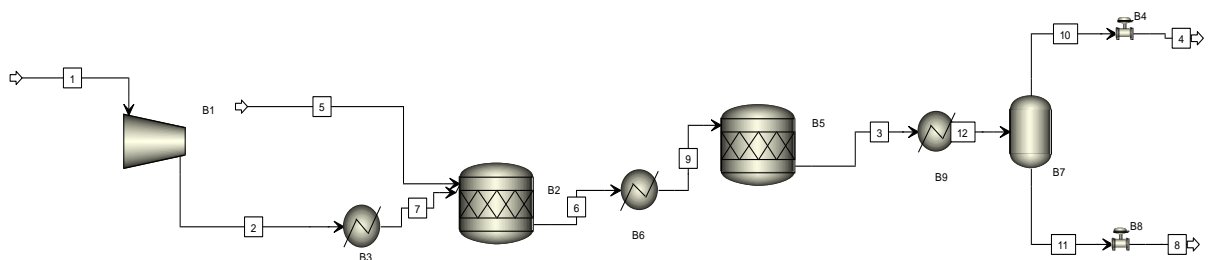


Figure 21: Air UCG-FTS simulation diagram

The above figure represents the process of an air-blown UCG system coupled with downstream FTS and separation. The system is divided into three specific parts – air compression, UCG reaction and FTS reaction.

Air is compressed in compressor B1 from ambient conditions (25°C, 1 atmosphere) to 15 atmospheres via a multistage compressor. From this, it is heated to 1200K in heater B3.

Carbon and water vapour from stream 5 (already at 1200K) combines with the heated air in the UCG reactor B2. The reaction scheme follows as per above and the product stream is then cooled to 220°C in cooler B6.

The stream is then reacted in the FT reactor B5 according to the traditional FT reaction to produce octane. This product stream is then cooled down to 298K in another cooler to liquefy the octane. The gas byproducts and inerts are separated from the liquid stream in separator B7.

Aside from the general assumptions mentioned earlier, the following process specific assumptions were made:

- The FTS reactor is assumed to operate via the traditional FTS reaction scheme
- Although capable of producing a wide product spectrum, the simulation only uses octane to represent the FTS product.
- Nitrogen is an inert within the system
- It is assumed that CO has a conversion of 0.955 to produce octane

The following results were obtained from the simulation.

Table 30: Main UCG & FTS simulation results

Component	FTS product stream	UCG product stream
Carbon	0.00	0.00
Oxygen	0.00	0.00
Nitrogen	0.61	0.44
Water	0.00	0.00
Carbon Monoxide	0.02	0.28
Carbon Dioxide	0.29	0.07
Methane	0.01	0.01
Hydrogen	0.05	0.19
Octane	0.02	0.00

Using the simulation data obtained (see Appendix B for full simulation data), it was possible to calculate the physical exergy using equation 15 for gases and equation 16 for solids and liquids. The enthalpy difference was calculated assuming the following equation:

$$\Delta H = (h - h_0) = \sum \dot{m}C_p(T - T_0) \quad (31)$$

Where:

- \dot{m} is the mass flow of the stream of individual components in the stream in kg/s
- C_p is the heat capacity of the component in J/kg.K – this is assumed to be constant
- $T - T_0$ is the difference between the stream temperature and the reference temperature (298.15K)

The chemical exergy is calculated via equation 17.

The following data was obtained from the exergy analysis:

Table 31: Total exergy results of Air UCG & FTS

Stream	Flow (kmol/sec)	Physical (kW)	Chem (kW)	Total (kW)
1	3.095	12.77	412.88	425.65
2	3.095	34,291.73	412.88	34,704.61
3	4.02893	31,028.31	19,559.22	50,587.53
5	3.12	-238,853.45	527,949.56	289,096.12
6	5.513	108,984.93	164,381.79	273,366.72
7	3.095	57,801.53	412.88	58,214.41
9	5.513	43,378.92	164,381.79	207,760.70
10	3.922472	26,356.85	8,307.86	34,664.71
11	0.1064576	70.85	400,299.96	400,370.81
4	3.922472	15,658.92	8,307.86	23,966.78
8	0.1064576	-7.13	400,299.96	400,292.82
12	4.02893	28,788.55	19,559.22	48,347.77

Table 32: Equipment exergy analysis

Equipment Balance	MW	Efficiency
Compressor	34.28	81.53
UCG Reactor	-73.94	0.79
FTS Reactor	-157.17	0.24
Heater B3	23.51	1.68
Cooler B6	-65.61	0.76
Seperator	384.45	8.60
Valve B4	-10.70	0.69
Valve B8	-0.08	1.00
Cooler B9	-2.24	0.96
Overall	150.47	1.50
Fuel efficiency	111.20	1.38

The above tables represent the physical and chemical exergy results for the air-blown UCG coupled with FTS system as well as the exergy lost or gained from the system and the overall efficiency.

The exergy gains/losses are represented by the exergy flow diagram below:

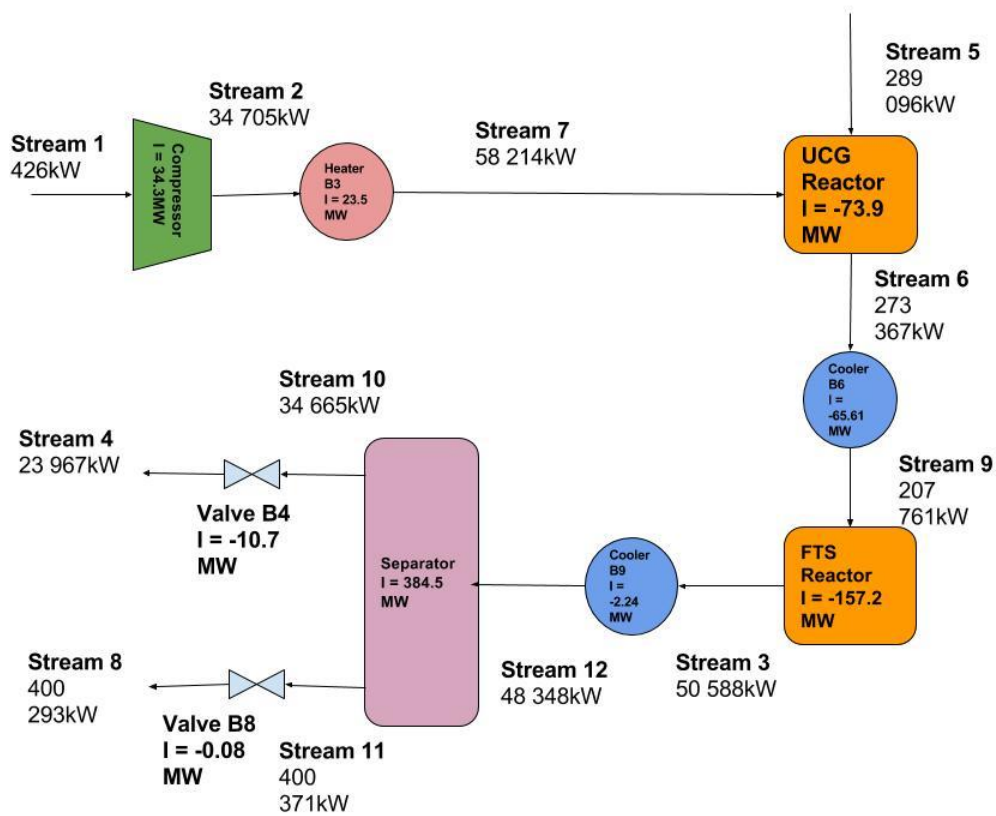


Figure 22: Exergy flow diagram of air-blown UCG with downstream FTS

There is a positive gain of exergy from the compressor input, as can be seen from its gain of 34.28MW and its efficiency of 81.53. This occurs due to work being added to the air stream in the form of compression. The compressor was modelled in the default ASPEN efficiency of 0.72. The benefit of a multistage compressor in terms of exergy is that it offers the ability to add work to the system without the need for a separate piece of equipment. Translated to financial benefits, this means that this requires a lower capital investment.

Heater B3 has an exergy gain of 23.51MW and an exergy efficiency of 1.68. In reality, this would be lower, as the simulation does not take the energy required to produce and compress steam to act as the heating agent within the exchanger. Again, this represents an energy gain, as the stream has work added in the form of heat. This is in comparison to the cooler B6, which takes out work to cool the UCG product stream down to base temperature. Again, the cooling medium

production and pressurisation is not taken into account, so the exergy efficiency for a realistic scenario would be less than the current 0.76.

The UCG reactor losses stem mainly from the loss of chemical exergy from the carbon stream to the product stream. This could be attributed to the dispersion of carbon molecules to the different gases within the system, i.e. the carbon is stream 5 reacts to form a variety of gases, though each gas amount is less than the original total. Even so, this reactor manages to maintain 79% of the incoming work ability.

The FTS reactor presents the converse story with the lowest exergy efficiency of the system. The composition change in the conversion of CO and H₂ to octane and CO₂ represents a loss in chemical exergy as well. The high CO₂ content coming out of the reactor account for these losses as the component contains a lower standard chemical exergy than both CO and H₂ as well as a lower heat capacity. For optimization around this process, the conversion of carbon monoxide and hydrogen would have to be lower so as not to drastically increase the carbon dioxide content.

The separator represents the biggest gain in exergy as well as efficiency. Though no work is added to the system in terms of heat or compression, the separation offers a split in terms of liquid from gas and thus produces a stream with a greater liquid phase concentration. Liquids are more ordered than gas molecules, and thus contain more exergy. The bottom stream is rich in octane, which offers a huge gain in terms of the chemical exergy when compared to the other components due to the change in composition. The waste gas stream still offers a chance to be used further as its total exergy is comparable to the compressed air in stream 2. Overall, the exergy efficiency and fuel efficiency values represent that there is a net gain in workable energy in the system, mainly from compression and the lack of pressure drops.

4.2.2 Oxygen (ASU) UCG

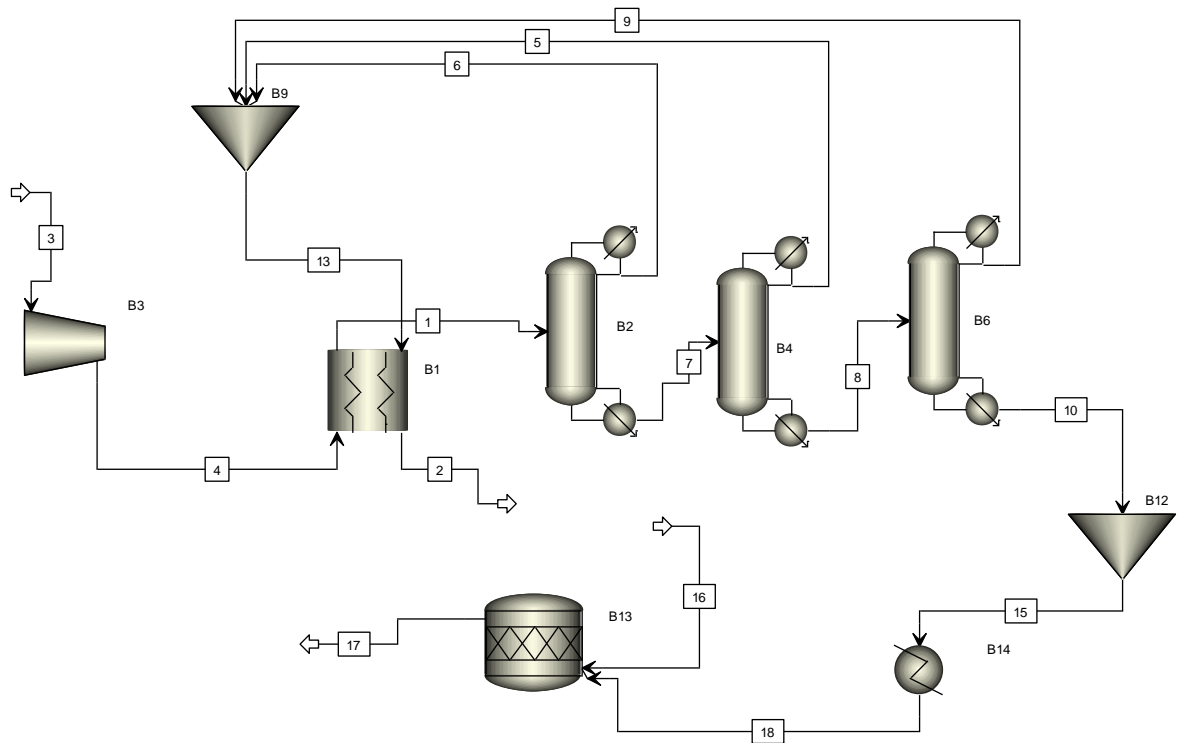


Figure 23: ASU-UCG simulation diagram

The above figure represents the process diagram for the UCG process that utilizes oxygen produced from an air separation unit (ASU). It is divided into four distinct areas: air compression, cooling, distillation and UCG reaction.

Air is compressed from ambient conditions to 5bar via compressor B3. The stream is then cooled to 98.15K in heat exchanger B1 from an outgoing waste nitrogen stream. The cooled stream then goes to the distillation unit, where all three columns operate at 5bar. The bottom streams are oxygen-rich and are sent for further refining in the successive columns. The top streams are nitrogen-rich and are mixed together to act as a cooling agent for the air stream in B1, before being discarded as waste. The table below represents the operating conditions for each column:

Table 33: Distillation unit summary

Column	Number of stages	Reflux ratio	Feed Stage
B2	100	40	25
B4	100	40	20
B6	100	45	50

Stream 10 is considered to be the oxygen product stream from the ASU and heated to 1200K, and 100% purity. This is sent into the UCG reactor to produce syngas.

Aside from the general assumptions mentioned earlier, the following process specific assumptions were made:

- The distillation columns were simulated using the Edimister method
- There is a slight pressure increase of 0.5atm assumed in the heater B4
- There is a pressure drop of 2atm in the waste mixer B9

The following results were obtained from the simulation.

Table 34: Main UCG composition results

Component	UCG product stream
Carbon	0.00
Oxygen	0.05
Nitrogen	0.00
Water	0.00
Carbon Monoxide	0.49
Carbon Dioxide	0.13
Methane	0.01
Hydrogen	0.33

Table 35: Total exergy analysis of oxygen (ASU) UCG simulation

Stream	Flow (kmol/sec)	Physical (kW)	Chem (kW)	Total (kW)
1	10	117,516.22	1,334.26	118,850.48
2	8.75	-19,854.47	3,370.27	-16,484.20
3	10	41.26	1,334.26	1,375.51
4	10	53,762.80	1,334.26	55,097.05
5	2.5	58,762.29	1,800.00	60,562.29
6	5	117,560.07	3,600.00	121,160.07
7	5	120,879.65	878.71	121,758.36
8	2.5	61,564.98	6,049.60	67,614.58
9	1.25	30,606.83	1,538.28	32,145.12
10	1.25	30,907.17	4,937.49	35,844.66
13	8.75	182,423.74	3,370.27	185,794.00
15	1.25	30,906.98	4,937.49	35,844.47
16	5	-169,645.86	850,066.54	680,420.68
17	5.122307	81,474.72	462,199.21	543,673.92
18	1.25	16,034.26	4,937.49	20,971.74

Table 36: Equipment exergy analysis

Equipment	MW	Efficiency
Compressor	53.72	40.06
Main HX	-138.52	0.42
Column B2	124.07	2.04
Column B4	6.42	1.05
Column B6	0.38	1.01
Waste Mixer	-28.07	0.87
Heater	-14.87	0.59
UCG Reactor	-157.72	0.78
Overall	-154.61	0.77
Fuel Efficiency	-136.75	0.80

As with the air simulation, the compressor has an exergy efficiency greater than 1. This is due to the addition of work via compression of the feed air stream. The advantage of a multistage stream compressor is that there is a greater addition of work without the need for separate equipment.

The subsequent Grassman diagram represents the exergy flows throughout the system.

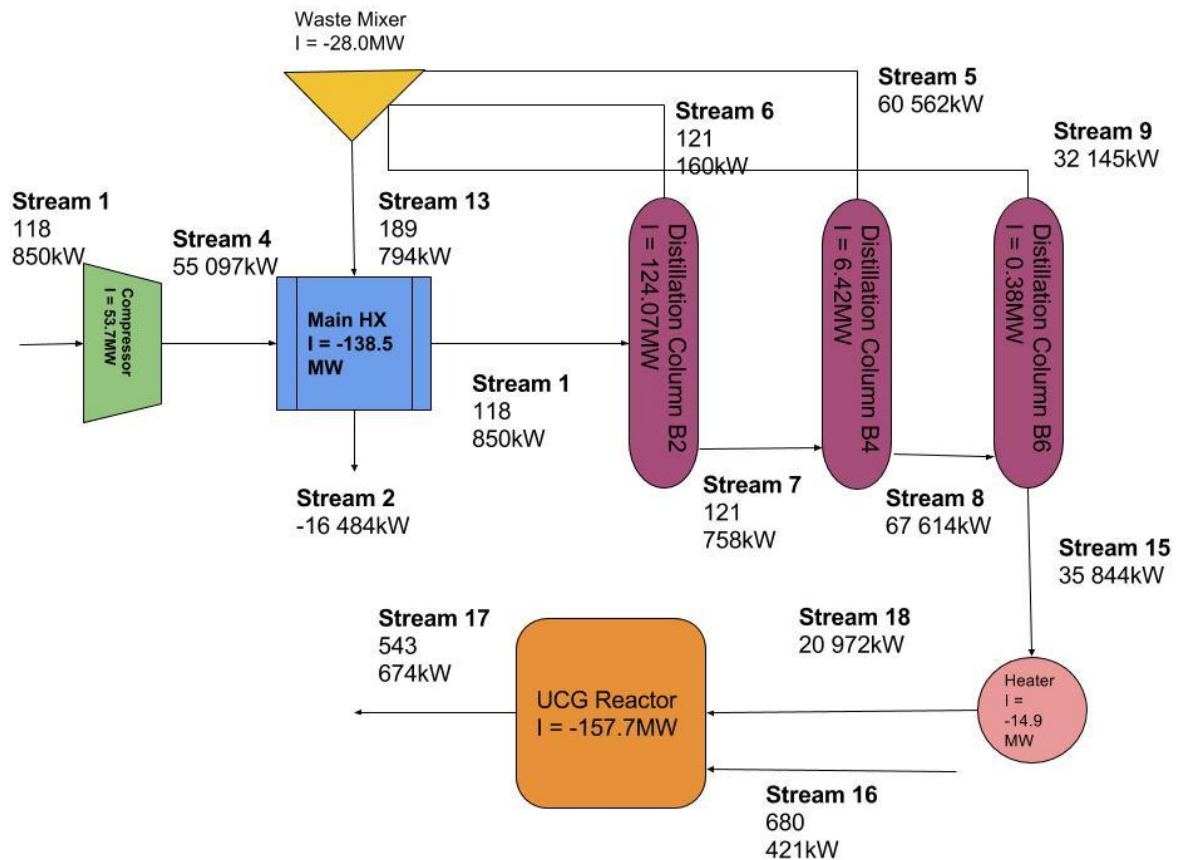


Figure 24: Exergy flow Oxygen-blown (ASU) UCG

Analysis of the main heat exchanger offers insight as to the cooling down of the main air stream with waste products. No change of composition happens over this equipment, therefore most of the exergy comes from the physical component. The main air stream is not fully liquefied due to its compression. In reality, the exergy efficiency of this equipment would be lower due to pressure drops and an increased discharge temperature of the main air stream. One method to prevent such losses would be to ensure insulation around the heat exchanger to prevent heat ingress.

The high efficiency over the waste mixer are expected as there isn't much pressure change across the stream.

The distillation train offers particular insight into the chemical changes of the system, since most of the changes occur within the composition of the air streams. Most of the changes occur across the chemical exergy of the streams, which is expected due to the separation of the oxygen from nitrogen. The oxygen-rich streams from the bottom of the columns contain more work than the top streams. From a chemical point of view, this is due to oxygen having a higher standard chemical exergy (3950kJ/kmol) than nitrogen (720kJ/kmol). In terms of the physical exergy, oxygen is intrinsically heavier than nitrogen and is more stable in the liquid form, thus making it capable of more work potential.

The heater efficiency of 0.59 is surprising in the sense that work is being added to the stream in the form of heat, therefore the efficiency should be greater than 1. A possible reason for this is that stream 15 (input stream to the heater) is liquid oxygen – much of the heat would go towards vaporizing the liquid and sustaining the temperature of the exit gas stream.

The UCG reactor has an efficiency of 0.78. Although there is a gain of physical exergy, the reactor is unable to preserve nearly half of the coal's chemical potential in stream 16. This would be a function of the syngas product exiting the reactor. In reality, a higher CO₂ content would be present in the product stream, thus making the chemical exergy of the system lower.

4.2.3 Comparative Simulation Discussion

In terms of the total system, the efficiency of the entire system as well as compared to the fuel stream (streams with carbon regarded as the input) only would be lower due to several factors:

- Pressure and temperature drops across the system
- Losses in steam production or other heating mediums for heaters
- Losses in cooling water or other coolant mediums in coolers
- Power generation and consumption thereof

Of most importance is the overall exergy efficiency of the air simulation (1.5) compared to that of the ASU simulation (0.77).

The air simulation has a higher conservation of the work inputs through its processes, mainly due to its lack of pressure drops. Although the FTS reactor does not offer a high exergy efficiency, its addition to the system prevents the overall chemical exergy from being lost due to the production of octane, which has a standard chemical potential exergy of 5413.1kJ/mol, the highest of any component modelled in both systems. This is somewhat offset by the production of carbon dioxide as well, thus contributing to the low efficiency of the reactor.

The overall fuel efficiency offers insight as to the conservation of the coal stream inputs compared to the desired product stream exergy. Again, the air simulation has a higher value (1.38 compared to the ASU's 0.8). The following table compares the UCG product stream exergies of both simulations:

Table 37: Comparison of UCG product stream exergies

Simulation	Physical Exergy (kW)	Chemical Exergy (kW)
Air	108 984.83	164 381.79
Oxygen	81 474.72	462 199.21

The air simulation stream contains a higher physical exergy, but is far outranked by the oxygen simulation stream's chemical exergy. This is due to the high content of nitrogen in the air simulation: it accounts for 44% of the air stream, and

contains the lowest standard chemical exergy out of all components modelled (720kJ/kmol).

The UCG reactors of both simulations have similar results. This is expected as the reaction scheme used for both simulations is the same.

The air-blown FTS system offers a particularly exciting proposition when compared to the ASU-coupled UCG for several other reasons as well:

- It offers a lower capital investment and operational expenses. The main expenses would occur within processing and storage of octane and related FTS products. An ASU is usually outsourced to an external gas company for construction and operation and presents a higher expense rate, depending on the service level agreement with said company, even though production rates could be greater.
- The waste stream still contains a significant amount of CO and hydrogen, which can be further combusted to produce energy. The production of the ASU simulation still contains 18% of oxygen, a significant amount when compared to the investment required for the actual ASU. Though the air input can be adjusted to lower flows, this would be a waste of the ASU.
- Whilst the ASU system only produces syngas, octane (along with other hydrocarbons produced in FTS) can be used processed into vehicle fuel in addition to being an energy source.
- Though the Air-FTS plant is smaller, it offers more benefits in terms of less human resources requirement, which reduces the probability of serious safety incidents occurring. A smaller plant also means easier control systems and operations, with quicker start-up and shutdown times as well as less maintenance required. It is also easier to add redundancy to the plant, e.g. additional compressor in case the main one goes down.

4.2.4 Hoe Creek Simulation

In this section, the exergy properties of Hoe Creek, an existing UCG site, was studied to compare to the idealized situation mentioned above. As stated previously, Hoe Creek was a UCG site using air as an oxidant.

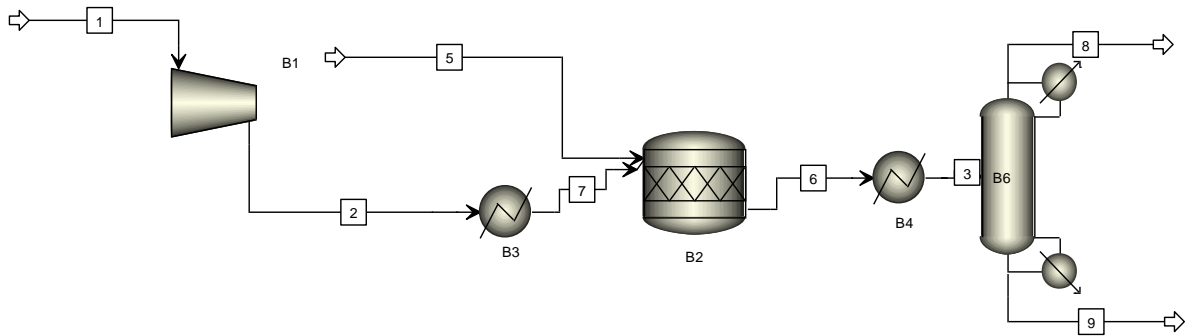


Figure 25: Hoe Creek simulation diagram

Though no formal description is given by Thorsness *et al*, the process has been modified from the original air simulation by removing the FTS reactor and adding a condenser and water separator at the end of the process. Once again, carbon is assumed to be the feed for simplification of the simulation. The same reaction scheme as the previous simulations with the following conversions of carbon applied:

- R1: 0.326
- R2: 0.144
- R3: 0.13
- R4: 0.2
- R5: 0.1
- R6: 0.1

Air is compressed to 25psia and then heated to 1200K. The coal stream (stream 5) contains a 2.5:1 water ratio. This is due to the high water influx that formed

part of the experiment to see the parameter impact as well as the fact that steam accounts for 30% of the gas composition and that a considerable quantity of water was produced by pumps located at the product well.

The UCG reactor is also assumed to operate at 1200K, with the same reaction scheme as the previous two simulations. The following tables describe the conversions applied as well as the composition of gas obtained from the simulation in comparison to Thorsness *et al*:

Table 38: Comparison of Hoe Creek syngas composition to simulation

Component	UCG gas composition (simulation)	UCG gas composition (Thorsness <i>et al</i>)
Carbon (tar)	0.00	0.014
Oxygen	0.03	0.00
Nitrogen	0.33	0.381
Water	0.35	0.304
Carbon Monoxide	0.10	0.061
Carbon Dioxide	0.08	0.11
Methane	0.02	0.011
Hydrogen	0.10	0.119

The following exergy results were obtained from the simulation:

Table 39: Hoe Creek simulation exergy results

Stream	Flow (kmol/sec)	Physical (kW)	Chem (kW)	Total (kW)
1	2.142857	8.84	285.91	294.75
2	2.142857	2,998.32	285.91	3,284.23
5	3.5	-184,919.20	132,090.99	52,828.21
6	5.16919	-43,317.75	31,789.33	11,528.41
7	2.142857	8,247.88	285.91	8,533.79
3	5.16919	34,160.21	31,789.33	65,949.55
8	3.365857	-62,500.79	42,994.10	19,506.69
9	1.803333	-1.19	17,131.66	17,130.48

Table 40: Hoe Creek simulation exergy efficiency

Equipment Balance	MW	Efficiency
Compressor	2.99	11.14
UCG Reactor	32.77	0.26
Heater B3	5.25	2.60
Cooler B4	77.48	5.72
Separator B6	-68.33	0.04
Overall	-55.50	0.05
Fuel efficiency	33.32	0.37

As expected, the compressor and heater efficiencies indicate that work is being added to the system in the form of compression and heat respectively.

The UCG reactor has the lowest efficiency of the equipment. In terms of chemical exergy, this is due to the considerable amount of nitrogen in the system, accounting for 33% of the UCG product content. When compared to the ideal air-FTS simulation, there is a high amount of water vapour coming from the reactor and lowers the chemical exergy of the system. Extrapolating from this, this means that the reactor at its current reaction conversions cannot contain the potential work of the incoming air and carbon streams. Given the amount of carbon monoxide being produced, it would not be useful to install a downstream FTS reactor to produce hydrocarbons.

Surprisingly, there is a gain in exergy across the cooler. This is due to the water condensing out of the gas phase and reversing the vaporization process. Liquid contains the potential to do more work than gas as it has less entropy.

The Hoe Creek simulation is far worse than the original air simulation, based on the overall and fuel exergy efficiencies. A suggestion to improve the process (if the mine was still in operation) would be to adjust the pressures and coal seam temperatures (via ignition) to control the composition of the outcoming gas – more carbon monoxide and hydrogen would be an added benefit. Thorsness *et al* also mentions an influx of water done as an experiment to see if gas compositions would change. This is also mentioned cited by Brown as an example of poor control by allowing such an influx from nearby water bodies. Had this been

controlled, Hoe Creek would not have contained as much water in its syngas and perhaps would have been more efficient at containing its feed exergy.

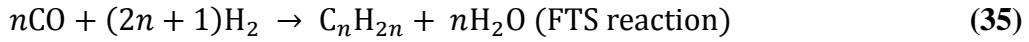
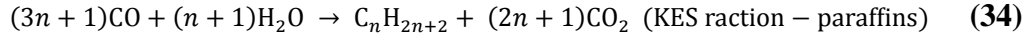
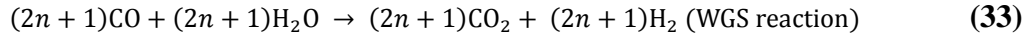
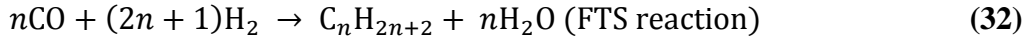
4.2.5 Improvements

Improvements on the exergy analysis could be made by transitioning the ideal situations to more realistic scenarios. This would add complexities in terms of additional components to consider – coal contains many other components such as sulphur, mercury and nitrogen, though these may be modelled as separate reactions within the reactor to produce SO_x and NO_x gases. If the standard chemical exergy can be found for the coal, it is a simple matter of finding the standard enthalpy and entropy of the coal, which can be done by modelling an ASPEN stream at standard conditions for the exact coal composition.

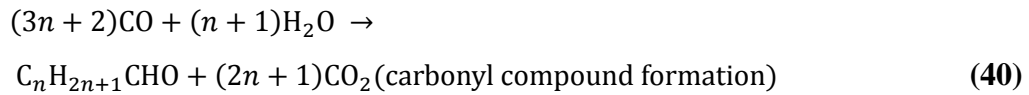
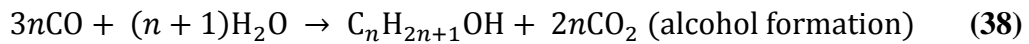
In terms of the FTS reactor, kinetics of the system could be studied to produce a wider yield of hydrocarbons. The effect of different catalysts should also be considered for yield of products as well as effects of the spectrum of reaction rates. Kölbel-Engelhardt should also be considered as an alternative to the traditional FTS mechanism for a comparative study.

Kölbel & Ralek (1984) as well as Larkins & Khan (1989) make reference to the Kölbel-Engelhardt synthesis (KES), a reaction mechanism that is similar to FTS in that it is able to produce hydrocarbons from a gas feed. Developed from research based on the water-gas shift reaction and its designated role in the overall Fischer-Tropsch mechanism, and is useful to develop hydrocarbon products from hydrogen-poor or hydrogen-free gas feeds. Depending on operating conditions, the main products are unbranched aliphatic hydrocarbons which may consist of olefins whereby the double bond between carbon atoms is located terminally (Kölbel & Ralek, 1984).

KES can be considered a combination of FTS and WGS, with two different sets of reactions for paraffins and olefins:



Oxygenates are formed as by-products, with the following reactions representing the synthesis of alcohols, organic acids and carbonyl compounds respectively:



Unwanted side reactions that occur include methanation and CO decomposition:



Both Kölbel & Ralek and Larkins & Khan state that metals which are typically used in FTS; such as iron, cobalt, nickel and ruthenium; may also be used in the KES process. It is important to note that a certain ratio of CO to H₂O must be maintained to avoid catalyst oxidation from excess steam and carbon deposition from excess CO. Kölbel and Ralek advise that this ratio must correspond to the reaction stoichiometry. They also note that infusing the catalyst with nitrides inhibits CO decomposition, whilst alkali salts can be used to suppress

methanation. Copper and silver promote catalyst reduction and enables metal formation at lower temperatures to avoid sintering.

Overall, further study would be required on the individual components of the simulation equipment. For example, compressors consist of electric motors, compression stages and aftercoolers (Kotas, 1985). By taking these as individual pieces that make a whole process, a more accurate idea of the exergy flow, losses and gains can be obtained.

Generally, ASU's are the only means to have a high production rate of oxygen, though smaller coal seams may allow for a more varied selection of oxidant production. Smith & Klosek detail an entire range of air separation methods, including adsorption methods.

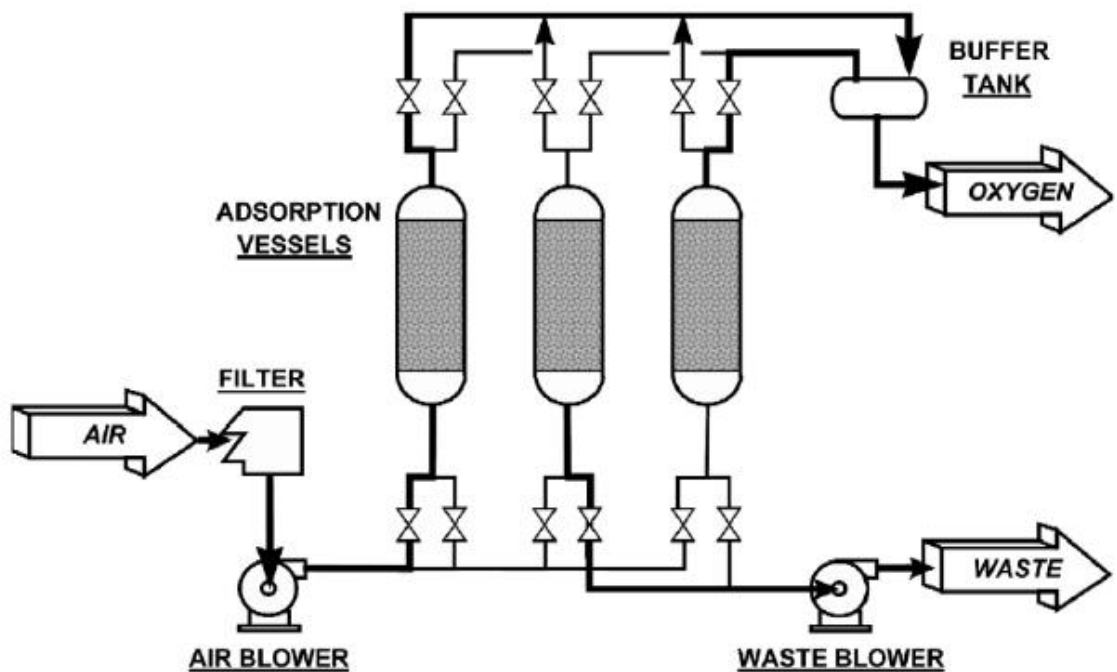


Figure 26: Process flow diagram of air separation via adsorption (Smith & Klosek, 2001)

Air is filtered and compressed in the feed stage before being passed through vessels filled with zeolite-based packing. Zeolite has a property of creating non-uniform electrical fields in the void spaces of the vessel, which preferentially adsorb nitrogen due to it being more polarisable than oxygen. Having more than one

vessel in the process mean that supply occurs continuously whilst the other vessels regenerate by heating or pressure drops to release their stored waste gas.

5 Conclusion

Using the BED method of analysis, UCG operations can be analyzed in terms of their input and production. The air-blown sites studied (Hoe Creek and Chinchilla) give valuable insight by their comparison on their respective BED's. Though they contain similar (dry, without nitrogen) compositions of carbon dioxide and hydrogen, the higher methane content in Chinchilla causes the overall system to be endothermic. The higher carbon monoxide formation in the Hoe Creek site causes its system to be exothermic in contrast.

The same method of evaluation applied to the oxygen-blown sites yields similar information. The laboratory study considered the excess use of oxidant – it pushes operations out of the stoichiometric region. Comparison of Rocky Mountain's ELW and CRIP method show that their differing ratios of steam to oxygen produce different results: the CRIP run has a higher steam to oxygen ratio, thus lowering the seam temperature to produce a higher carbon monoxide and hydrogen content. On average, the oxygen-blown sites have more carbon dioxide than their air-blown counterparts due to higher temperatures in their respective seams. Optimal UCG operations, such as the ELW run, should lie on a thermally balanced line or within a thermally balanced region.

The exergy simulations analyze UCG from a more idealized situation, but it is still important for determining how best to make use of the work potential in coal and oxidant feed inputs. The air simulation contains a higher overall exergy efficiency, though the oxygen simulation has a higher fuel efficiency. This is due to the constant presence of nitrogen within the air simulation, which heavily lowers the chemical exergy of the UCG product stream. However, latter simulation offers other advantages over the oxygen simulation, mainly due to its smaller size, easier operations and lower capital investment.

The Hoe Creek simulation, in comparison to the original air simulation highlights the poor operations carried out at the site. The high water influx and poor carbon monoxide content contribute to a highly inefficient system, in terms of both fuel and overall efficiencies.

Improvements can be made by considering additional coal inputs such as sulphur and nitrogen as well as considering alternative methods of air separation and the Kölbl-Engelhardt process. Further study would also be needed on the individual components of the equipment to gain a more accurate study.

6 References

Arabpour M., Rahimpour M.R., Iranshahi D. & Raeissi S. (2012); *Evaluation of Maximum Gasoline Production of Fischer-Tropsch Synthesis Reaction in GTL Technology: A Discretized Approach*; Journal of Natural Gas Science and Engineering, vol. 9, pgs 209-219

Bell D.A., Towler B.F. & Fan M. (2011); *Coal Gasification & Its Applications*; William Andrew Applied Science Publishers, chapter 5, pgs 101-111

Bhutto A.W., Bazmi A.A. & Zahedi G. (2013); *Underground Coal Gasification: From Fundamentals To Applications*; Progress in Energy and Combustion Science, vol. 39, pgs 189-214

Bialecka, B. (2009); *Analysis of criteria for UCG siting and operation*, Acta Motanistica Slovaca, vol. 14, pgs 298-305

Boroumandjazi G., Rismanchi B. & Saidur R. (2013); *A Review on Exergy Analysis of Industrial Sector*; Renewable and Sustainable Energy Reviews, vol. 28, pgs 198-203

Brown, K.M. (2012); *In Situ Coal Gasification: An Emerging Technology*; Journal of the American Society of Mining and Reclamation; vol. 1, pgs 103-122

Chodhury H.A. & Moholkar V.S. (2013)¹; *An Optimization Study of Fischer-Tropsch Synthesis Using Commercial Cobalt Catalyst*; International Journal of Scientific Engineering and Technology, vol. 2, pgs 31-39

Chodhury H.A. & Moholkar V.S. (2013)²; *Synthesis and Characterization of Fe-Catalyst for Fischer-Tropsch Synthesis using Biosyngas*; International Journal of Scientific Engineering and Technology, vol. 2, pgs 817-821

Cornelissen R.L. & Hirs G.G. (1998); *Exergy Analysis of Cryogenic Air Separation*; Energy Conversion Management, vol. 39, pgs 1821-1826

Dennis S. (2006); *Rocky Mountain , Underground Coal Gasification Test Project (Hanna, Wyoming): Final Technical Report for the Period 1986 to 2006* ; National Energy Technology Laboratory, U.S. Department of Energy, pgs 1-51

Domalski E.S. (1972); *Selected Values of Heats of Combustion and Heats of Formation of Organic Compounds Containing the Elements C, H, N, O, P and S*; Journal of Physical and Chemical Reference Data, vol. 1, pgs 221-277

European Industrial Gases Association (EIGA) (2011); *Environmental Impacts of Air Separation Units*; Doc 94/11, pgs 1-14

Eftekhari A.A., Van Der Kooi H., & Bruining H. (2012); *Exergy analysis of Underground Coal Gasification with Simultaneous Storage of Carbon Dioxide*; Energy, vol. 45, pgs 729-745

Ghamarian A. & Cambel A.B. (1982); *Exergy Analysis of Illinois No. 6 Coal*; Energy, vol. 7, pgs 483-488

Hu J., Yu F. & Lu Y. (2012); *Application of Fischer-Tropsch Synthesis in Biomass to Liquid Conversion*; Catalysts, vol. 2, pgs 303-32

Iandoli C.L. & Kjelstrup S. (2007); *Exergy Analysis of a GTL Process based on a Low-Temperature Slurry F-T Reactor Technology with a Cobalt Catalyst*; Energy & Fuels, vol. 21, pgs 2317-2324

Imran M., Kumar D., Kumar N., Quayyum A., Saeed A. & Bhatti M.S. (2014); *Environmental Concerns of Underground Coal Gasification*; Renewable and Sustainable Energy Reviews, vol. 31, pgs 600-610

Kačur J., Durdán M., Laciak M. & Flegner P. (2014); *Impact Analysis of the Oxidant in the Process of Underground Coal Gasification*; Measurement, vol. 51, pgs 147-155

Kapusta K., Stańczyk K., Wiatowski M. & Chećko J (2013); *Environmental Aspects of a Field-Scale Underground Coal Gasification Trial in a Shallow Coal Seam at the Experimental Mine Barbara in Poland*; Fuel, vol. 113, pgs 196-208

Kölbel H. & Ralek M. (1984); *The Fischer-Tropsch Synthesis*; Academic Press Inc. (London) Ltd, chapter 7 (The Kölbel-Engelhardt Synthesis), pgs 205-292

Kotas T.J. (1985); *The Exergy Method of Thermal Plant Analysis*; Anchor Brendon Ltd, section 3.5 (Pictorial representation of the exergy balance), pgs 84-85

Kumar H., Udayakumar D.L., Stojcevski A & Oo A.M.T. (2014); *Underground Coal Gasification: An Alternate, Economical and Viable Solution for future sustainability*; International Journal of Engineering Science Invention, vol. 3, pgs 57-68

Larkins F.P. & Khan A.Z. (1989); *Investigation of Kölbel-Engelhardt Synthesis over Iron-Based Catalysts*; Applied Catalysis, vol. 47, pgs 209-227

Lillebø A.H., Holmen A, Enger B.C. & Blekkan E.A. (2013); *Fischer-Tropsch Conversion of Biomass-Derived Synthesis Gas to Liquid Fuels*; WIREs Energy Environ, vol. 2, pgs 507-524

Lior N., Sarmiento-Darkin W. & Al-Sharqawi H.S. (2006); *The Exergy Fields In Transport Processes: Their Calculation and Use*; Energy, vol.31, pgs 553-578

Maloney J.O. (2008); *Perry's Chemical Engineers' Handbook*; The McGraw-Hill Companies Inc.; 8th edition; chapter 2; pgs 2-157, 2-158, 2-160, 2-179, 2-180

Mirzaei A.A., Arsalanfar M., Ebrahimzadeh F., Atashi H. & Moghaddam S.H.M. (2013); *Kinetic Study of Fischer Tropsch Synthesis over co Precipitated Iron-Cerium Catalyst*; Physical Chemistry Research, vol. 1, pgs 69-80

National Energy Technology Laboratory (2012); *Quality Guidelines for Energy System Studies: Detailed Coal Specifications*; U.S. Department of Energy, pgs 1-55

Pillay O. (2013); *Evaluation of Processes for Landfill Gas Utilization*; University of Witwatersrand, pgs 1-70

Prabu V. & Jayanti S. (2012); *Laboratory Scale Studies on Simulated Underground Coal Gasification of High Ash Coals for Carbon-Neutral Power Generation*; Energy, vol. 46, pgs 351-358

Prins M.J., Ptasinaki K.J. & Janssen F.J.J.G. (2004); *Exergetic Pptimization of a Production Process of Fischer-Tropsch Fuels from Biomass*; Fuel Processing Technology, vol. 86, pgs 375-389

Queensland Department of Mines & Energy (1999); *Utilisation of Walloon Coals of Southern Queensland for Power Generation*, Department of Mines & Energy (Queensland, Australia), pgs 1-38

Romero J.C. & Linares P. (2014); *Exergy as a Global Energy Sustainability Indicator: A Review of the State of the Art*; Renewable and Sustainable Energy Reviews, vol. 33, pgs 427-442

Saiba A.M., Moodley D.J., Ciobîca I.M., Hauman M.M., Sigwebela C.J. Westrate, Niemantverdriet J.W., van de Loosdrecht J. (2010); *Fundamental Understanding of Deactivation and Regeneration of Cobalt Fischer-Tropsch Synthesis Catalysts*; Catalysis Today, vol. 154, pgs 271-282

Sapali S.N. & Raibhole V.N. (2013); *Exergy Analysis of Cryogenic Air Separation Unit Integrated with Biomass Gasifier*; Lecture Notes in Engineering and Computer Science, vol. 2208, pgs 621-625

Schulz H. (2013); *Principles of Fischer-Tropsch Synthesis – Constraints on Essential Reactions Ruling FT-selectivity*; Catalysis Today, vol. 214, pgs 140-151

Self S.J., Reddy B.V. & Rosen M.A. (2012); *Review of underground coal gasification technologies and carbon capture*; International Journal of Energy and Environmental Engineering, vol. 3, pgs 1-8

Smith A.R. & Klosek J. (2001); *A Review of Air Separation Technologies and Their Integration with Energy Conversion Processes*; Fuel Processing Technology, vol. 70, pgs 115-134

Sohel M.I. & Jack M.W. (2011); *Thermodynamic Analysis of Lignocellulosic Biofuel Production via a Biochemical Process: Guiding Technology Selection and Research Focus*; Bioresource Technology, vol. 102, pgs 2617-2622

Srivastava A. (1988); *Second Law (Exergy) Analysis of Various Types of Coal*; Energy Conversion Management, vol. 28, pgs 117-121

Thorness C.B., Hill R.W. & Stephens D.R. (1977); *Preliminary Results From an In-Situ Coal Gasification Experiment Using Explosive Fracturing*; Lawrence Livermore Laboratory (University of California), pgs 1-21

van de Loosdrecht J., Botes F.G., Ciobica I.M., Ferreira A., Gibson P., Moodley D.J., Visagie J.L., Westrate C.J., & Niemantsverdriet J.W. (2013); *Comprehensive Inorganic Chemistry II*; Elsevier, chapter 7.20 (Fischer-Tropsch Synthesis: Catalysts and Chemistry), pgs 525-557

Wilson K.B., Woodward D.W. & Erickson D.C. (1988); *New Low Energy Processes for Cryogenic Air Separation*; Proceedings of the Twelfth International Cryogenic Engineering Conference (Southampton, UK – 12 to 15 July 1988), pgs 355-359

Yao M., Yao N., Shao Y., Han Q., Ma C., Yuan C., Li C. & Li X. (2014); *New Insight Into the Activity of ZSM-5 Supported Co and CoRu Bifunctional Fischer-Tropsch Synthesis Catalyst*; Chemical Engineering Journal, vol. 239, pgs 408-415

http://www.engineeringtoolbox.com/density-solids-d_1265.html, accessed 17 March 2015 at 19:18PM

http://www.engineeringtoolbox.com/specific-heat-fluids-d_151.html, accessed 17 March 2015 at 19:28PM

http://www.engineeringtoolbox.com/specific-heat-solids-d_154.html, accessed 17 March 2015 at 19:15PM

Appendix A: Bond Equivalent Diagram

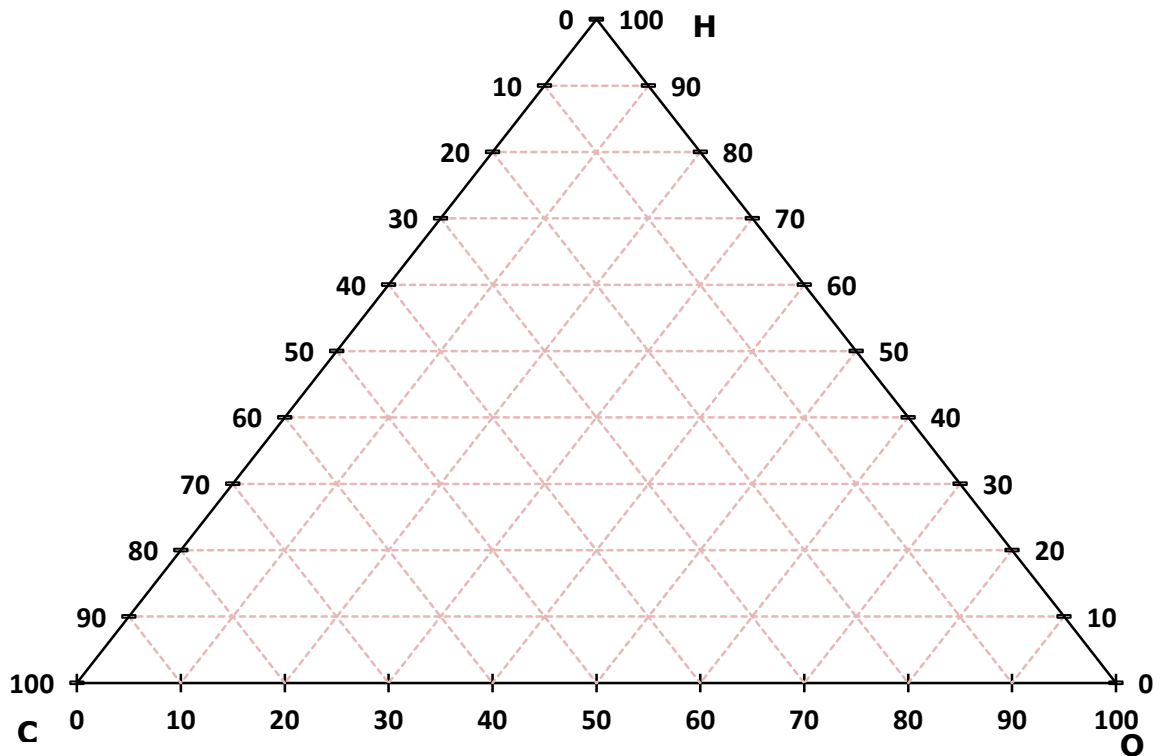


Figure A1: Bond Equivalent Diagram (C-H-O ternary system)

Figure A1 above represents the bond equivalent diagram. This system is used to plot and analyze various mass and concentration systems that contain three main components, signified by each of the triangle's apexes. In this research, carbon (C), hydrogen (H) and oxygen (O) are considered. The closer a point is to an apex, the more of that particular component it contains.

The molar composition (x) of a particular substance must be known in order to find the exact co-ordinates on the bond equivalent diagram. Each of the three co-ordinates can be found by multiplying the composition by the number of valence electrons for that particular element and dividing it by the sum of products (Pillay, 2013):

$$C = \frac{4x_C}{4x_C + x_H + 2x_O} \quad (\text{A1})$$

$$H = \frac{x_H}{4x_C + x_H + 2x_O} \quad (\text{A2})$$

$$O = \frac{2x_O}{4x_C + x_H + 2x_O} \quad (\text{A3})$$

Substances such as carbon monoxide, carbon dioxide and methane can be plotted by using the ratio of atoms designated by the compound and substituting the numerical values into equations A, B and C. This is illustrated by Table A below:

Table A1: Molar concentration inputs for various CHO substances

Substance	x_C	x_H	x_O
Carbon	1	0	0
Hydrogen	0	1	0
Oxygen	0	0	1
Carbon monoxide	1	0	1
Carbon dioxide	1	0	2
Methane	1	4	0
Water	0	2	1

To model a mixture of various compounds, equation D must be applied to each component in the system:

$$N_Z = n_Z F_Y \quad (\text{A4})$$

Where:

- N_Z is the number of atoms for a particular element Z in compound Y in the mixture
- n_Z is the number of atoms for element Z in compound Y (e.g. oxygen atoms in carbon dioxide equals 2)
- F_Y is the amount of compound Y in the mixture (molar)

Once this is done for each compound in terms of C, H and O, the total number of atoms can be summed up and the molar compositions for C, H and O can be calculated:

$$x_Z = \frac{\sum N_Z}{N} \quad (\text{A5})$$

Where:

- x_Z is the molar component of element Z
- N is the total number of atoms in the system

Reactions are essentially modelled in the same way, except the stoichiometric coefficients are substituted for the amounts. Either the reactants or products can be modelled as the same number of atoms for each elements are involved in both sides of the reaction.

The following tables represent the data obtained for each of the BED's in section 4.1 (compound elements are common to all of them, and will thus only be shown in the first table):

Table A2: Hoe Creek BED data points

Compound	Mol % of compound			BED Co ordinates		
	C	H	O	H	O	C
Methane	1	4	0	0.50	0.00	0.50
Carbon dioxide	1	0	2	0.00	0.50	0.50
Carbon Monoxide	1	0	1	0.00	0.33	0.67
Water	0	2	1	0.50	0.50	0.00
Hydrogen	0	1	0	1.00	0.00	0.00
Carbon	1	0	0	0.00	0.00	1.00
Oxygen	0	0	1	0.00	1.00	0.00
Hoe Creek r1	0.40816	0.18367	0.40816	0.07	0.31	0.62
Hoe Creek r 2	0.28986	0.13043	0.57971	0.05	0.47	0.47
Hoe Creek r3	0.2281	0.5438	0.2281	0.28	0.24	0.48
Hoe Creek r4	0.13543	0.59372	0.27086	0.35	0.32	0.32
Hoe Creek r5	0.31338	0.49765	0.18897	0.23	0.18	0.59
Hoe Creek r6	0.24414	0.53516	0.2207	0.27	0.23	0.50

Hoe Creek coal	0.674	0.3039	0.0221	0.10	0.01	0.89
Hoe Creek syngas	0.24431	0.37847	0.37722	0.18	0.36	0.46
Thermally balanced point A	0.23404	0.53193	0.23404	0.27	0.24	0.48
Thermally balanced point B	0.19677	0.40969	0.39354	0.21	0.40	0.40

Table A3: Chinchilla BED data points

Compound	Mol % of compound			BED Co Ordinates		
	C	H	O	H	O	C
Chinchilla r1	0.40816	0.18367	0.40816	0.50	0.00	0.50
Chinchilla r2	0.28986	0.13043	0.57971	0.00	0.50	0.50
Chinchilla r3	0.23031	0.53938	0.23031	0.00	0.33	0.67
Chinchilla r4	0.1362	0.59139	0.27241	0.50	0.50	0.00
Chinchilla r5	0.31546	0.49211	0.19243	1.00	0.00	0.00
Chinchilla r6	0.24477	0.53139	0.22384	0.00	0.00	1.00
Chinchilla coal	0.6658	0.2981	0.0361	0.00	1.00	0.00
Chinchilla syngas	0.21935	0.49032	0.29032	0.07	0.31	0.62
Thermally balanced point A	0.38217	0.17197	0.44586	0.05	0.47	0.47
Thermally balanced point B	0.26056	0.3316	0.40784	0.28	0.24	0.48
Thermally balanced point C	0.1945	0.4166	0.3889	0.35	0.32	0.32
Thermally balanced point D	0.2974	0.23699	0.46561	0.23	0.18	0.59
Thermally balanced point E	0.26404	0.35963	0.37633	0.27	0.23	0.50

Table A4: Rocky Mountain BED data points

Compound	Mol % of compound			BED Co ordinates		
	C	H	O	H	O	C
Rocky Mountain r1	0.41494	0.17012	0.41494	0.50	0.00	0.50
Rocky Mountain r2	0.29326	0.12023	0.58651	0.00	0.50	0.50
Rocky Mountain r3	0.23529	0.52941	0.23529	0.00	0.33	0.67
Rocky Mountain r4	0.13793	0.58621	0.27586	0.50	0.50	0.00
Rocky Mountain r5	0.32	0.48	0.2	1.00	0.00	0.00
Rocky Mountain r6	0.24615	0.52308	0.23077	0.00	0.00	1.00
Rocky Mountain coal	0.6709	0.2726	0.0565	0.00	1.00	0.00
Rocky Mountain syngas (ELW)	0.23478	0.39985	0.36537	0.06	0.31	0.62
Rocky Mountain syngas (CRIP)	0.21813	0.46889	0.31297	0.05	0.48	0.48
Thermally balanced point A	0.3881	0.15912	0.45278	0.27	0.24	0.48
Thermally balanced point B	0.2639	0.3277	0.4084	0.35	0.33	0.33
Thermally balanced point C	0.18857	0.4343	0.37714	0.22	0.19	0.59
Thermally balanced point D	0.30702	0.3043	0.38868	0.27	0.23	0.50
Thermally balanced point E	0.26272	0.38139	0.35589	0.09	0.04	0.87

Table A5: Lab coal run (Prabu & Jayanti, 2012) BED data points

Compound	Mol % of compound			BED Co ordinates		
	C	H	O	H	O	C
Lab run r1	0.3937	0.2126	0.3937	0.50	0.00	0.50
Lab run r2	0.28249	0.15254	0.56497	0.00	0.50	0.50
Lab run r3	0.22727	0.54545	0.22727	0.00	0.33	0.67
Lab run r4	0.13514	0.59459	0.27027	0.50	0.50	0.00
Lab run r5	0.3125	0.5	0.1875	1.00	0.00	0.00
Lab run r6	0.2439	0.53659	0.21951	0.00	0.00	1.00
Lab coal	0.62112	0.3354	0.04348	0.00	1.00	0.00
Lab run syngas (oxygen run)	0.28877	0.16586	0.54537	0.08	0.31	0.61
Lab run syngas (air run)	0.20045	0.2445	0.55505	0.06	0.47	0.47
Thermally balanced point A	0.36111	0.19444	0.44444	0.29	0.24	0.48
Thermally balanced point B	0.2583	0.3243	0.4173	0.35	0.32	0.32
Thermally balanced point C	0.19902	0.40294	0.39804	0.24	0.18	0.59
Thermally balanced point D	0.29602	0.30928	0.3947	0.28	0.23	0.50
Thermally balanced point E	0.26212	0.36021	0.37766	0.12	0.03	0.85

The thermally balanced line represents a particular set of conditions in system operations whereby the product outlet temperature is equal to the reactant inlet temperature by balancing out the endothermic reactions with the exothermic ones. Under these conditions, no heat is added or lost to the system and is considered to be adiabatic (Pillay, 2013).

In order to find the molecular formula for the different coals considered, the ratio of carbon to hydrogen to oxygen was taken based on the ultimate analysis. The coal formulas are tabulated in table A7.

In the process simulation, the only area where chemical reactions occur is assumed to be the UCG reactor. Reactions A6 to F are assumed to be the only reactions in the system:



To balance out the reactions, each one must be classified as endothermic (heat of reaction greater than zero) or exothermic (heat of reaction less than zero). For this, equation G is used:

$$\Delta H_{rxn} = \sum n\Delta H_{products} - \sum m\Delta H_{reactants} \quad (\text{A12})$$

Where:

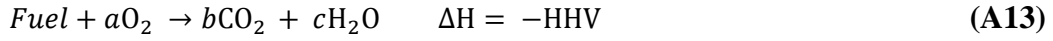
- ΔH_{rxn} is the heat of reaction in kJ
- $\sum n\Delta H_{products}$ is the sum of the product between the stoichiometric coefficients of the products and their respective heat of formations in kJ
- $\sum m\Delta H_{reactants}$ is the sum of the product between the stoichiometric coefficients of the reactants and their respective heat of formations in kJ

For the heat of formations, data from Felder & Rosseau (2005) was given at a reference basis of 25°C and 1atm. This was taken down to a reference temperature of 273K and is summarized in table A6:

TableA6: Heats of formation

Element	Heat formation (kJ/mol)
Carbon	0.00
Oxygen	0.00
Hydrogen	0.00
Water	-242.69
Carbon monoxide	-111.25
Carbon dioxide	-394.45
Methane	-75.75

To calculate the heat of formation of the coal, it was necessary to calculate the complete combustion of the fuel into carbon dioxide and water:



Where:

- Fuel is the coal considered
- a , b & c are the stoichiometric coefficients of oxygen, carbon dioxide and water respectively. These are calculated by balancing the above equation
- HHV is the higher heating value of the coal in kJ/mol

Using equation A12 and the heats of formation in table A6 to solve for the heat of formation of the coal, the following heating values and heats of formation:

Table A7: Summary of coal properties

Coal	Coal Formula	HHV (kJ/mol)	Source of HHV & Empirical Analysis Data	Coal Heat of Formation (kJ/mol)
Hoe Creek	$\text{CH}_{0.45}\text{O}_{0.033}$	290.778	Thorsness <i>et al</i> , 1977	-151.93
Chinchilla	$\text{CH}_{0.45}\text{O}_{0.054}$	348.249	Queensland Department of Mines & Energy, 1999	-94.552
Rocky Mountain	$\text{CH}_{0.41}\text{O}_{0.08}$	272.705	National Energy Technology Laboratory, 2012	-165.2
Laboratory Study	$\text{CH}_{0.54}\text{O}_{0.07}$	290.412	Prabu & Jayanti, 2012	-180.85

Once the heats of the reactions have been calculated, they can either be classified as endothermic or exothermic. In order to balance the reactions, the endothermic reactions must be added to the exothermic reactions based on the ratios of their heats of the reactions. The balanced reactions can be found in section 4.1.

Appendix B: Exergy Analysis

In order to calculate the exergy analysis, the simulation data was needed to be obtained first. Simulations were performed as per the descriptions and diagrams in section 4.2.

The following tables represent the data obtained from the ASPEN simulations.

Table B1: ASPEN Simulation results for air-FTS simulation

	1	2	3	4	5	6	7	8	9	10	11	12
	B1	B3	B7		B2	B6	B2		B5	B4	B8	
		B1	B5	B4		B2	B3	B8	B6	B7	B7	
<i>Substream: MIXED</i>												
<i>Mole Flow kmol/sec</i>												
<i>CARBO-01</i>	0	0	0	0.00E+00	2	0	0	0.00E+00	0.00E+00	0.00E+00	0.00E+00	0.00E+00
<i>OXYGE-01</i>	0.65	0.65	0.016	1.59E-02	0	0.016	0.65	8.37E-06	1.60E-02	1.59E-02	8.37E-06	1.60E-02
<i>NITRO-01</i>	2.445	2.445	2.445	2.44E+00	0	2.445	2.445	1.02E-03	2.45E+00	2.44E+00	1.02E-03	2.45E+00
<i>WATER</i>	0	0	0.01	7.14E-04	1.12	0.01	0	9.29E-03	1.00E-02	7.14E-04	9.29E-03	1.00E-02
<i>CARBO-02</i>	0	0	0.06993	6.99E-02	0	1.554	0	3.15E-05	1.55E+00	6.99E-02	3.15E-05	6.99E-02
<i>CARBO-03</i>	0	0	1.154035	1.15E+00	0	0.412	0	7.34E-03	4.12E-01	1.15E+00	7.34E-03	1.15E+00
<i>METHA-01</i>	0	0	0.034	3.40E-02	0	0.034	0	3.81E-05	3.40E-02	3.40E-02	3.81E-05	3.40E-02
<i>HYDRO-01</i>	0	0	0.207211	0.207241	0	1.042	0	5.93E-06	1.042	0.207241	5.93E-06	0.207211
<i>N-OCT-01</i>	0	0	0.092754	4.02E-03	0	0	0	0.08873	0	4.02E-03	0.08873	0.092754
<i>Total Flow kmol/sec</i>	3.095	3.095	4.02893	3.922472	3.12	5.513	3.095	0.106458	5.513	3.922472	0.106458	4.02893
<i>Total Flow kg/sec</i>	89.29217	89.29217	133.4913	122.8351	44.19911	133.4913	89.29217	10.65623	133.4913	122.8351	10.65623	133.4913
<i>Total Flow cum/sec</i>	75.71921	12.89708	10.86896	13.40772	7.331304	36.19	20.31708	0.086946	14.87258	4.469241	0.022494	6.412479
<i>Temperature K</i>	2.98E+02	7.62E+02	4.93E+02	2.98E+02	1.20E+03	1.20E+03	1.20E+03	2.98E+02	4.93E+02	2.98E+02	2.98E+02	2.98E+02
<i>Pressure N/sqm</i>	101325	1519880	1519880	506625	1519880	1519880	1519880	506625	1519880	1519880	1519880	1.52E+06
<i>Vapor Frac</i>	1	1	1	1	0.357503	1	1	0.058614	1	1	0	0.973577
<i>Liquid Frac</i>	0	0	0	0	0.642497	0	0	0.941386	0	0	1	0.026423
<i>Solid Frac</i>	0.00E+00	0.00E+00	0.00E+00	1.18E+08	0.00E+00	0.00E+00						
<i>Enthalpy J/kmol</i>	2.94E-09	1.40E+07	1.13E+08	1.06E+08	3.43E+08	3.21E+07	2.85E+07	2.61E+08	5.56E+07	1.06E+08	2.61E+08	1.22E+08
<i>Enthalpy J/kg</i>	1.02E-10	4.85E+05	3.42E+06	3.46E+06	2.42E+07	1.33E+06	9.86E+05	5.59E+06	2.29E+06	3.46E+06	5.59E+06	3.67E+06
<i>Enthalpy Watt</i>	9.11E-09	43313800	-4.6E+08	3.93E+08	1.07E+09	-1.8E+08	88065500	-1.1E+08	3.06E+08	3.93E+08	1.12E+08	
<i>Entropy J/kmol-K</i>	4273.383	9892.253	-10737.5	-4497.9	205309	57372.25	24843.41	7.30E+05	28184.63	-13632.1	7.30E+05	-32553.8
<i>Entropy J/kg-K</i>	148.1218	342.8802	-324.069	-435.303	14492.7	2369.392	861.1096	-5222.56	1163.985	-734.163	-5228.55	
<i>Density kmol/cum</i>	0.040875	0.239977	0.370682	0.276973	0.425572	0.152335	0.1523349	3.627051	0.370682	0.830918	14.01951	
<i>Density kg/cum</i>	1.179254	6.923443	12.28188	8.46526	6.02882	3.688623	4.394932	229.9281	8.975663	25.39578	888.7327	
<i>Average MW</i>	28.85046	28.85046	33.13319	30.56354	14.16638	24.21391	28.85046	63.39258	24.21391	30.56354	63.39258	
<i>Liq Vol 60F cum/sec</i>	0.165761	0.165761	0.225488	0.198891	0.035127	0.294909	0.1657614	0.026597	0.294909	0.198891	0.026597	

TableB3: ASPEN Simulation results for ASU UCG

	1	2	3	4	5	6	7	8	9	10	13	15	16	17	18	
Entering	B2		B3	B1	B9	B9	B4	B6	B8	B12	B1	B14	B13		B13	
Exiting	B1	B1		B3	B4	B2	B2	B4	B6	B6	B9	B12		B13	B14	
	LIQUID	VAPOR	VAPOR	VAPOR	LIQUID	LIQUID	LIQUID	LIQUID	LIQUID	LIQUID	MIXED	LIQUID	MIXED	VAPOR	VAPOR	
Substream: MIXED																
Mole Flow kmol/sec																
CARBO-01	0	0	0	0	0	0	0	0	0	0	0	0	3.21279	0	0	
CARBO-02	0	0	0	0	0	0	0	0	0	0	0	0	0	2.496338	0	
CARBO-03	0	0	0	0	0	0	0	0	0	0	0	0	0	0.661835	0	
NITRO-01	7.9	7.9	7.9	7.9	2.499999	5	2.9	0.400001	0.400001	0	7.9	0	0	0	0	
OXYGE-01	2.1	0.850003	2.1	2.1	6.65E-14	1.95E-15	2.1	2.1	0.850003	1.249997	0.850003	1.249997	0	0.231542	1.249997	
HYDRO-01	0	0	0	0	0	0	0	0	0	0	0	0	0	1.673864	0	
WATER	0	0	0	0	0	0	0	0	0	0	0	0	1.787209	4.11E-03	0	
METHA-01	0	0	0	0	0	0	0	0	0	0	0	0	0	0.054617	0	
Total Flow kmol/sec	10	8.75	10	10	2.5	5	5	2.5	1.25	1.25	8.75	1.25	5	5.122307	1.25	
Total Flow kg/sec	2.89E+02	2.49E+02	2.89E+02	2.89E+02	7.00E+01	1.40E+02	1.48E+02	7.84E+01	3.84E+01	4.00E+01	2.49E+02	4.00E+01	7.08E+01	1.11E+02	4.00E+01	
Total Flow cum/sec	1.26E+01	1.00E+03	2.45E+02	8.79E+01	0.09675	0.1935	0.17561	0.079724	0.041343	0.038464	4.44E+01	0.038464	3.52E+01	1.01E+02	2.24E+01	
Temperature K	98.15	475.152	298.15	535.9062	94.17049	94.17049	98.68354	105.434	102.4979	108.9911	70.01223	108.9921	1200	1200	1200	
Pressure N/sqm	5.07E+05	34473.79	1.01E+05	5.07E+05	34473.79	5.07E+05	5.07E+05	5.07E+05	5.57E+05							
Vapor Frac	0.775393	1	1	1	0	0	0	0	0	0	0.298946	0	0.356951	1	1	
Liquid Frac	0.224607	0	0	0	1	1	1	1	1	1	0.701054	1	0.643049	0	0	
Solid Frac	0	0	0	0	0	0	0	0	0	0	0	0	0	0	0	
Enthalpy J/kmol	-	7.02E+06	5.19E+06	7.45E-09	7.02E+06	1.08E+07	1.08E+07	1.12E+07	1.15E+07	1.14E+07	1.16E+07	1.09E+07	1.16E+07	3.45E+08	7.54E+07	2.98E+07
Enthalpy J/kg	-	2.43E+05	1.83E+05	2.58E-10	2.43E+05	3.84E+05	3.84E+05	3.77E+05	3.67E+05	3.71E+05	3.62E+05	3.82E+05	3.62E+05	2.43E+07	3.49E+06	9.30E+05
Enthalpy Watt	-	7.02E+07	4.54E+07	7.45E-08	7.02E+07	2.69E+07	5.38E+07	5.60E+07	2.88E+07	1.43E+07	1.45E+07	9.50E+07	1.45E+07	1.72E+09	3.86E+08	3.72E+07
Entropy J/kmol-K	-53578	25272.43	4273.205	8187.812	-98234	-98234	-93258.4	-95085.1	-93721.1	-98373.3	-90248.4	-98372.7	2.09E+05	85122.68	30673.36	
Entropy J/kg-K	-1857.1	889.8546	148.116	283.8024	-3506.67	-3506.67	-3141.36	-3031.94	-3050.47	-3074.28	-3177.69	-3074.26	14769.41	3935.797	958.5785	
Density kmol/cum	0.795584	8.73E-03	4.09E-02	1.14E-01	25.83982	25.83982	28.47226	31.35838	30.23455	32.49813	0.197216	32.49795	1.42E-01	5.08E-02	5.59E-02	
Density kg/cum	22.95291	0.247832	1.179251	3.280367	723.8632	723.8632	845.2649	983.4349	928.9111	1039.901	5.601065	1039.895	2.013095	1.098223	1.787329	
Average MW	28.8504	28.40063	28.8504	28.8504	28.01348	28.01348	29.68731	31.36115	30.7235	31.9988	28.40063	31.9988	14.15718	21.62781	31.9988	
Liq Vol 60F cum/sec	0.535578	0.468631	0.535578	0.535578	0.133895	0.267789	0.267789	0.133895	0.066947	0.066947	0.468631	0.066947	0.056212	0.274194	0.066947	

TableB3: ASPEN Simulation results for Hoe Creek

	1	2	5	6	7
Entering	B1	B3	B2		B2
Exiting		B1		B2	B3
	VAPOR	VAPOR	MIXED	VAPOR	VAPOR
Substream: MIXED					
Mole Flow kmol/sec					
CARBO-01	0	0	1	0	0
OXYGE-01	0.45	0.45	0	0.143	0.45
NITRO-01	1.692857	1.692857	0	1.692857	1.692857
WATER	0	0	2.5	1.803333	0
CARBO-02	0	0	0	0.522667	0
CARBO-03	0	0	0	0.394	0
METHA-01	0	0	0	0.083333	0
HYDRO-01	0	0	0	0.53	0
Total Flow kmol/sec	2.142857	2.142857	3.5	5.16919	2.142857
Total Flow kg/sec	61.82227	61.82227	57.0492	118.8715	61.82227
Total Flow cum/sec	52.42502	37.79973	101.2801	209.8035	86.97277
Temperature K	298.15	365.702	673.15	673.15	673.15
Pressure N/sqm	1.01E+05	1.72E+05	1.38E+05	1.38E+05	1.38E+05
Vapor Frac	1	1	0.71293	1	1
Liquid Frac	0	0	0.28707	0	0
Solid Frac	0	0	0	0	0
Enthalpy J/kmol	7.45E-09	1.97E+06	1.98E+07	-1.14E+08	1.12E+07
Enthalpy J/kg	2.58E-10	68452.23	1.21E+06	-4.97E+06	3.89E+05
Enthalpy Watt	1.60E-08	4.23E+06	6.92E+07	-5.91E+08	2.40E+07
Entropy J/kmol-K	4273.205	5825.686	1.38E+05	29521.79	25970.98
Entropy J/kg-K	148.116	201.9274	8479.046	1283.771	900.1948
Density kmol/cum	0.040875	0.05669	0.034558	0.024638	0.024638
Density kg/cum	1.179251	1.635522	0.563281	0.566585	0.710823
Average MW	28.8504	28.8504	16.29977	22.99615	28.8504
Liq Vol 60F cum/sec	0.114767	0.114767	0.05258	0.212818	0.114767

Once the data was obtained, the exergy analysis was broken down into distinct sections. The following equation represents the calculation for the entire stream:

$$\dot{E} = \dot{E}_k + \dot{E}_p + \dot{E}_{phys} + \dot{E}_{chem} \quad \text{(B1)}$$

Where:

- \dot{E} is the total rate of exergy in a stream in J/s
- \dot{E}_k is the kinetic exergy (associated with speed) of a stream in J/s
- \dot{E}_p is the potential exergy (associated with altitude) of a stream in J/s
- \dot{E}_{phys} is the physical exergy (work obtainable from a substance through a reversible process) of a stream in J/s
- \dot{E}_{chem} is the chemical exergy (work obtainable from a substance through heat transfer and matter exchanges with the environment) of a stream in J/s

For the purpose of this calculation, it is assumed that all exergies apart from the physical and chemical exergies are negligible. The following equations define the non-zero components of the analysis:

$$\dot{E}_{phys} = \dot{m}[(h - h_0) - T_0(S - S_0)] \quad \text{(B2)}$$

Where:

- \dot{m} is the stream flow rate in kg/s
- $h - h_0$ refers to the enthalpy difference of the stream at its current state (T, P) and the 'dead' or reference state in J/kg (T_0, P_0) respectively (Note – environmental considerations are in K and Pa for temperature and pressure respectively).
- $S - S_0$ refers to the entropy difference of the stream at its current state and the dead state in J/kg.K

h_0 and S_0 were calculated by simulating streams with the same composition as their simulation counterparts at standard conditions.

For solids and liquids, the physical exergy can be defined as:

$$E_{phys} = \dot{m} \left[C \left((T - T_0) - T_0 \ln \frac{T}{T_0} \right) - v_m (P - P_0) \right] \quad (\text{B3})$$

Where:

- C is the heat capacity of the solid or liquid in J/kg.K
- v_m is the specific volume of the solid or liquid at temperature T_0 in m³/kg

Chemical exergy can be defined as:

$$E_{chem} = \dot{m} \sum_i x_i (e_{0,i} + RT_0 \ln x_i) \quad (\text{B4})$$

Where:

- x_i is the molar fraction of the component i in the stream
- $e_{0,i}$ is the standard chemical exergy of the stream in J/kg

The simple exergy efficiency of the process is defined as:

$$\eta = \frac{E_{out}}{E_{in}} \quad (\text{B5})$$

Where:

- E_{in} and E_{out} are the exergies of the streams flowing into and out of a particular system boundary in J/s

The fuel exergy efficiency takes individual components or desired components and compares them to the exergy used:

$$\Psi = \frac{E_{desired\ component(s)}}{E_{coal\ stream}} \quad (\text{B6})$$